SPATIAL AND GEOCHEMICAL CHARACTERIZATION OF AN ANOMALOUS, MAP-SCALE DOLOMITE BRECCIA IN THE MONTEREY FORMATION, SANTA MARIA BASIN, CALIFORNIA

A THESIS

Presented to the Department of Geological Sciences

California State University, Long Beach

In Partial Fulfillment

of the Requirements for the Degree

Master of Science in Geology

Committee Members:

Richard J. Behl, Ph.D. (Chair)
Lora R. Stevens, Ph.D.
Sean J. Loyd, Ph.D.

College Designee:

Richard J. Behl, Ph.D.

By Maia C. Davis

B.S., 2009, University of California, Santa Barbara

May 2018

ABSTRACT

SPATIAL AND GEOCHEMICAL CHARACTERIZATION OF AN ANOMALOUS, MAP-SCALE DOLOMITE BRECCIA IN THE MONTEREY FORMATION, SANTA MARIA BASIN, CALIFORNIA

By

Maia C. Davis

May 2018

An approximately eighteen-square-kilometer dolomite breccia mapped by Dibblee and Ehrenspeck in 1988 outcrops at or near the base of the Monterey formation in the southern margin of the Santa Maria Basin (SMB). Although not recognized as such by the original mappers, it marks the location of an extensive detachment surface, along which large amounts of fluids flowed that dolomitized and cemented an undulating fault zone. This surface is key to allowing excess folding of Monterey strata relative to older strata.

The dolomite breccia exposed in the old Grefco Quarry road cut is analyzed in detail using outcrop description, macro- and micro- rock fabric description, thin section petrography, X-ray diffraction data, carbon and oxygen isotopes, and trace element geochemistry. Deformation, mineralogy, and isotope signatures are consistent with hydrothermal dolomite (HTD) emplacement from evolved, Monterey-sourced connate fluids that ranged in temperature from 36.6 to 99.5ºC. Clasts of dolomite, Monterey siliceous rocks and sandstone from underlying formations are locally supported by >35% micritic dolomite and microcrystalline quartz cement in a dilation breccia. A minimum of 128,000-231,000 cm^3 of fluid per cm^3 of breccia volume were required to deposit the dolomite cements.

ACKNOWLEDGMENTS

Thank you to my esteemed committee members, Dr. Richard Behl, Dr. Lora Stevens, and Dr. Sean Loyd. You are brilliant, and your guidance and friendship are invaluable.

I would also like to give a big "THANK YOU!" to the MARS Project and affiliates for supporting this research. And thank you to my extraordinary field and lab assistants, Amber Tucker, Casey Slatten, and Melissa Lizarraga for your help and contributions to this research.

Many, many thanks to the Poett and Mott families at Rancho San Julian, the Isaacson and Hames families at El Chorro Ranch, Christopher Ryan and the Vandenberg Air Force Base, Morgan Emmett, Phil Hogan and the Hollister Ranch Owners Association and Co-op, and the City of Santa Barbara for not only allowing me access to my study areas but welcoming me with open arms and warm hospitality. I am forever grateful.

Thanks to Dr. Greg Holk for your guidance and assistance with the IRMS and isotope data analysis, and thank you, Dr. Tom K. Kelty and Dr. Jayne Bormann, for keeping me sane, grounded, and on track. Also, thank you, Peter Eichhubl for your kindness and generosity, allowing me access to your tabulated data.

I would like to give another big "THANKS!" to my MARS family – Rick Behl, John "Jack" Farrell, Pam Hill, Wanjiru Njuguna, Alex Sedlak, Ryan Weller, and Yannick Wirtz – for their thoughtfulness, collaboration, support, and friendship through this process, and for making my graduate school experience so rich.

Thank you, Michael Hong, for your support through this process. Marie, Sidney, and Nathan Davis, Strawn Cathcart, Lakisha Witzel, and Mollie Richards: thank you for your endless encouragement and support. No adventure would be the same without you.

This work is dedicated to my parents.

TABLE OF CONTENTS

LIST OF TABLES

LIST OF FIGURES

CHAPTER 1

INTRODUCTION

The Miocene Monterey Formation is largely composed of fine-grained biogenic and siliciclastic sediments and diagenetic material (Bramlette, 1946; Isaacs, 1981; Behl, 1998). Authigenic precipitates, such as dolomite or carbonate fluorapatite, are less common, yet still characteristic minerals. Dolomite occurs throughout the formation on millimeter to meter scales, more commonly in the lower members compared to the upper members (Compton and Siever, 1984), and in higher concentrations in the Santa Maria Basin (hereafter SMB) than in the Santa Barbara Basin (hereafter SBB) (Compton and Siever, 1984). Dibblee and Ehrenspeck (1986, 1987, 1988b, 1988c, 1988d) and Dibblee et al. (1994) mapped four dolomite bodies in the SMB and three limestones in the SBB (Fig. 1) on a 1:24,000 scale. This scale of carbonate occurrence is atypically large for the Monterey Formation, and little is known about the origin of these carbonates. This study examines the outcrop structure, macro- and microfabrics of the rock, $\delta^{13}C$ and $\delta^{18}O$ isotopic signatures, and trace element concentrations of the most extensive occurrence of atypical Monterey dolomites (Fig.1, location 6; Fig. 3.6) in the SMB in order to provide insight to the origin of these rocks.

Geologic Setting

The onshore SMB is a depositional and tectonic basin bounded to the south by the east-west trending Santa Ynez Mountains of the Western Transverse Ranges and to the northeast by the northwest-southeast trending Coast Ranges (Tennyson and Isaacs, 2001) (Fig. 1). The SBB is directly south of the SMB, bounded to the north by the Santa Ynez Mountains, and is predominantly an east-west trending offshore basin (Tennyson and Isaacs, 2001) (Fig. 1). These basins developed during the Miocene to Quaternary in conjunction with the 90° clockwise

rotation of the western Transverse Ranges (Hornafius et al., 1986) that was initiated in the early Miocene by capture of the Monterey microplate by the Pacific plate (Nicholson et al., 1994). The SMB is mostly underlain by the Jurassic-Cretaceous Franciscan Assemblage and the Cretaceous Great Valley Sequence; however, Paleocene to Eocene strata comprise the basement rocks in the southern part of the SMB and northern part of the onshore SBB (McLean, 1995; Tennyson and Isaacs, 2001). The SBB is underlain by Cretaceous to Eocene or Oligocene (varies locally) strata (Tennyson and Isaacs, 2001).

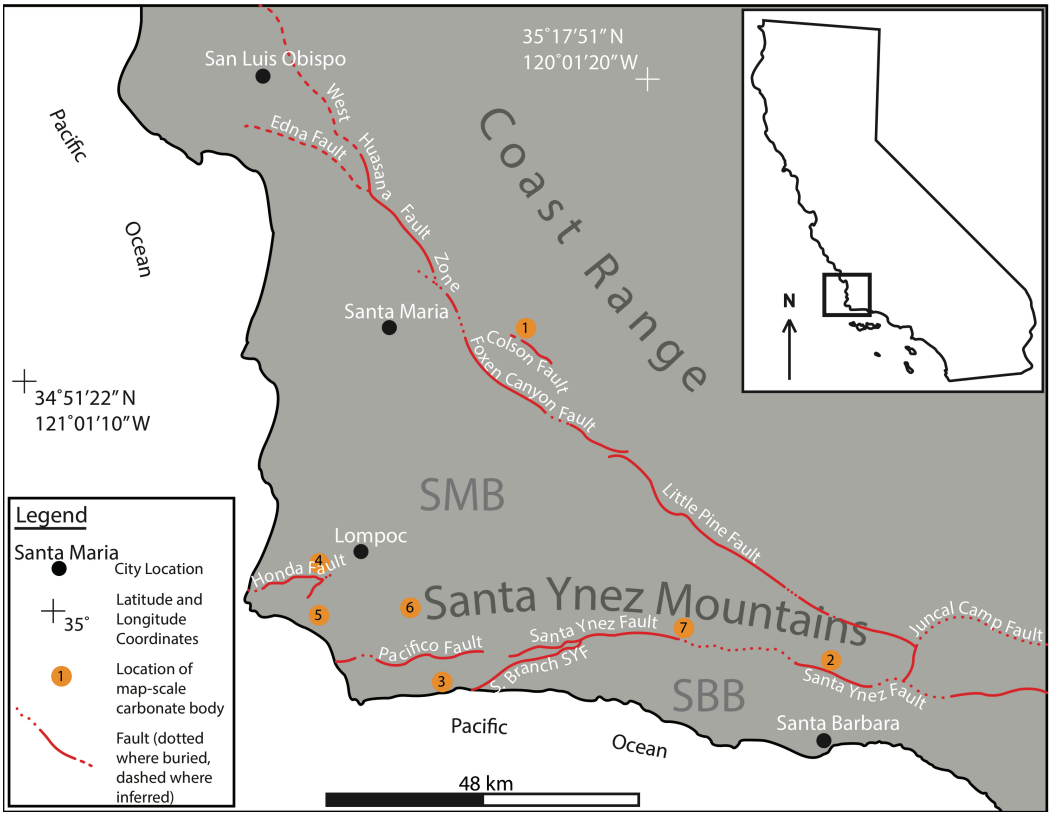

FIGURE 1. Location of carbonate bodies mapped on a 1:24,000 scale (Dibblee and Ehrenspeck, 1988b, 1988c, 1988d; Dibblee et al., 1994) in Central California. The Santa Maria Basin is indicated by "SMB" and the Santa Barbara Basin is indicated by "SBB." Numbers within circles correspond to specific location names. 1 – Tepusquet Canyon; 2 – Gibraltar Road; 3 – Hollister Ranch; 4 – La Salle Canyon Road; 5 – Sudden Canyon Road; 6 – Old Grefco Quarry Road; 7 – Bee Rock Quarry (not included in study). Carbonate and fault locations determined from Little Pine Mountain (Dibblee and Ehrenspeck, 1986), Lake Cachuma (Dibblee and Ehrenspeck, 1987), Santa Rosa Hills and Sacate (Dibblee and Ehrenspeck, 1988b), Lompoc Hills and Point Conception (Dibblee and Ehrenspeck, 1988c), Point Arguello and Tranqioon Mountain (Dibblee and Ehrenspeck, 1988d) and Tepusquet Canyon (Dibblee et al., 1994) quadrangles.

Dolomite in the Monterey Formation

The Monterey Formation in the SMB has been subdivided into members differently by various workers. Woodring and Bramlette (1950) differentiated lower, middle, and upper members. MacKinnon (1989) identified four members, from bottom to top: Lower Calcareous-Siliceous Member, Phosphatic Member, Upper Calcareous-Siliceous Member, and the Clayey-Siliceous Member. Dibblee and Ehrenspeck (1988b, 1988c) divided the formation into two main mappable units, which have been correlated to MacKinnon's four members (Fig. 2), and a number of locally significant subunits. Tmls (Monterey Limestone) is Dibblee and Ehrenspeck's map unit designated for map-scale carbonates in the SMB and SBB, but it is not included in the correlation of Dibblee map units to MacKinnon members because it does not occur consistently in the Monterey Formation stratigraphy.

Typical Dolomite Occurrence in the Monterey Formation

Dolomite in the Monterey Formation is typically authigenic or diagenetic, formed in association with the breakdown of organic matter (Pisciotto, 1981; Loyd et al., 2012a). It occurs as concretions, laminations and beds, and often replaces other lithologies (Murata et al., 1969, 1972; Pisciotto, 1981; Pisciotto and Mahoney, 1981; Loyd et al., 2012a; Behl, 2014). Such occurrences of dolomite within the Monterey Formation will be referred to as "stratigraphic dolomite" throughout this work in order to distinguish between typical (laminations, nodules, etc.) and atypical (map-scale breccias) Monterey dolomite occurrences.

Compton and Siever (1984) documented greater dolomite occurrences in the lower members of the Monterey Formation than in the upper members, and they also noted that the SMB has more dolostone and less calcareous rock types than equivalent strata in the SBB.

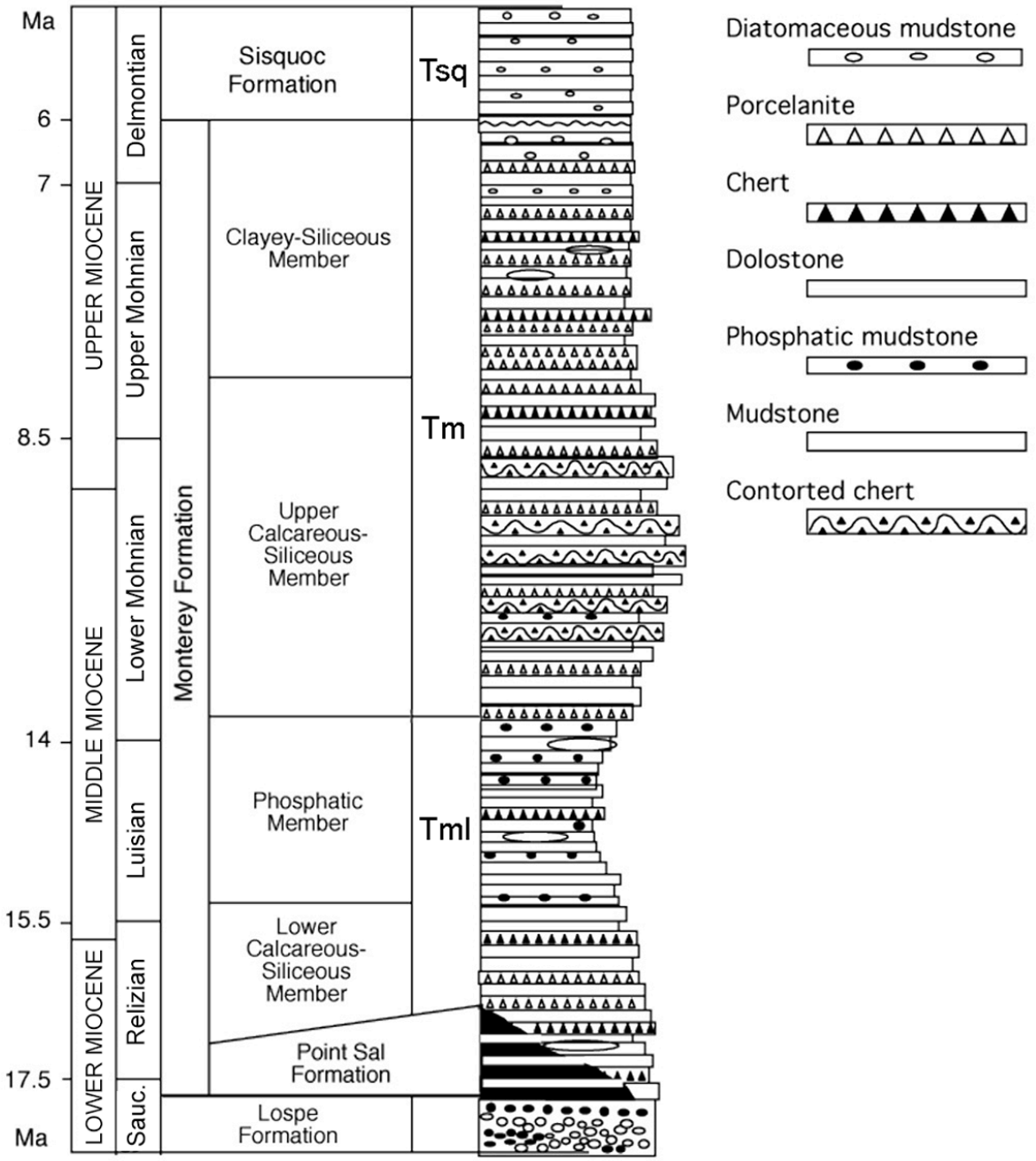

FIGURE 2. Composite stratigraphic section of the Monterey Formation in the Lompoc area (after Ijeoma, 2014, modified from MacKinnon (1989) and Dibblee and Ehrenspeck (1988b, 1988c)). Tmls is not depicted in this figure because it does not occur at consistent stratigraphic intervals.

Atypical Dolomite Occurrence in the Monterey Formation

Dibblee and Ehrenspeck (1986, 1987, 1988b, 1988c, 1988d) and Dibblee et al. (1994) mapped seven carbonate bodies on a quadrangle scale within the Monterey Formation, predominantly in the Tml map unit or along its basal contact (Fig. 3). These bodies are massive, isolated, and enigmatic due to their large size. They exist adjacent to faults and along contact or unconformable surfaces locally throughout the Monterey. With the exception of the dolomite breccia in Tepusquet/Colson Canyons, which is mapped and described as dolomite (Dibblee et al., 1994), the carbonate bodies in the western portion of the SMB and along the northwest margin of the SBB are mapped as limestone although they were described as dolomite. Carbonate bodies along the northeast margin of the SBB are mapped and described as limestones (Dibblee and Ehrenspeck, 1986, 1987). These dolomites and the dolomite breccia in Tepusquet and Colson Canyons (Redwine, 1981; Roehl, 1981; Malone et al., 1996; Martin and Rymerson, 2002) (Fig. 3) resemble what Davies and Smith (2006) have described as hydrothermal dolomite (HTD). As far as we know, occurrences of these dolomite bodies are largely confined to the SMB and along the northern margin of the SBB.

Hydrothermal Dolomite (HTD)

Davies and Smith (2006) documented in the mid-continent how wrench and normal faults associated with releasing bends or step-overs in strike-slip fault systems created conduits for hydrothermal brines stored in sandstones to travel upward into finer-grained, lower-permeability rocks (carbonates in this case) dolomitizing other lithologies and precipitating hydrothermal dolomite (HTD). Central California is presently characterized by both compressional and extensional structures formed during the initial rifting and 90° clockwise rotation of the western Transverse Ranges from the early Miocene to the present (Hornafius et al., 1986; Nicholson et

al., 1994). Reverse and normal faults, potentially including detachment faults, in the SMB and SBB act as conduits for fluid migration. Eichhubl and Boles (2000b) calculated high rates of fluid flow related to hydrothermal dolomite in the Monterey west of Santa Barbara. Behl (1998) calculated that 2,500-20,000 volumes of formation fluid had traveled through intraformational chert breccias in the Monterey Formation of SMB. Large volumes of fluids have flowed through faults and breccias in the Monterey Formation, and fluid flow and dilation structures are also both elemental in the formation of HTD elsewhere in North America (Davies and Smith, 2006).

Dolomite Breccia at Tepusquet and Colson Canyons

Prior to the 1970s, a dolomite breccia spanning Tepusquet and Colson Canyons east of Santa Maria was merely included in the lithologic description of the lower members of the Monterey Formation as a lenticular dolomitic carbonate (Woodring and Bramlette, 1950; Dibblee, 1950). In the late 1970s, increased interest in fractured dolomite reservoirs in the SMB developed (Roehl, 1981), and Redwine (1981) delineated and described the four-kilometer-long and 20-meter-wide exposure of the breccia, discussing its importance to understanding dolomite reservoirs in the SMB.

Roehl (1981) compared the isotopic signature of this dolomite breccia to other carbonate occurrences within the continental United States (Michigan and Texas) and to isotope data previously compiled by Murata et al. (1969) from stratigraphic dolomites in Pacific Miocene strata, including the Monterey Formation. He found distinct $\delta^{13}C$ isotopic signatures for Pacific Miocene stratigraphic dolomites and greater dolomitization in the lower Monterey Formation relative to upper members of the Monterey. Isotopic information from Tepusquet Canyon (Roehl, 1981; Martin and Rymerson, 2002), along with dolomite isotopic studies from Jalama Beach (Winter and Knauth, 1992; Eichhubl and Boles, 2000a; Martin and Rymerson, 2002) and

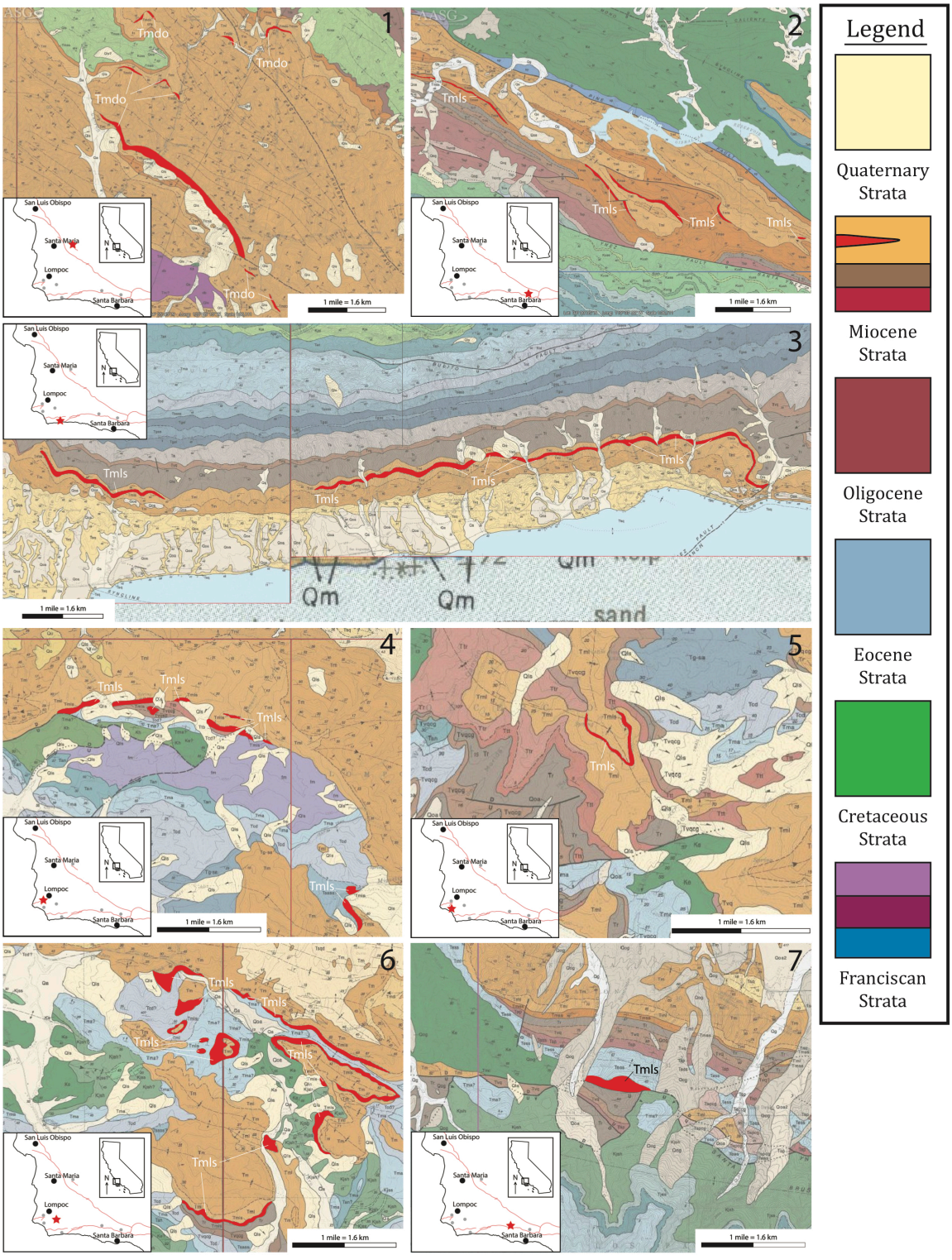

FIGURE 3. Maps of isolated, map-scale carbonate occurrences (highlighted in red) in the Santa Maria and Santa Barbara basins, mapped by Dibblee and Ehrenspeck (1986, 1987, 1988b, 1988c, 1988d) and Dibblee et al. (1994). Each map corresponds to locations denoted by red the red star on inset location figure with numbering scheme in upper right corner consistent with Figure 1.

from stratigraphic dolomites throughout the SMB and SBB (Murata et al., 1969; Pisciotto, 1981; Kushnir and Kastner, 1984; Loyd et al., 2012a), are used as a comparison for $\delta^{13}C$ and $\delta^{18}O$ collected in this study. The studies at Tepusquet Canyon and Jalama Beach are significant because they are evidence of HTD in the SMB.

In 1994, Dibblee et al. mapped the dolomite breccia as a separate map unit within the Monterey Formation on the Tepusquet Canyon quadrangle. The breccia is mapped as a lenticular, discontinuous dolomite breccia along the contact between the lower and upper members of the Monterey Formation (Fig. 3). The largest portion of this body extends just over three kilometers from northwest to southeast, and it is accessible from the Tepusquet and Colson Canyon roads. The outcrop displays rock fabrics such as dilational, floating-clast breccias with massive dolomite cement and saddle dolomite that are consistent with HTD (Davies and Smith, 2006).

Study Area

Seven exposures of isolated carbonate bodies in various locations in the SMB and the northern margin of the SBB (Fig. 1) were evaluated for this project, six of which were visited and described (Appendix A). Location 7 was excluded from the study due to our inability to obtain access to private property. In most cases, each carbonate body is in proximity to, or underlain by, Cretaceous marine strata or the Mesozoic Franciscan Assemblage (Tennyson and Isaacs, 2001).

The six study locations are of different sizes, ranging from approximately 1.5 to 10 kilometers long. Most of the carbonate occurrences are close to or in contact with mapped regional or local faults (Fig. 1), with exception of the “Sudden Canyon Road” occurrence and the “Old Grefco Quarry Road” occurrence (Fig. 3). The Sudden Canyon Road occurrence is

apparently confined to Monterey strata and conforms to local geologic structure. However, this occurrence is near the convergence of two synclines, indicating an association with complex geologic structure. The Old Grefco Quarry Road occurrence has been mapped along an unconformable surface between the Monterey Formation and older Miocene, Eocene, and Cretaceous strata. This location has the most extensive and continuous exposure of the Monterey's atypical dolomite, making it the best candidate for the primary detailed site study.

CHAPTER 2

METHODS

Six locations of carbonate bodies (Fig. 1, locations 1-6) previously mapped on a 1:24,000 scale in the Santa Maria and Santa Barbara Basins (Dibblee and Ehrenspeck, 1988b, 1988c, 1988d; Dibblee et al., 1994) were visited and described (Table 1). Lithology, composition, rock fabric, and stratigraphic location of dolomite occurrences were documented and compared at outcrop and hand-sample scales, and four to fifty hand-samples were collected at each location. Descriptions for locations 1 through 5 (Fig. 1) are in Appendix A. The dolomite breccia at the Grefco Quarry Road location (Fig. 1, location 6; Fig. 3) was chosen to be the focus of this study, which includes detailed petrographic and geochemical analysis. A subset of selected hand-samples from this location represent different stratigraphic and spatial positions within the dolomite breccia. These samples were cut into slabs, polished, and mapped for variation in color and breccia pattern. Mapped hand-sample slabs guided isotope and trace element analyses and thin section location for composition and microfabric analysis.

Thin sections of portions of the slabs, showing the best representation of pattern and color variation across the slabs, were conventionally analyzed with a petrographic microscope in plane- and cross-polarized light. Blue epoxy impregnation highlights porosity and Aliziran Red S and potassium ferricyanide stains identify calcite and iron-rich carbonates, respectively.

Multiple episodes of brecciation were identified both in hand-sample and in thin section. The relative timing of these episodes was determined using the principle of crosscutting relations. Cement from each breccia zone was powdered for X-ray powder diffraction (XRD), $\delta^{18}O$ and $\delta^{13}C$ isotopic, and trace metal analysis.

Mineralogical and geochemical analyses were done on equipment at California State University, Long Beach in the Department of Geological Sciences and the Institute for Integrated Research in Materials, Environments, and Society (IIRMES). XRD analysis was performed on a Rigaku MiniFlex diffractometer equipped with a Cuα tube, using the Reference Intensity Ratio (RIR) technique, as outlined by the International Centre for Diffraction Data (2008). Minerals were identified with X'Pert Highscore Plus.

Oxygen and carbon isotopic analyses were made on a ThermoFinnigan DeltaPlusXP isotope-ratio mass spectrometer (IRMS) with a Finnigan GasBench-II inlet device. Approximately 200-300μg of powdered dolomite was measured into vials, which were purged of atmosphere with ultra-high purity helium (UPH). One hundred percent phosphoric acid was injected into the purged vials, and dolomite was digested for 15 to 18 hours at 90°C to produce CO_2. Data were calibrated using a three-point calibration with International Atomic Energy Agency (IAEA) standards NBS-18 and NBS-19 and one internal standard (STD-A). Reproducibility was determined using carbonate reference material (CRC 200) from Dr. Sean Loyd at California State University, Fullerton. Isotopic compositions and analytical precision are presented in Table 2. Values are reported as per mil (‰) in $\delta^{13}C$ and $\delta^{18}O$ notation relative to Vienna PeeDee Belemnite (VPDB).

Trace metal concentrations were measured with an Agilent 7500ce inductively coupled plasma mass spectrometer (ICP-MS). A known quantity of each sample ranging from 0.03-0.04g was digested over night at 90°C in one milliliter of 50% Optima®-grade nitric acid solution. Samples were calibrated against the SPEX CertiPrep multi-elemental standard (CL-CAL-2) and internal standards of SPEX CertiPrep rhodium (PL-RH3-2Y) and thulium (PLTM2-2Y). Relative

percent differences (RPD) were calculated for each element from two blank spikes and one replicate sample (Table 3).

TABLE 1. Secondary Mapping Scales of Described Carbonate Occurrences

Location 2 – E	Gibraltar Road – East	1:12,930
Location 2 – W	Gibraltar Road – West	1:11,520
Location 3	Hollister Ranch	1:7,680
Location 4	La Salle Canyon Road	1:16,000
Location 5	Sudden Canyon Road	1:11,520
Location 6	Grefco Quarry Road	1:1,516

TABLE 2. Isotopic Values of Standards and Precision Using CSULB Equipment

Standard	Value (‰VPDB)		Standard Deviation	
	$\delta^{13}C$	$\delta^{18}O$	$\delta^{13}C$	$\delta^{18}O$
NBS-18	–5.014	–23.2	0.29	0.83
NBS-19	+1.95	–2.20	0.09	0.05
STD-A	–39.75	–19.15	0.12	0.43
CRC 200*	+1.82	–8.37	0.44	0.85
	+2.91	–6.16		
	+1.97	–8.25		
	+2.12	–8.21		
	+2.14	–7.96		

Note: *Carbonate reference material provided by Dr. Sean Loyd, CSU Fullerton.

TABLE 3. Analytical Precision of Trace Elements

Element Measured	* Blank Spike 1 (µ g/g)	* Blank Spike 2 (µ g/g)	011116-09-01 (µ g/g)	011116-09-01 Replicate (µ g/g)	RPD Blank 1	RPD Blank 2	RPD Duplicate
Be	51.96	51.92	0.19	0.19	3.84	3.76	2.01
B	54.25	54.40	12.04	11.13	8.15	8.43	7.81
Al	49.77	50.95	989.0	973.2	0.45	1.89	1.60
Ti	49.21	49.12	49.13	47.50	1.60	1.78	3.37
V	56.02	55.79	110.83	108.93	11.36	10.94	1.72
Cr	55.77	55.65	17.78	17.49	10.91	10.69	1.63
Mn	56.05	55.75	115.20	115.66	11.40	10.87	0.39
Fe	50.35	50.02	1740.70	1751.03	0.69	0.05	0.59
Co	56.52	56.50	0.31	0.32	12.24	12.25	1.36
Ni	57.18	57.09	4.52	4.54	13.40	13.23	0.42
Cu	57.87	57.83	2.43	2.42	14.60	14.52	0.56
Zn	54.01	54.41	13.70	13.76	7.71	8.45	0.39
As	49.27	49.75	0.25	0.24	1.47	0.49	1.35
Se	50.03	50.20	0.00	0.00	0.07	0.40	NA
Sr	57.50	57.31	180.19	182.50	13.95	13.63	1.27
Mo	57.08	57.43	0.00	0.00	13.22	13.84	NA
Ag	58.11	57.61	0.19	0.19	15.01	14.15	0.04
Cd	55.29	55.06	1.40	1.40	10.04	9.63	0.33
Sn	56.50	56.89	0.16	0.17	12.20	12.89	1.61
Sb	56.93	57.10	0.00	0.00	12.96	13.26	NA
Ba	56.98	56.78	72.96	73.47	13.05	12.70	0.71
Tl	50.18	50.60	0.00	0.00	0.36	1.19	NA
Pb	57.56	57.74	0.66	0.68	14.05	14.37	2.57

Note: * Blank spikes have true value of 50µ g/g.

CHAPTER 3

RESULTS

The Grefco Quarry road outcrop of the San Julian occurrence is the largest of seven map-scale carbonate exposures that were evaluated (Fig. 1, location 6). This location was chosen as the focus of this thesis, and in-depth analyses including outcrop description, hand-sample slab analysis, thin section analysis, and $\delta^{13}C$ and $\delta^{18}O$ isotope analysis were conducted for this site.

Exposure Description Along Grefco Quarry Road Cut

The carbonate occurrence approximately sixteen kilometers southeast of Lompoc (Fig. 1, location 6) occurs primarily along the unconformable contact between the base of the Monterey Formation and Paleogene and Cretaceous strata (Dibblee and Ehrenspeck, 1988b, 1988c) (Fig. 4). The exposures occur discontinuously over an area of approximately eighteen square kilometers and are lenticular bodies ranging from 0.16 to 2.3 kilometers long and 40 to 204 meters wide. This entire unit is thus named the "San Julian Carbonate Breccia" for its location on the Rancho San Julian – one of the original Spanish land grants. Though mapped discontinuously, exposure patterns are consistent with local structure and geomorphology, suggesting this carbonate feature may have formed along a continuous surface that undulates from the base of, to within, the Monterey Formation in this location. However, lithology varies between exposures, despite being mapped as the same unit (Dibblee and Ehrenspeck, 1988b, 1988c), and includes calcareous mudstone, sucrosic dolomite, dolomitic sandstone, dolomitized siliceous rocks (diatomite, porcelanite, and chert), and dolomitic breccia. Most silica in this area is biogenic or a diagenetic derivative of biogenic silica. Veins of quartz cement are observed in one location along the road to the old Grefco Quarry.

A road cut for the out-of-operation Grefco Quarry exposes two intersecting orientations of the dolomitic breccia, allowing for ease of access and near three-dimensional analysis of a location that had not precisely been analyzed in detail.

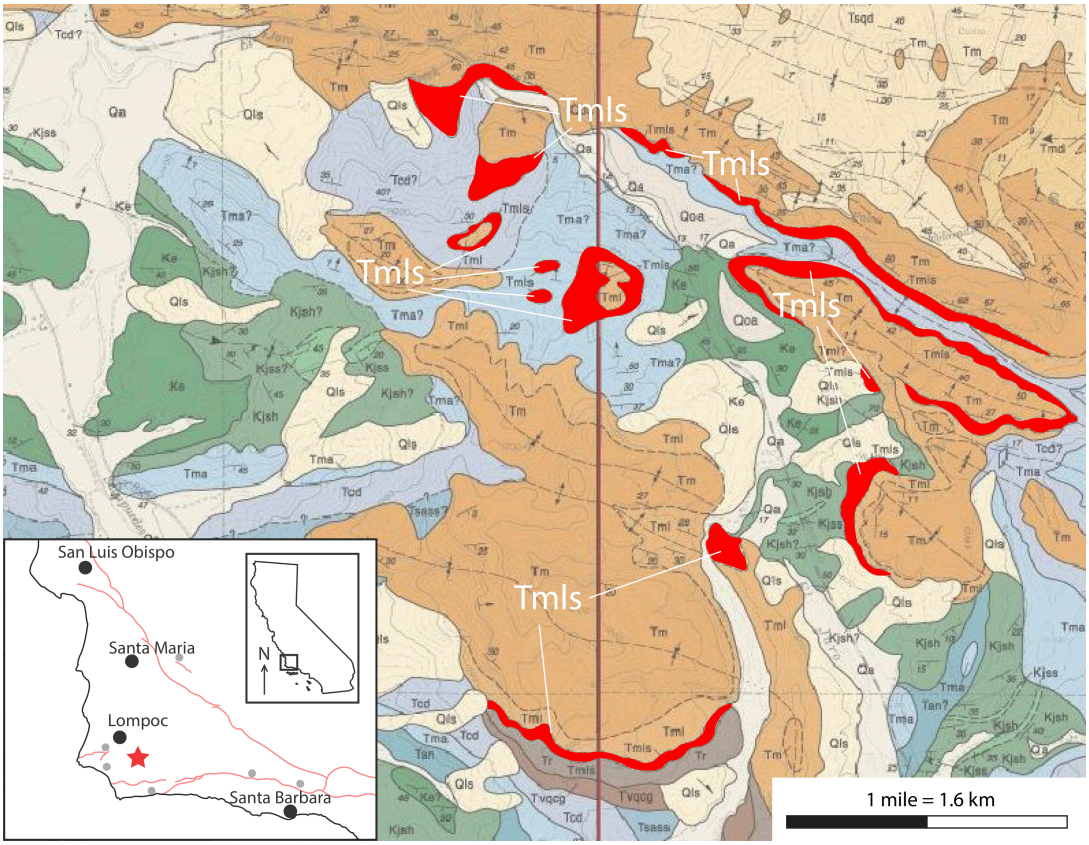

FIGURE 4. Geologic map of carbonate occurrence south of Lompoc, California (after Dibblee and Ehrenspeck, 1988b, 1988c). Carbonate occurrences are highlighted in red, Monterey strata are shades of orange, Paleogene strata are shades of blue, and Cretaceous strata are shades of green.

Two transects were studied along the old Grefco Quarry road on Rancho San Julian (Fig. 5). Transect A-A' has a bearing of 353° and approximately 213 meters of exposed deformed Monterey strata. Transect B-B' is roughly parallel to bedding strike on a bearing of 280° and exposes a massive dolomitic breccia in the cliff face.

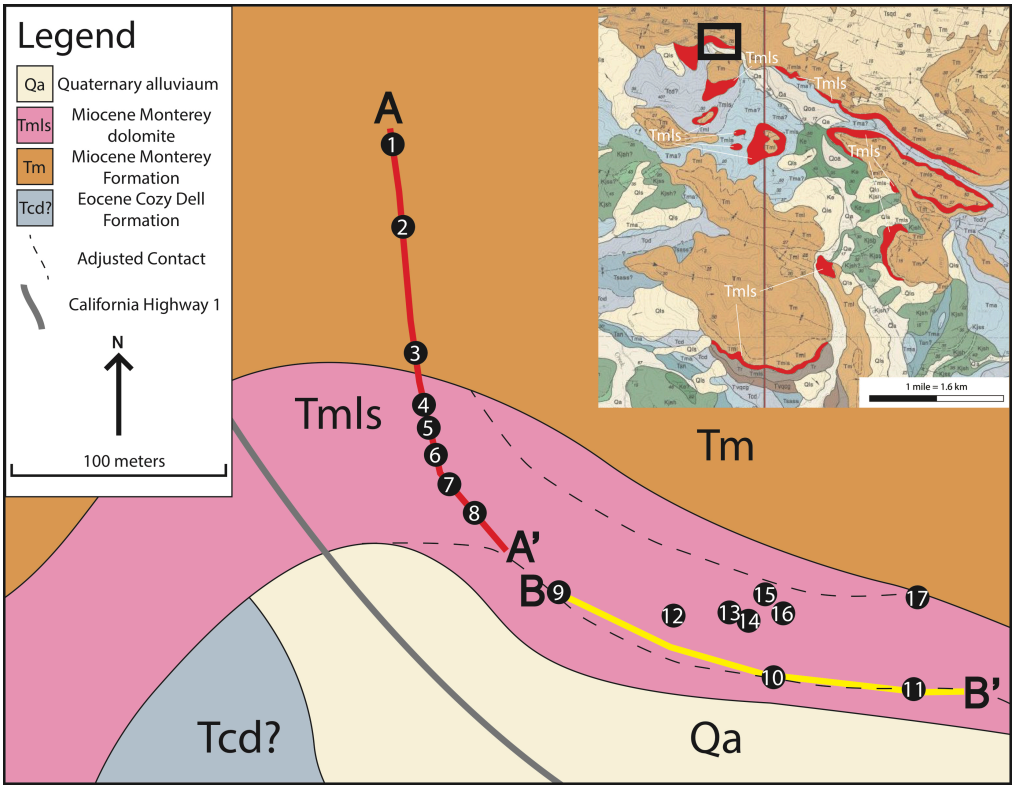

FIGURE 5. Location of transects in study area (after Dibblee and Ehrenspeck, 1988c). Scale on inset map is the same as in Figure 4. Tmls contact is adjusted (dashed lines) to only include carbonate, separating the carbonate from overlying Monterey strata and underlying Tertiary conglomeritic sandstone.

Transect A-A'

Transect A-A' reveals local structure as depicted in the schematic sketches below (Figs. 6-7). Folded muddy diatomite and porcelanite with fractured and highly contorted chert beds are presented from north to south at points 1-8. Pockets of brecciation occur within fold cores, and in some cases, along bedding contacts. The degree of brecciation is variable. Within fold cores, breccias are coarse and very hard. Layer-parallel breccias are less resistant than fold core breccias, but both breccias react with hydrochloric acid.

Figure 8 is a graphical summary of how structure, brecciation, lithology, and mineralogy vary along transect A-A' from north to south. Small-scale folds that are less than a half meter in height are present from points 1 to 6, increasing in concentration from around point 4 to 6. Large

folds (greater than a half meter in height) are present along the whole transect but are more common from point 1 to 5. Small faults (less than 1.5 meters in length) are present throughout the transect with consistent abundance. Large faults that are greater than 1.5 meters are present from point 1 to just beyond 7, where they disappear into the massive dolomite breccia at the southern end of the transect.

Bedding plane breccias are present along the transect leading up to point 8, increasing in occurrence and intensity to the south, disappearing at the dolomite breccia around point 8, as bedding planes are no longer visible within the massive breccia. Fold core breccias also increase in occurrence and intensity from point 1 to 8 and are more common from point 4 to the end of the transect.

Diatomaceous, porcelaneous, and cherty strata are present from point 1 up to halfway between points 7 and 8 where rocks become more or less completely dolomitized. Porcelanite is the dominant rock-type, regularly interbedded with diatomite, and increasing amounts of chert from north to south along the transect. Dolomitization trends parallel fold core breccia trends, increasing in occurrence and intensity from north to south, reaching maximum intensity around point 8. Saddle dolomite was only observed at the southern end of the transect.

At the southern end of the transect, approaching A', the breccia contacts an underlying conglomeritic sandstone – mapped as the Eocene Cozy Dell Formation with a question mark (Dibblee and Ehrenspeck, 1988c), but may alternatively be the Eocene Matilija Formation. Clasts ranging from two to greater than 65 millimeters are composed of red volcanics and green chert (Franciscan-type rocks) and are fractured in place near the contact. The conglomerate exposed at the base of the road cut is highly indurated. A small, more friable exposure of the conglomerate is exposed about three meters up slope.

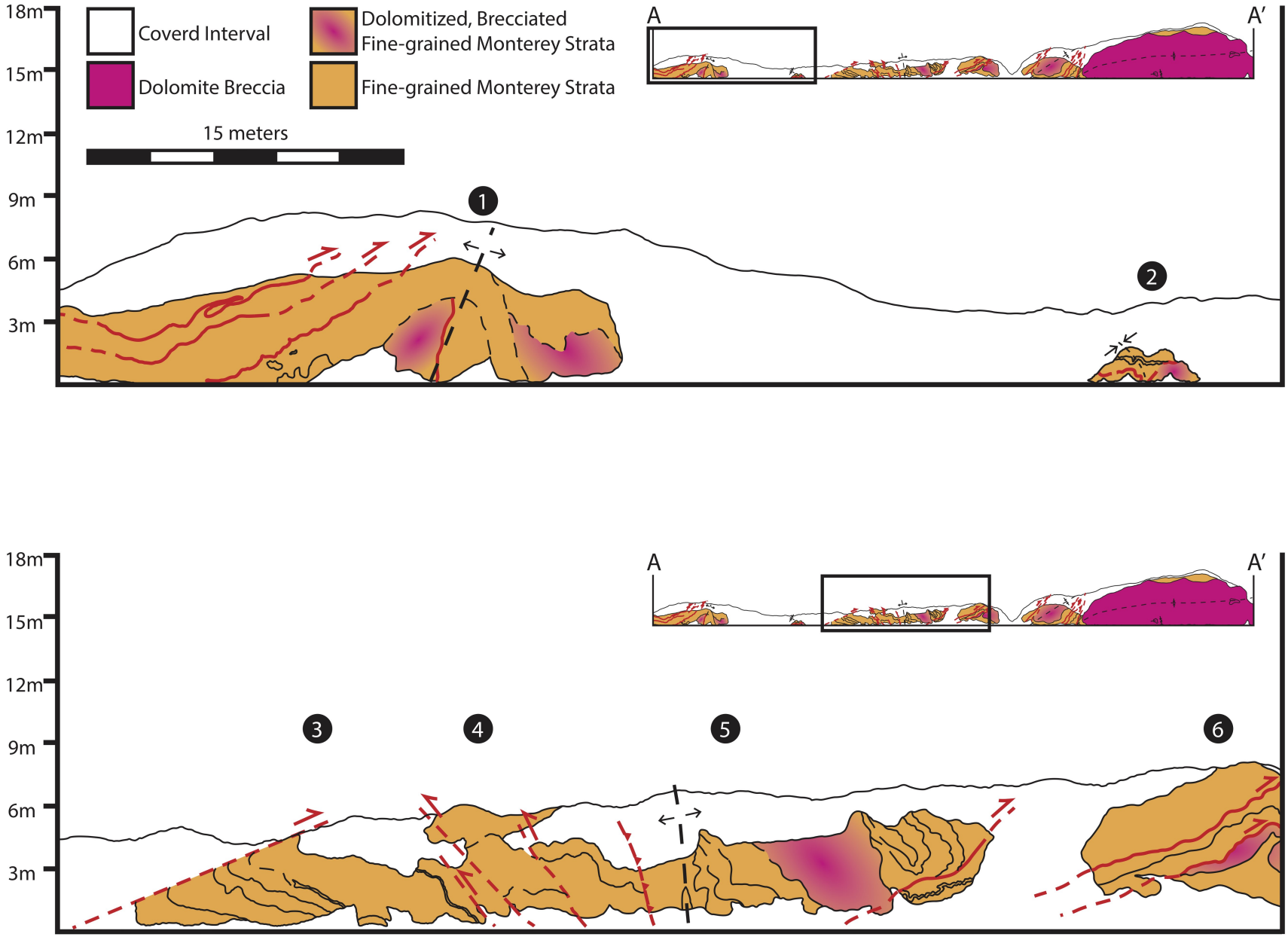
18m
15m
12m
9m
6m
3m
Coverd Interval
Dolomite Breccia
Dolomitized, Brecciated
Fine-grained Monterey Strata
Fine-grained Monterey Strata
15 meters
A
A′
1
2
3
4
5
6

FIGURE 6. Schematic sketch of outcrop characteristics along transect A-A', points 1-6. Orange represents stratified Monterey diatomite, porcelanite, and chert. Pink represents zones of brecciation and dolomitization. Brecciation and dolomitization are confined to fold cores and along bedding planes. Faults are layer-parallel at points 1 and 2 and between points 5 and 6 but crosscut strata at locations 3 and 4.

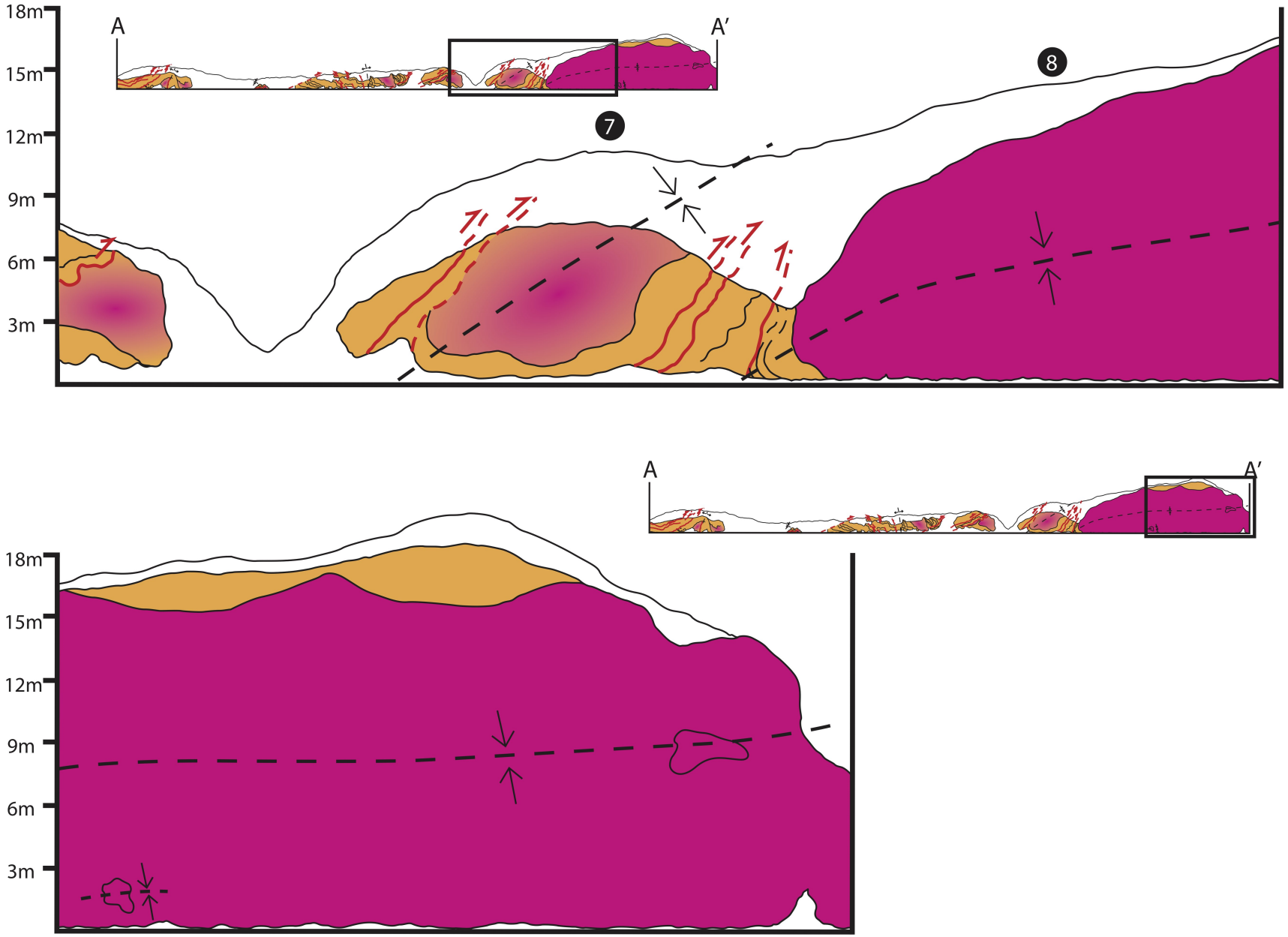
18m
15m
12m
9m
6m
3m
A
A′
7
8
A
A′
18m
15m
12m
9m
6m
3m

FIGURE 7. Continued schematic of outcrop characteristics along transect A-A', points 7-8. Degree of brecciation and dolomitization increase to south-southeast between points 6 and 7. Monterey rocks become completely unstratified and dolomitized where outcrop is colored solid pink, just after point 7 to the end of the transect.

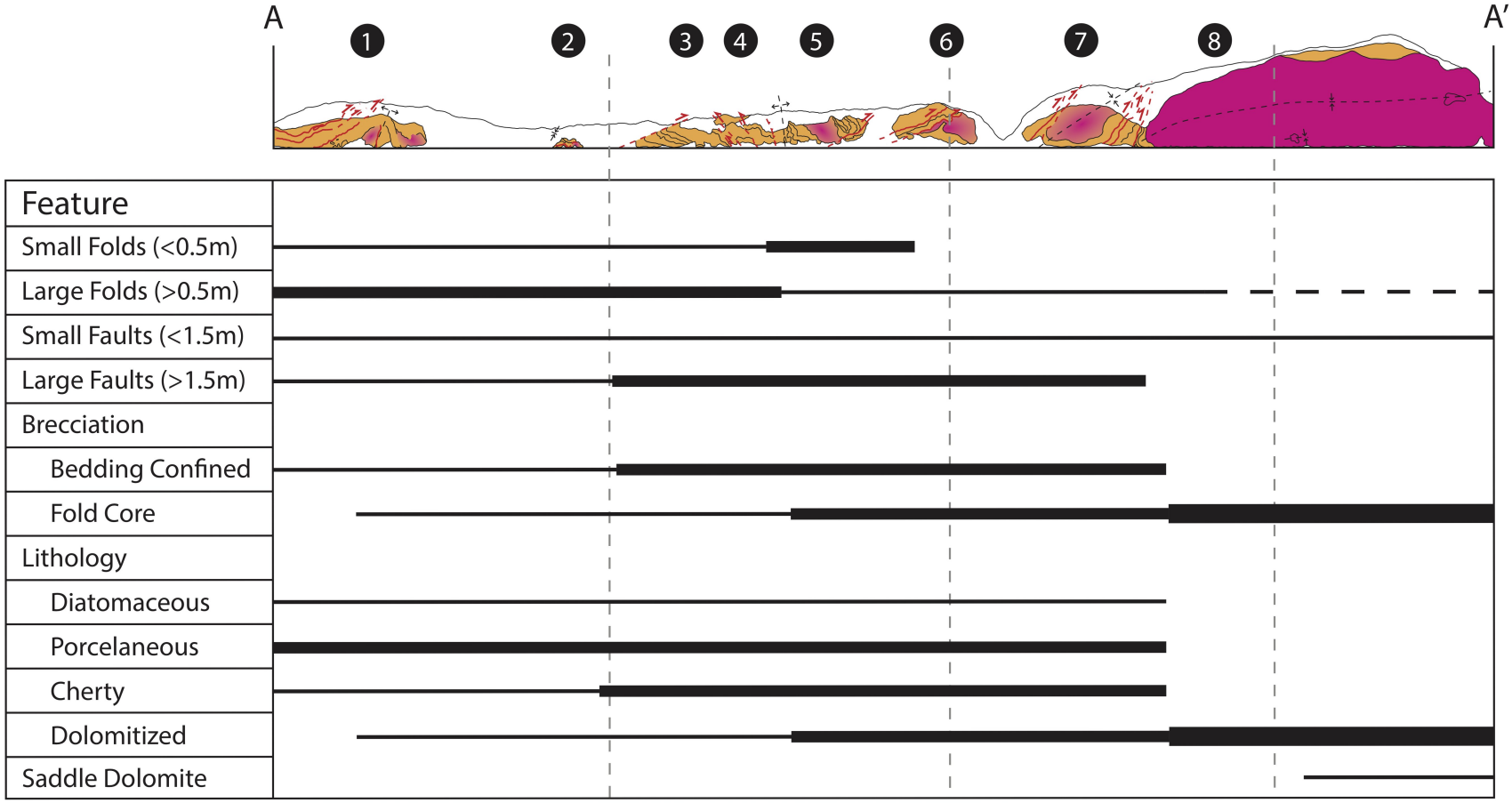

FIGURE 8. Graphic summary of outcrop character trends along transect A-A'. Solid line indicates presence of feature. Feature is believed to exist where line is dashed. Weight of line indicates relative abundance of a feature. Vertical dashed lines indicate sections of transect depicted in Figs. 6-7.

Transect B-B'

Transect B-B' (Fig. 5) exposes the lateral extent of the dolomitic breccia outcrop starting at location 8 (Fig. 7) at the southern end of transect A-A'. The breccia extends for approximately 152 meters from west-northwest to east-southeast (Fig. 9) and predominantly contains clasts of dolomitized Monterey strata and includes clasts from underlying Tertiary conglomeritic sandstone at the basal contact. Dibblee and Ehrenspeck (1988c) originally included the sandstone as a basal unit within the carbonate body, but the (dashed) contact of the carbonate has been adjusted to only include the carbonate within the Tmls map unit (Fig. 5). Nine locations along the transect are described and correlated based on stratigraphic position (Fig. 9). Locations 9-11 are along the basal contact of the unit with underlying Paleogene strata mapped by Dibblee and Ehrenspeck (1988c). Locations 12-16 are within the body of the breccia, and location 17 is at the upper contact of the breccia with stratified Monterey Formation. Lithologic characterization along this transect was done at outcrop and hand-sample scale, and X-ray powder diffraction (XRD) analyses were completed at each location indicated in Figure 9 to determine mineralogy. Results of these analyses are depicted in Figures 10-19. Thin sections of selected parts of hand-samples were analyzed to establish the spatial distribution and fabric of minerals identified by XRD analyses and to determine breccia characteristics on a finer scale.

A resistant, massive, cement-supported breccia is exposed discontinuously along Transect B–B' (Fig. 5). Both clasts and cements are dolomitic, except at location 9 (Fig. 9) where cements and clasts are silicified/quartzose.

Hand-samples collected at locations at locations along Transect B-B' (Fig. 9) were cut into slabs and mapped by cement color and/or breccia fabric variations. Different breccia zones identified in slabs were delineated and included on Figures 10 through 19. The locations of XRD

analyses of cements and clasts are identified in hand-samples indicated by the black, numbered dots on the "mapped" slab images on Figures 10-19. Dolomite and quartz are almost exclusively the only two minerals in these rocks, and dolomite is dominant. Other minerals were identified in breccia clasts derived from both superjacent Monterey Formation and subjacent sandstone, such as fluorapatite (Fig. 15, E) and albite (Fig. 12, C), respectively. These minerals reflect the primary rock composition of the clasts prior to dolomitization. XRD results for all cements and clasts sampled are in Appendix B.

Basal contact. Outcrops at locations 9 through 11 (Fig. 9) expose the basal contact of the dolomite breccia with an underlying sandstone (Fig. 10, 11, and 13, A-B). The contact at these locations is near vertical or dips steeply north-northwest. The sandstone is highly indurated and brecciated as well. Slabbed hand-samples reveal complex brecciation zones on a fine scale (Figs. 10, 11, and 13, C-D; Fig. 12, A-B). XRD results show high abundance of quartz in cements and clasts at location 9 (Fig. 10, E-I), with quartz abundance decreasing to the east at locations 10 and 11 (Plate 11, E; Fig. 12, C; Fig. 13, E). Quartz is most abundant in clasts and cement along the basal contact of the breccia.

Location 9 (Fig. 9) has an excellent exposure of a cement-supported breccia with multiple cementation events (Fig. 10, A-B) separating dolomitic breccia to the north from sandstone to the south. Five cementation zones are mapped on the slab (Fig. 10, C, zones delineated in D). Cements in this zone are composed predominantly of quartz (Fig. 10, E). Clasts in this zone are mainly composed of brecciated, re-cemented quartzose breccia fragments and clasts of stratified Monterey Formation. No sandstone clasts were identified in this breccia. XRD shows these zones exhibit both dolomite and quartz, and quartz percentages are generally high (Fig. 10, E).

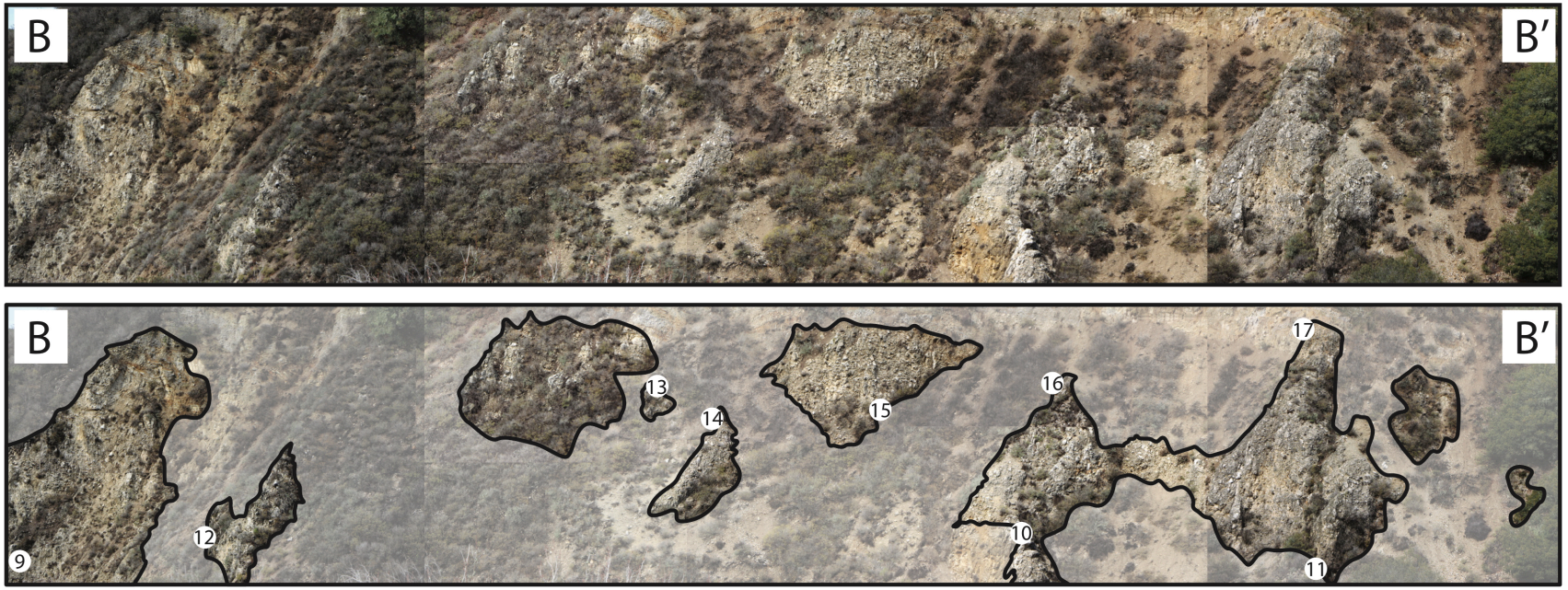

FIGURE 9. Photo of dolomite breccia exposure along Transect B-B' (Fig. 5), facing north. Top image is raw exposure. Bottom image depicts outline of breccia outcrops in cliff face. Numbers correspond to locations where hand-samples were collected for laboratory analyses. Exposure in image is approximately 152 meters long. Transect B-B' does not extend beyond location 10 in this image.

Location 10 (Fig. 9) reveals a brecciated, gradational contact between the dolomite breccia and underlying sandstone (Figs. 11 and 12). The basal contact is a brecciated zone approximately 30 centimeters wide (Fig. 11, B) containing dolomitized clasts of both sandstone and Monterey Formation rocks, such as chert and siliceous mudstone (Fig. 12, A). The dolomite breccia above the contact has a complex fabric (Fig. 11, C), and six cementation zones are delineated in a slabbed sample (Fig. 11, D). The brecciated sandstone also has complex fabrics and multiple cement zones in hand-sample (Figs. 12, A-B). The sandstone is well indurated within approximately 30 centimeters of the contact but becomes more friable with greater distance from the contact. Quartz content in the cements of both the dolomite breccia and the underlying sandstone range from 2% to 47% (Fig. 11, E); however, it is much lower than the concentration of quartz at location 9. High percentages of albite (Fig. 12, C) reflect the feldspar content of sandstone clasts that were likely incorporated into some of the cement.

The contact at location 11 (Fig. 9) was not as clearly exposed as at location 10. However, there is a notable difference in brecciation fabric. Figure 13C, reveals a gray jigsaw breccia with thin lighter-colored cement in the cracks between fragments, cut by a zone with millimeter-scale porosity (delineated in Fig. 13, D). XRD results show the sample is composed entirely of dolomite (Fig. 13, E).

Main body. The main body of the breccia is massive with no discrete zonation evident at the outcrop scale (Figs. 14-17, A-B; Fig. 18, A). Clast size ranges from three to greater than 65 millimeters in diameter and clast composition is dominated by dolomite. Hand-sample slabs (Figs. 14-17, C; Fig. 18, B) reveal complex breccia fabrics similar to those in samples from the basal contact with discrete zones at the hand-sample scale (Figs. 14-17, D). At locations 13 and 15 (Fig. 9), zones of very soft, powdery, porous white rock are visible in the slabs (Figs. 15 and

17, C). These zones are significantly less dense, and very friable and porous compared to any other zones.

XRD indicates that quartz content within the body of the breccia is lower than in the basal contact. Quartz is rarely present in cement within the main body of the breccia and shows no lateral trend. In contrast, approximately 67% of the cements sampled at the basal contact had a quartz component. Fluorapatite is present in a breccia zone with a matrix of white, friable rock with clasts less than one millimeter in diameter (Fig. 15, E4) at location 13 (Fig. 9).

Upper contact. The upper contact of the dolomite breccia with the Monterey Formation (Fig. 9, loc. 17) is poorly exposed and difficult to define, but has been approximated in Figure 19, A. The breccia exposed at this location thins toward the top of the cliff, and the white, friable material identified in the body of the breccia is visible in the hand-sample slab (Fig. 19, B). Cements sampled at this contact are exclusively dolomite (Fig. 19, D).

Thin Sections

Thin sections were analyzed for microfabric and composition of cement and clasts, and to compare with characteristics observed in outcrop and hand-sample. Microfabrics were related to stratigraphic position in order to determine any associated pattern.

Basal Contact

In rocks from the basal contact, microfabrics reveal a complex history of brecciation and cementation. Dolomitized Monterey rocks are fractured into sub-rounded to angular clasts (Fig. 20, A and C) that are supported primarily by dolomite cements (Fig. 20, D and F), and in some cases, distinct episodes of chalcedony and quartz cements fill veins and support clasts (Fig. 20, B). Angular to sub-angular clasts of fine-grained, fossiliferous dolostone are sporadically replaced with coarse-crystalline, rhombohedral dolomite cements (Fig. 20, C-D). Voids left by

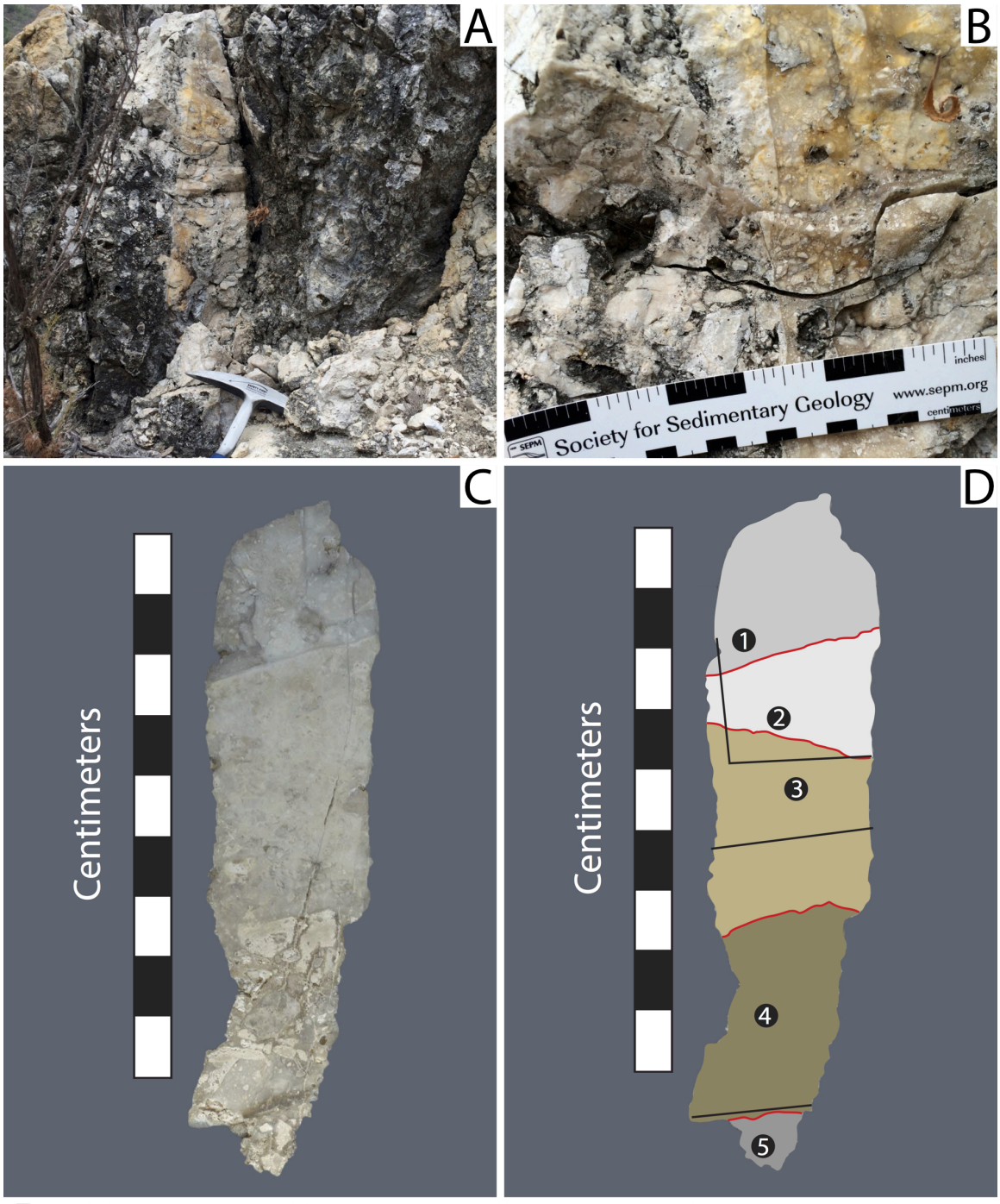
A
B
Society for Sedimentary Geology
www.sepm.org
C
Centimeters
D
Centimeters
1
2
3
4
5
E
93%
7%
67%
33%
72%
28%
75%
25%
59%
41%

FIGURE 10. Outcrop, hand-sample, and mineralogical characteristics of location 9 on transect B-B'. A) Outcrop photo showing a distinctly lighter zone within the predominantly gray outcrop. B) Closer photo of outcrop showing cement-supported breccia clasts of various sizes. C) Slabbed hand-sample showing definite lines within breccia, separating zones of cement with colors ranging from translucent gray to brown to white. Clasts are cement supported and are not larger than one centimeter. D) Mapped slab showing five distinct zones of brecciation and cementation. Numbers in mapped zones correspond to locations sampled for XRD analysis. E) Pie charts showing percent of minerals present within breccia zones mapped in slabs. Blue represents dolomite, and green represents quartz. Numbers in black circles in pie charts correspond to numbers on mapped slab.

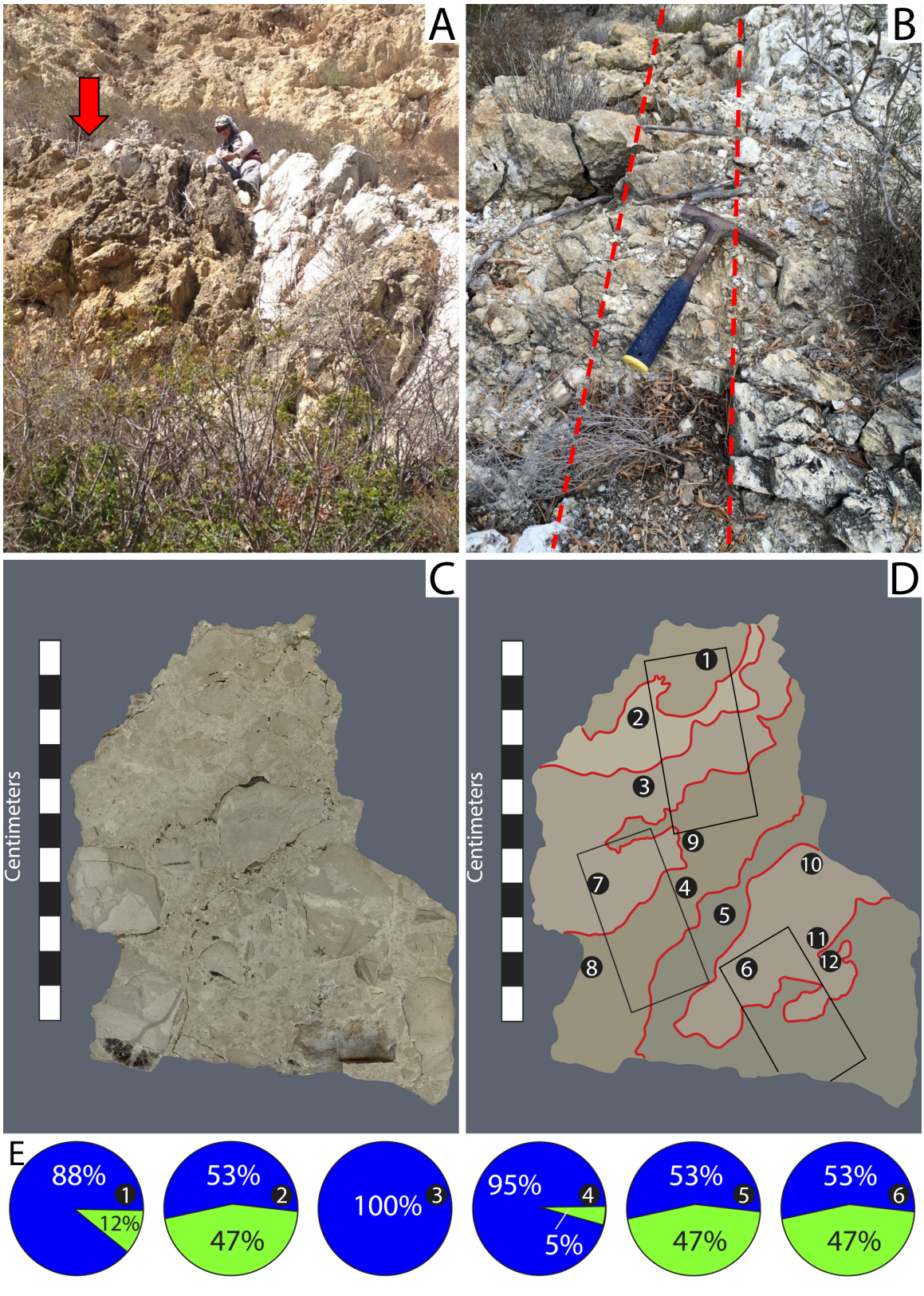
A
B
C
D
E
Centimeters
Centimeters
1
2
3
4
5
6
7
8
9
10
11
12
88%
12%
53%
47%
100%
95%
5%
53%
47%
53%
47%

FIGURE 11. Outcrop, hand-sample, and mineralogical characteristics of dolomite breccia above basal contact at location 10 on transect B-B'. Hand-sample was taken out of breccia above basal contact. A) Outcrop photo showing contact between white dolomite breccia and brown conglomeritic sandstone (geologist for scale). The contact is exposed on a large slip surface (white rock face). Red arrow indicates location of photo displayed in B. B) Photo basal contact of dolomite breccia. Red dashed lines indicate a breccia zone that is roughly twenty-five-centimeter wide and contains clasts of both dolomite breccia (Tmls) and sandstone. C) Slabbed hand-sample showing clasts of Monterey rocks. Clasts range in size from <1 centimeter to ~2.5 centimeters. Clasts are cement-supported. D) Mapped slab showing six distinct zones of brecciation and cementation. Numbers in mapped zones correspond to locations sampled for XRD analysis. E) Pie charts showing percent of minerals present within breccia zones mapped in slabs. Blue represents dolomite and green represents quartz. Numbers in black circles in pie charts correspond to numbers on mapped slab.

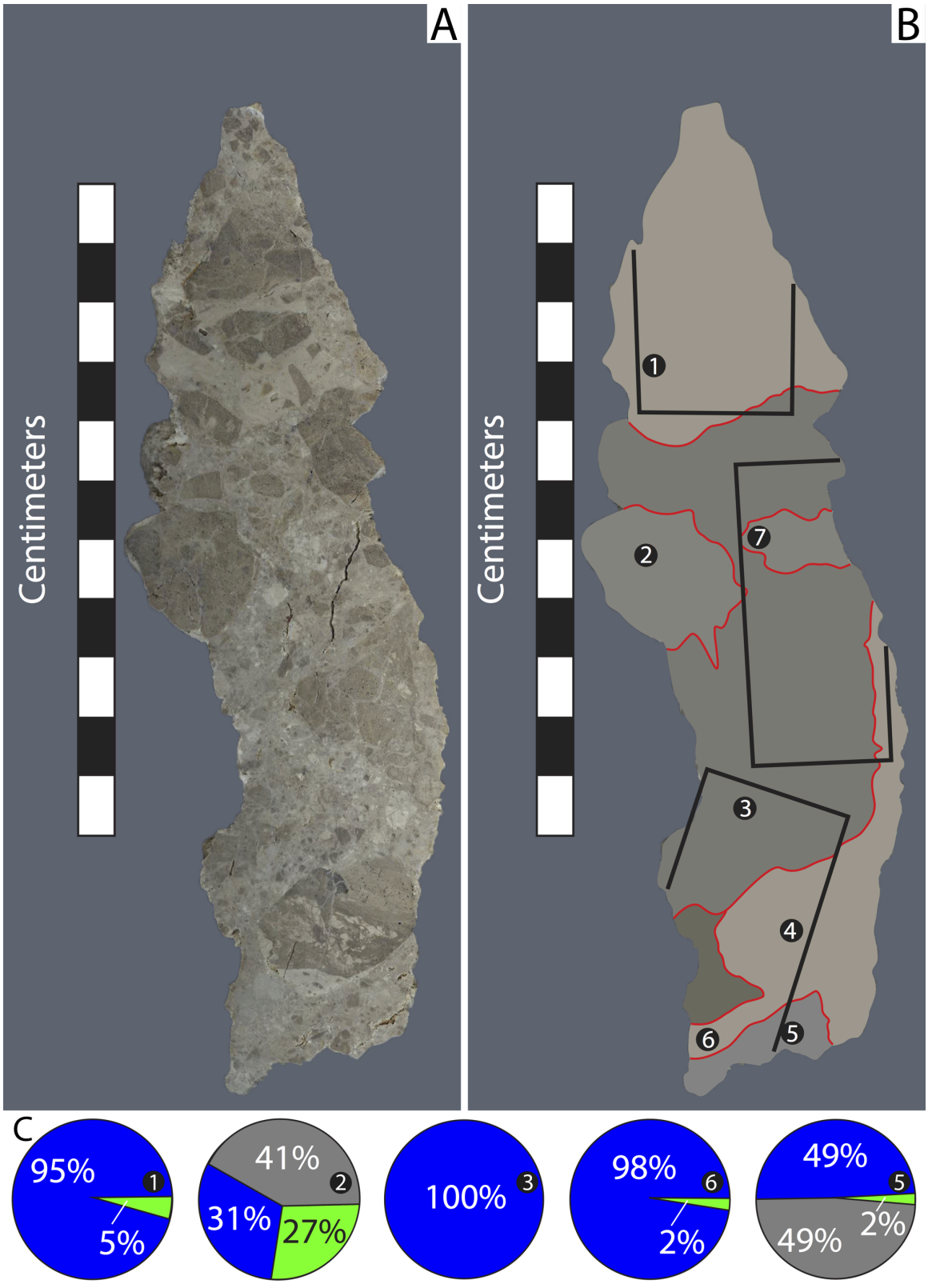
A
Centimeters
B
Centimeters
1
2
7
3
4
6
5
C
95%
1
5%
41%
2
31%
27%
100%
3
98%
6
2%
49%
5
49%
2%

FIGURE 12. Hand-sample and mineralogical characteristics of brecciated zone in basal contact at location 10 on transect B-B'. Hand-sample was taken from breccia zone containing clasts of Monterey strata and underlying sandstone identified within red dashed lines on Plate 2A. A) Slabbed hand-sample showing clasts of Monterey rocks and sandstone in gray to brown-gray cement. Clasts range in size from <1 centimeter to ~2.5 centimeters and are cement-supported. B) Mapped slab showing six distinct zones of brecciation and cementation. Numbers in mapped zones correspond to locations sampled for XRD analysis. C) Pie charts showing percent of minerals present within breccia zones mapped in slabs. Blue represents dolomite, green represents quartz, and gray represents albite. Numbers in black circles in pie charts correspond to numbers on mapped slab.

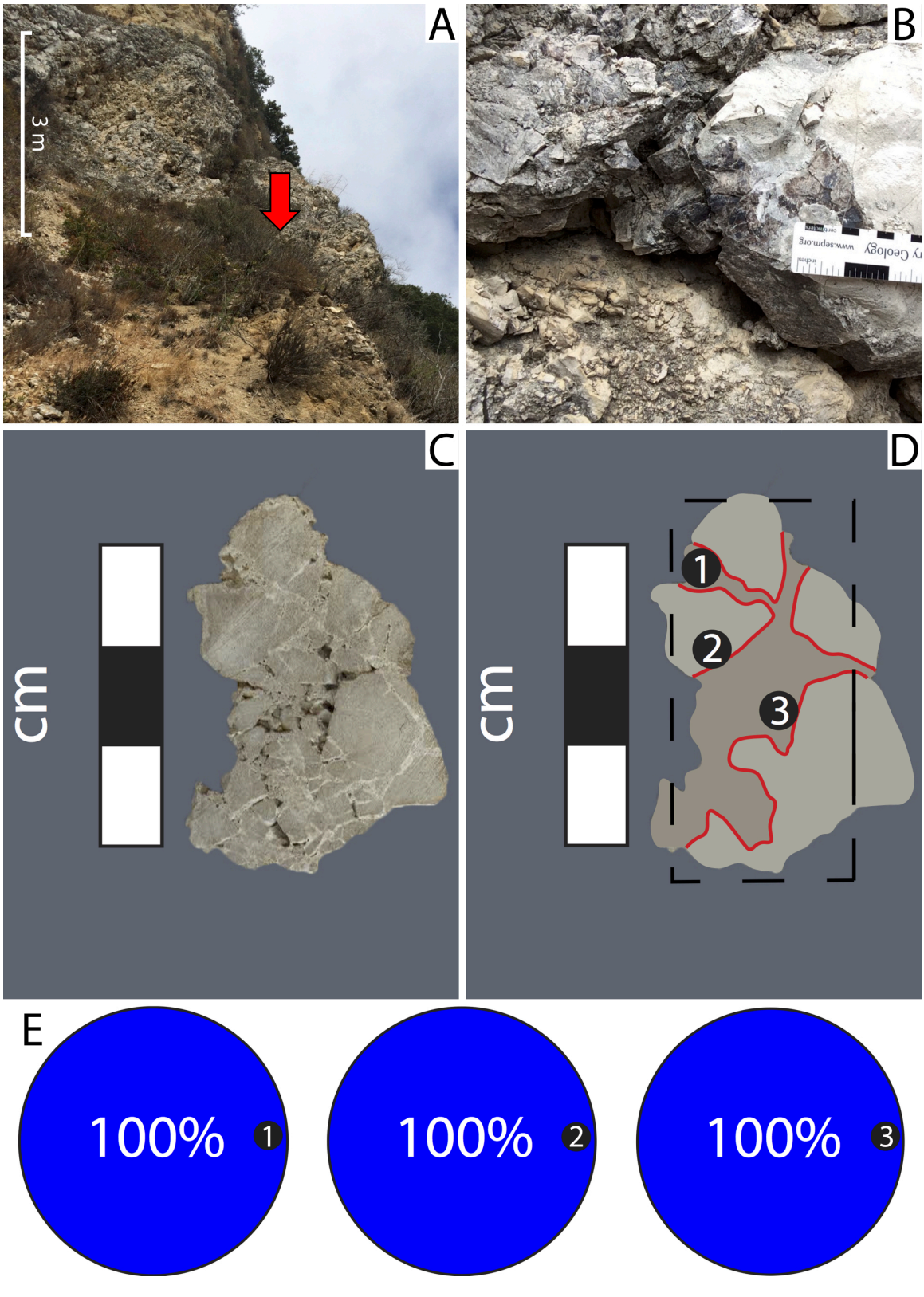
A
3 m
B
C
cm
D
cm
1
2
3
E
100%
1
100%
2
100%
3

FIGURE 13. Outcrop, hand-sample, and mineralogical characteristics of location 11 on transect B-B'. A) Outcrop photo showing the resistant outcrop of the dolomite breccia in contact with the less resistant underlying sandstone. Red arrow indicates location of contact. B) Closer photo of outcrop showing dolomitized clasts of chert (brown) and other Monterey strata (white) within the dolomite breccia. C) Slabbed hand-sample showing jigsaw breccia with lighter colored fracture-healing cement. A zone with millimeter-scale porosity cuts through center of sample. D) Mapped slab highlighting zone of millimeter-scale porosity (darker zone that divides lighter shaded areas). Numbers in mapped zones correspond to locations sampled for XRD analysis. E) Pie charts showing percent of minerals present within breccia zones mapped in slabs. Blue represents dolomite. Numbers in black circles in pie charts correspond to numbers on mapped slab.

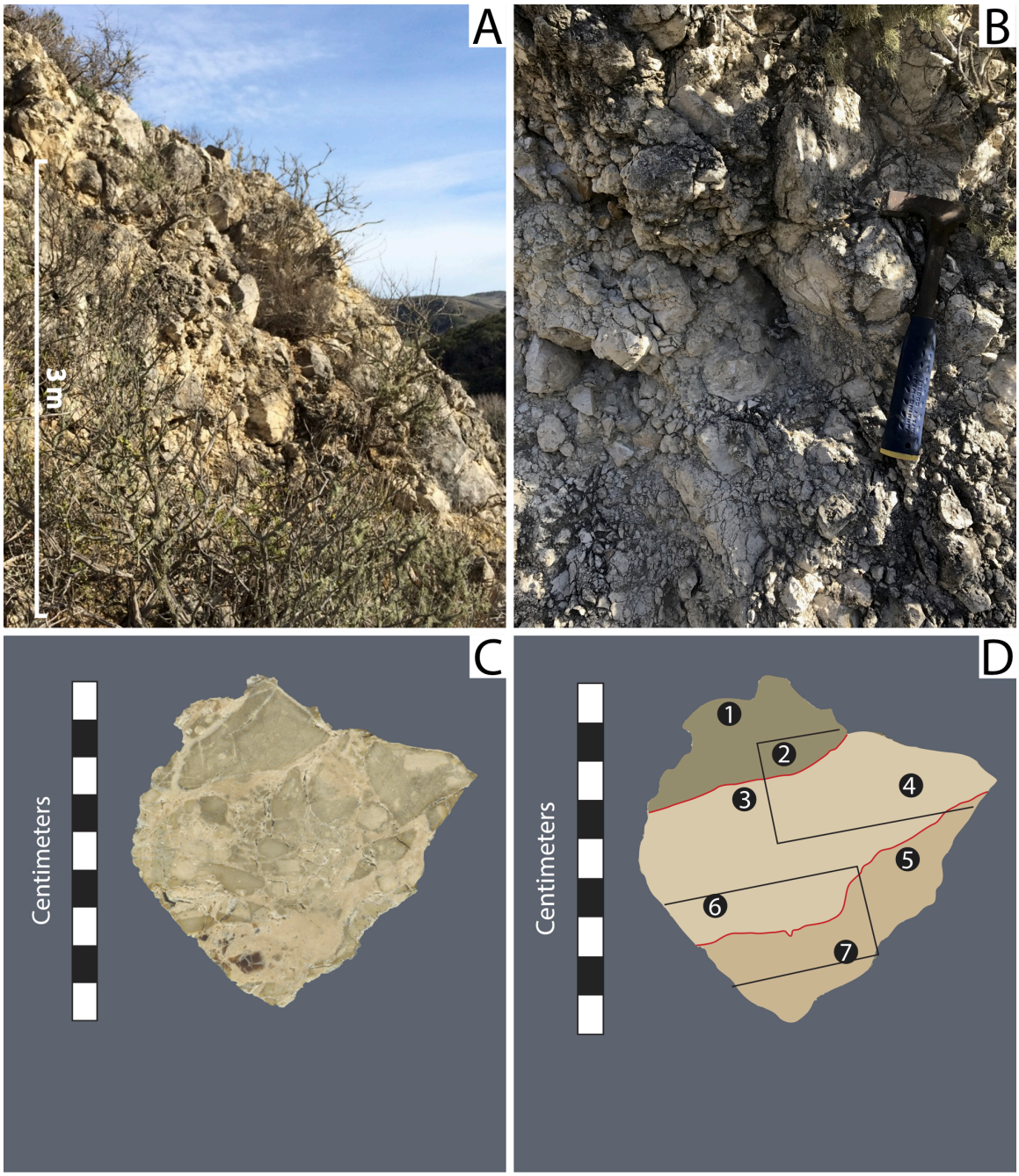
A
3m
B
C
Centimeters
D
Centimeters
1
2
3
4
5
6
7
E
69%
1
31%
100%
3
54%
6
46%
100%
7

FIGURE 14. Outcrop, hand-sample, and mineralogical characteristics of location 12 on transect B-B'. A) Outcrop photo showing large clasts (~0.5-meter diameter) are also present in breccia. B) Closer photo of breccia that exhibits wide range of clast sizes. C) Slabbed hand-sample showing brown clasts supported by buff and buff-pink cements. D) Mapped slab showing three distinct zones of brecciation and cementation. Numbers in mapped zones correspond to locations sampled for XRD analysis. E) Pie charts showing percent of minerals present within breccia zones mapped in slabs. Blue represents dolomite, and green represents quartz. Numbers in black circles in pie charts correspond to numbers on mapped slab.

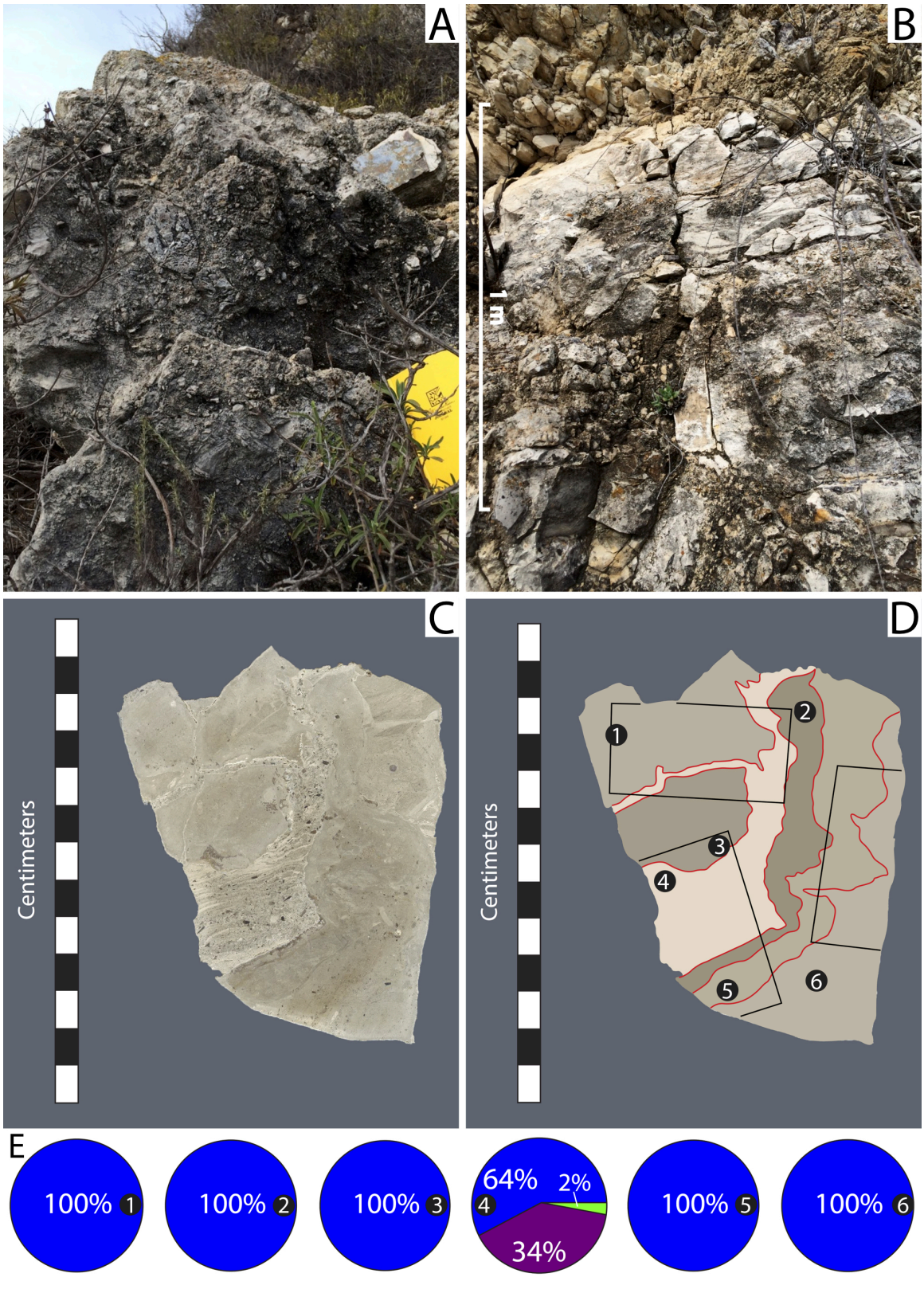
A
B
1 m
C
Centimeters
D
Centimeters
1
2
3
4
5
6
E
100% 1
100% 2
100% 3
64%
2%
4
34%
100% 5
100% 6

FIGURE 15. Outcrop, hand-sample, and mineralogical characteristics of location 13 on transect B-B'. A) Outcrop photo showing resistant breccia with differential weathering of cement, creating clast protrusions. B) Photo of breccia outcrop with slickensides on exposed slip surface. C) Slabbed hand-sample highlighting fractured Monterey strata with a through-cutting, highly brecciated zone with white cement. D) Mapped slab showing six distinct zones defined by color variation. Numbers in mapped zones correspond to locations sampled for XRD analysis. E) Pie charts showing percent of minerals present within breccia zones mapped in slabs. Blue represents dolomite, green represents quartz, and purple represents fluorapatite. Numbers in black circles in pie charts correspond to numbers on mapped slab.

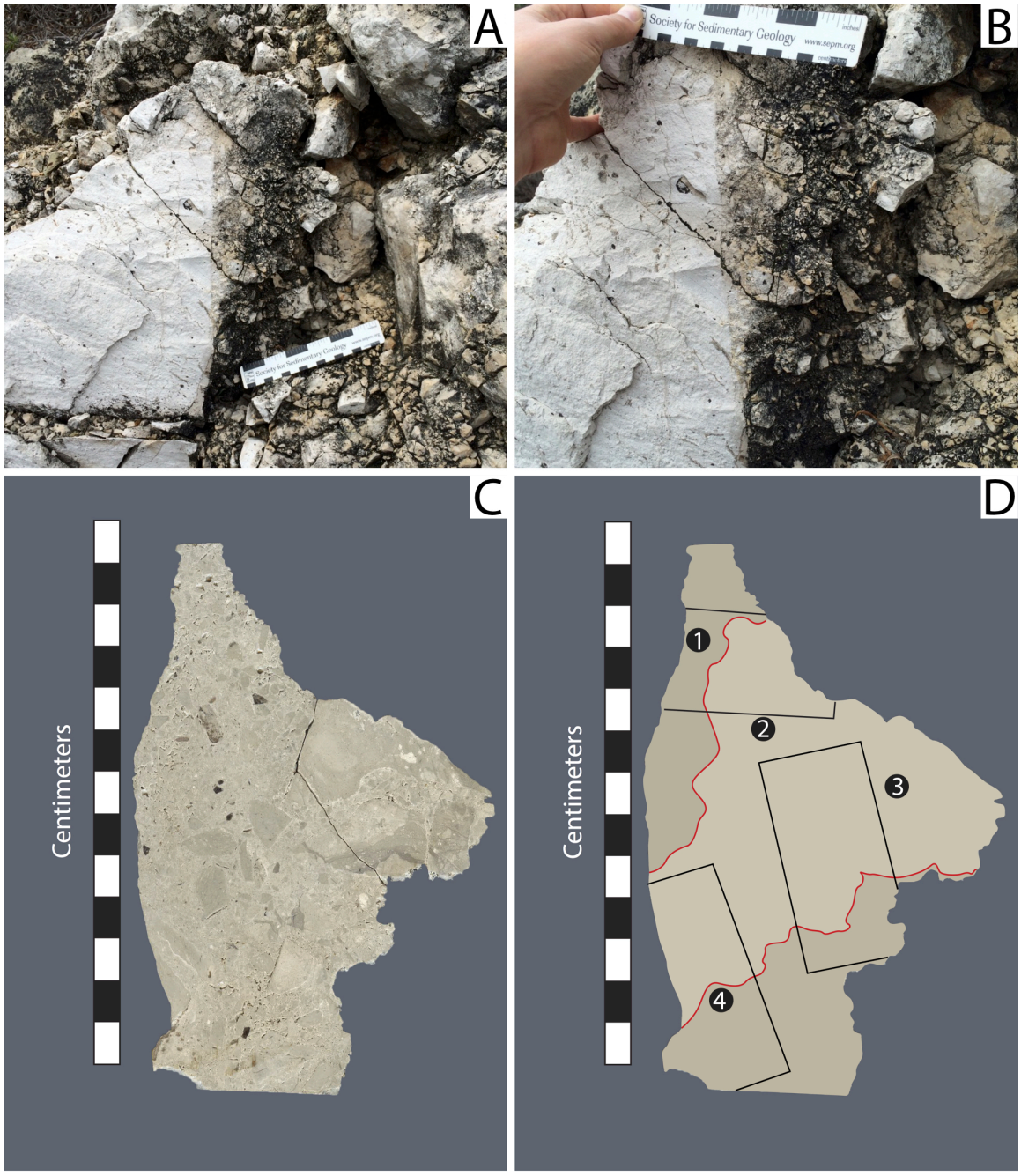
A
B
Society for Sedimentary Geology
www.sepm.org
C
Centimeters
D
Centimeters
1
2
3
4
E
92%
8%
1
96%
4%
2
100%
3
93%
7%
4

FIGURE 16. Outcrop, hand-sample, and mineralogical characteristics of location 14 on transect B-B'. A) Outcrop photo showing fractured Monterey strata with breccias lining fractures and separating fracture blocks exceeding 30 centimeters in size. B) Photo of fracture-lining breccia with clast size ranging from several millimeters to approximately three centimeters. C) Slabbed hand-sample showing breccia zone with clast size exceeding one centimeter cutting breccia zone comprised of millimeter-sized clasts with millimeter-scale porosity. D) Mapped slab showing two distinct breccia zones. The central lighter-colored zone divides a single zone of millimeter-scale breccia. Numbers in mapped zones correspond to locations sampled for XRD analysis. E) Pie charts showing percent of minerals present within breccia zones mapped in slabs. Blue represents dolomite, and green represents quartz. Numbers in black circles in pie charts correspond to numbers on mapped slab.

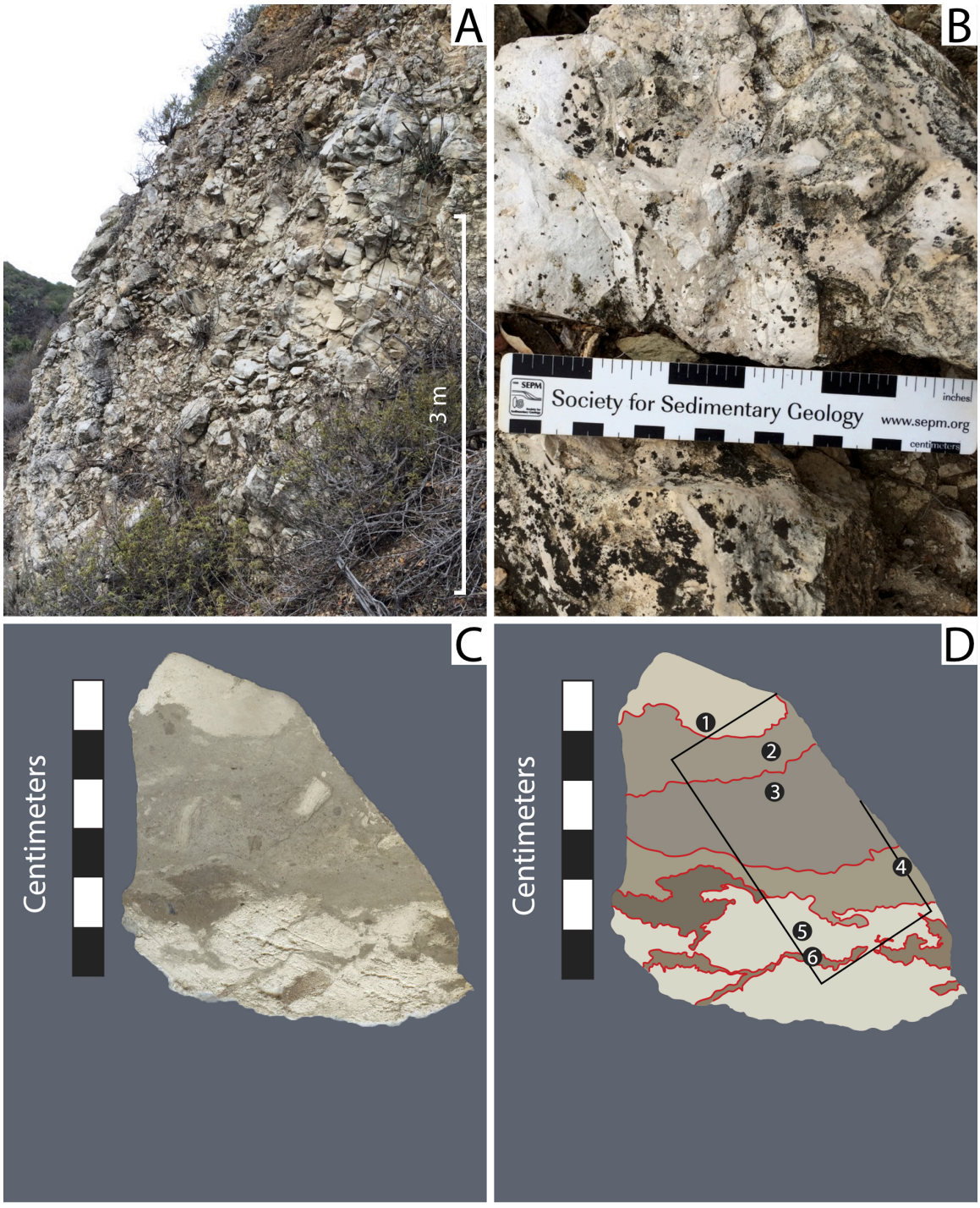
A
3 m
B
Society for Sedimentary Geology
www.sepm.org
C
Centimeters
D
Centimeters
1
2
3
4
5
6
E
100% 1
100% 2
100% 3
4 100%
100% 5
56%
6
44%

FIGURE 17. Outcrop, hand-sample, and mineralogical characteristics of location 15 on transect B-B'. A) Photo of dolomite breccia outcrop. B) Outcrop photo of white millimeter-scale to centimeter-scale clasts supported by brown cement. C) Slabbed hand-sample showing sinuous breccia fabric with some blocky clasts. Clast size does not exceed one centimeter. D) Mapped slab showing six breccia zones. Numbers in mapped zones correspond to locations sampled for XRD analysis. E) Pie charts showing percent of minerals present within breccia zones mapped in slabs. Blue represents dolomite, and green represents quartz. Numbers in black circles in pie charts correspond to numbers on mapped slab.

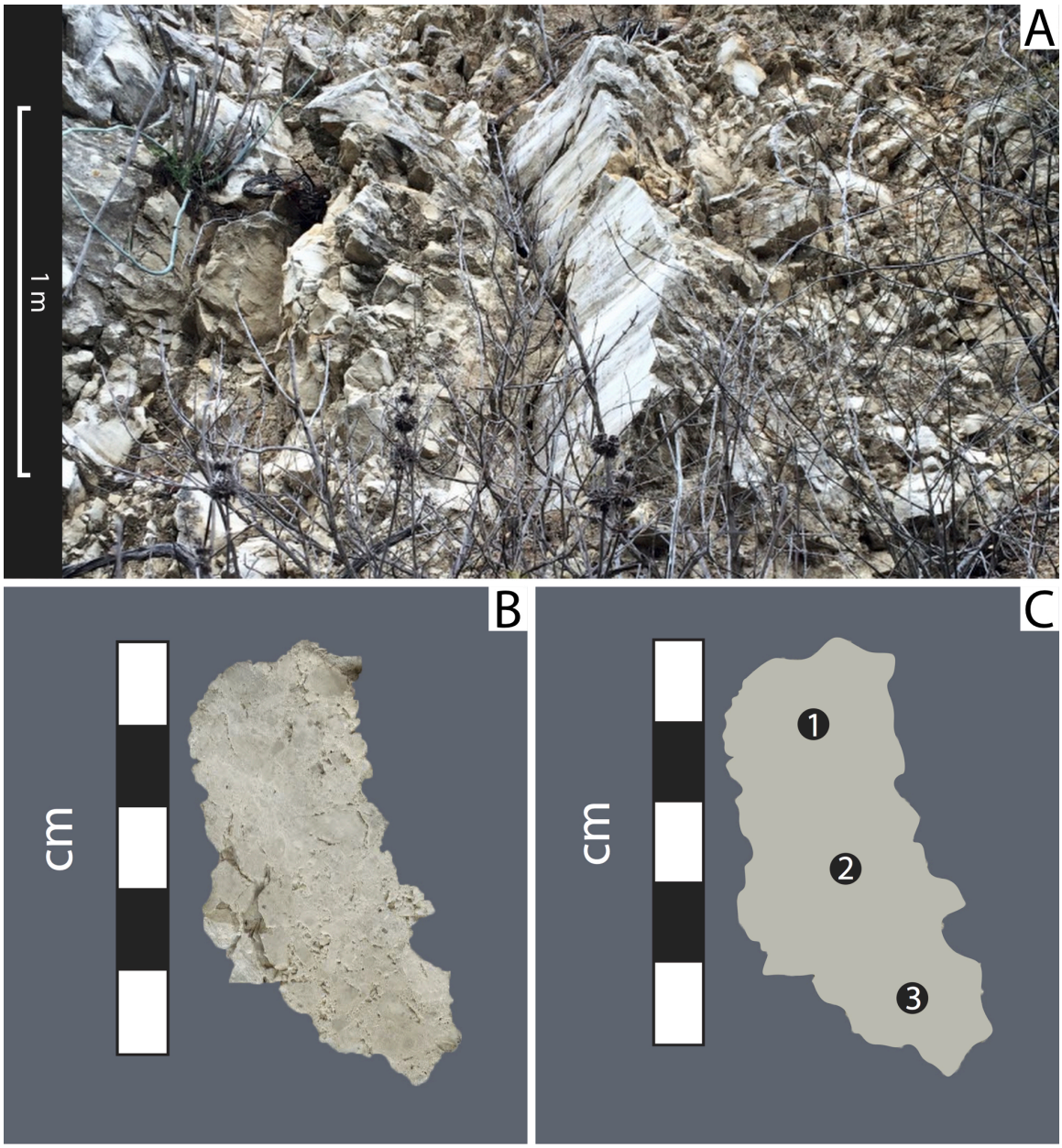
A
1 m
B
cm
C
cm
1
2
3
D
96%
1
4%
95%
2
5%
100%
3

FIGURE 18. Outcrop, hand-sample, and mineralogical characteristics of location 16 on transect B-B'. A) Photo of dolomite breccia outcrop with exposed slip surface with slickensides. B) Slabbed hand-sample showing fractured jigsaw breccia with millimeter-scale porosity between clasts. C) This sample did not display discrete breccia zones. Numbers in mapped zones correspond to locations sampled for XRD analysis. D) Pie charts showing percent of minerals present within breccia zones mapped in slabs. Blue represents dolomite, and green represents quartz. Numbers in black circles in pie charts correspond to numbers on mapped slab.

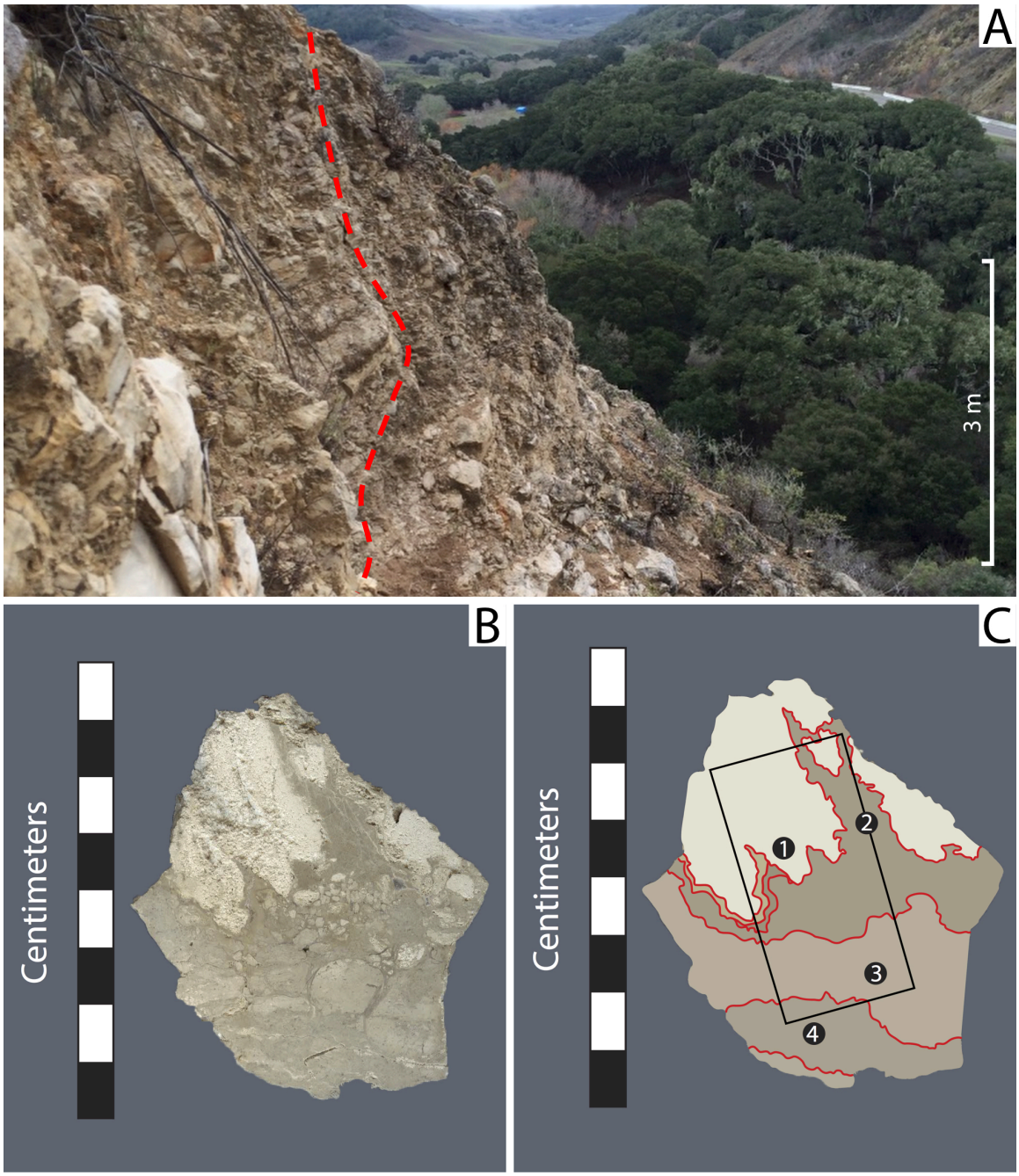
A
3 m
B
Centimeters
C
Centimeters
1
2
3
4
D
100%
1
100%
2
100%
3
100%
4

FIGURE 19. Outcrop, hand-sample, and mineralogical characteristics of location 17 on transect B-B'. A) Photo of upper contact between dolomite breccia and Monterey Formation, facing east-southeast. Red dashed line is interpreted contact location. B) Slabbed hand-sample showing two directions of aligned breccia fabric. White friable material is aligned from top left of sample diagonally down to the right. This trend is truncated by a nearly horizontal breccia zone with blocky clasts. Clast size does not exceed one centimeter. C) Mapped slab showing seven cementation zones. Aligned rock fabric is more apparent with mapped zones. Numbers in mapped zones correspond to locations sampled for XRD analysis. D) Pie charts showing percent of minerals present within breccia zones mapped in slabs. Blue represents dolomite, and green represents quartz. Numbers in black circles in pie charts correspond to numbers on mapped slab.

the dissolution of coarse dolomite rhombohedra are locally filled with chalcedony and/or quartz cements (Fig. 20, C-D). Dolomite cement with rhombohedra with relatively low birefringence and dark rhombohedral cores (Fig. 20, E-F) is the most common fabric. This fabric is cut by dolomite cement with larger rhombohedra that have a higher birefringence. This latter generation of dolomite veins are extensively replaced by microcrystalline quartz (Fig. 20, E-F).

Main Body

The main body of the breccia exhibits microfabrics similar to the basal contact. Figure 21 A and B show dolomite rhombohedra with cloudy cores and low birefringence in cross-polarized light. Replacive quartz locally preserves and includes the dark material at the dolomite crystal centers. Bands of micritic dolomite crystals create boundaries between episodes of dolomite cementation (Fig. 21, A-B).

Thin sections of the white friable zones identified in slabs (Fig. 17, C) reveal a fabric where dissolution of the cores of dolomite crystals created high intracrystaline porosity while preserving crystal boundaries (Fig. 21, C-D). Cement fabrics are increasingly complex in Figures 21 E-F, with angular fractured shards of first generation cement with darker, interstitial material. Clasts are difficult to discern, however, a triangular clast is evident in the top center of Figures 21 E-F. This shape is consistent with the sub-angular to sub-rounded average clast shape seen at hand-sample scale throughout the breccia.

Upper Contact

Cement microfabrics in the upper contact are equally complex as fabrics seen throughout the breccia, yet they vary somewhat in texture. Figures 22 A-B exhibit two directions of aligned fabric. The first is a zone of dolomite cement supporting sub-rounded clasts that are aligned from the bottom right corner of the figure diagonally up toward the top left of the figure. This zone,

however, is truncated in the middle of the figure by a dolomite cement zone that is oriented diagonally from the bottom left to the top right of the figure and paralleled by two additional dolomite cement zones distinguished by crystal size (Figs. 22, A-B). Within the dolomite in the cross-cutting zone, what were once large pore spaces created by the dissolution of dolomite crystals have been filled with coarse-crystalline dolomite and chalcedony cement. Figures 22 C-D show sub-angular clasts of fossiliferous, dolomitized Monterey rocks with fine-crystalline dolomite oriented radially into coarse-crystalline dolomite cement and void-filling chalcedony and quartz cement. Coarse-crystalline dolomite cement is also seen lining and filling fractures in dolomitized Monterey clasts (Figs. 22, E-F).

$\delta^{13}C$ and $\delta^{18}O$ Isotopes

The isotopic composition of dolomite ($\delta^{13}C$ and $\delta^{18}O$) was measured in order to gain insight to the environment of formation of the dolomite breccia exposed along the old Grefco Quarry Road. A subset of the samples used for XRD analysis were chosen to represent the exposure along the B-B' transect (Fig. 5) laterally and stratigraphically (i.e. samples adjacent to upper and lower contacts and within the body of the breccia). These isotopic data are compared to $\delta^{13}C$ and $\delta^{18}O$ isotopic compositions of "stratigraphic" dolomite collected from authigenic dolomite concretions within the Monterey Formation. These concretions are from Sweeney Road in Lompoc and Lion's Head on the northern end of the Vandenberg Air Force Base near Lompoc. Respectively, they are from the Upper (Tm) and Lower (Tml) members of the Monterey Formation as classified by Dibblee (1988a, 1988b). Details of $\delta^{13}C$ and $\delta^{18}O$ values for these samples are listed in Table 4.

Thirty-five of thirty-six samples analyzed from the dolomite breccia had $\delta^{13}C$ values between –8.7 and –14.3 ‰ with $\delta^{18}O$ values between –1.7 and +2.2 ‰ (Fig. 23). One outlier

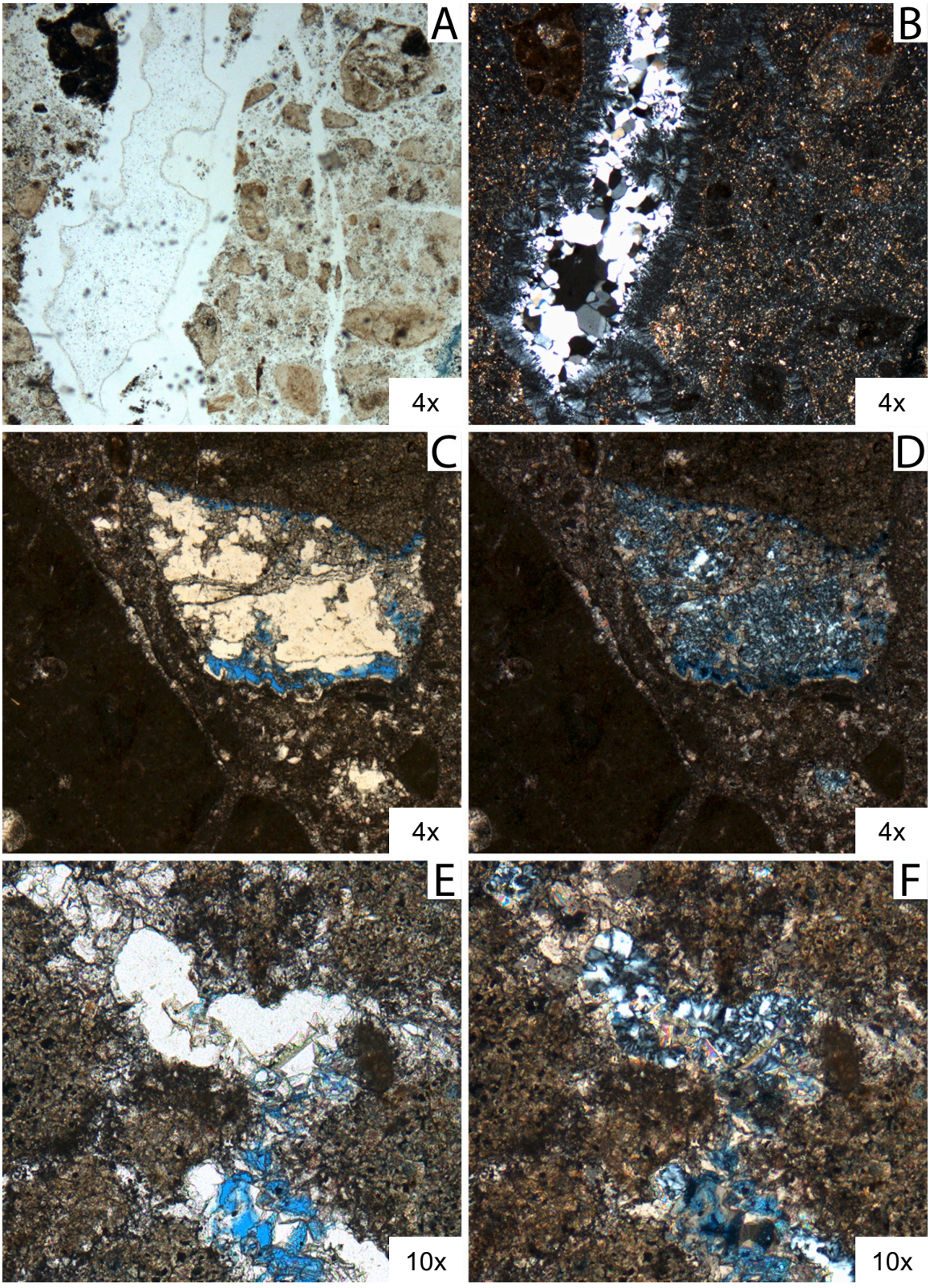
A
4x
B
4x
C
4x
D
4x
E
10x
F
10x

FIGURE 20. Microfabrics of dolomite breccia at basal contact. Figures on left side are in plane-polarized light, and figures on right are the same images in cross-polarized light. A) Subrounded clasts of fine-grained Monterey strata with cemented fracture dominating the left side of the image. Field of view is 3 mm. B) Cross-polars show micritic dolomite cement pervasively replaced with chalcedony. Chalcedony cement lines edges of large fracture at left. The rest of the fracture is filled by polycrystalline quartz cement. Field of view is 3 mm. C) Large sub-angular clast in predominantly fine-crystalline cement. Porosity developed around the rim of the clast with dissolution of centers of dolomite rhombohedra. Field of view is 3 mm. D) Cross-polarized light reveals the sub-angular clast is composed predominantly of microcrystalline quartz cement with sinuous remnants of dolomite cement. Field of view is 3 mm. E) Dolomite cement with visible interlocking rhombohedra with dark cores. Dolomite cement is cut in the center of the image by clear cement zone with intercrystaline porosity. Field of view is 1 mm. F) Central cement zone is composed of coarser-crystalline dolomite cement (visible at top of image) that has mostly dissolved. Microcrystalline quartz fills voids left by dissolution of dolomite. Field of view is 1 mm.

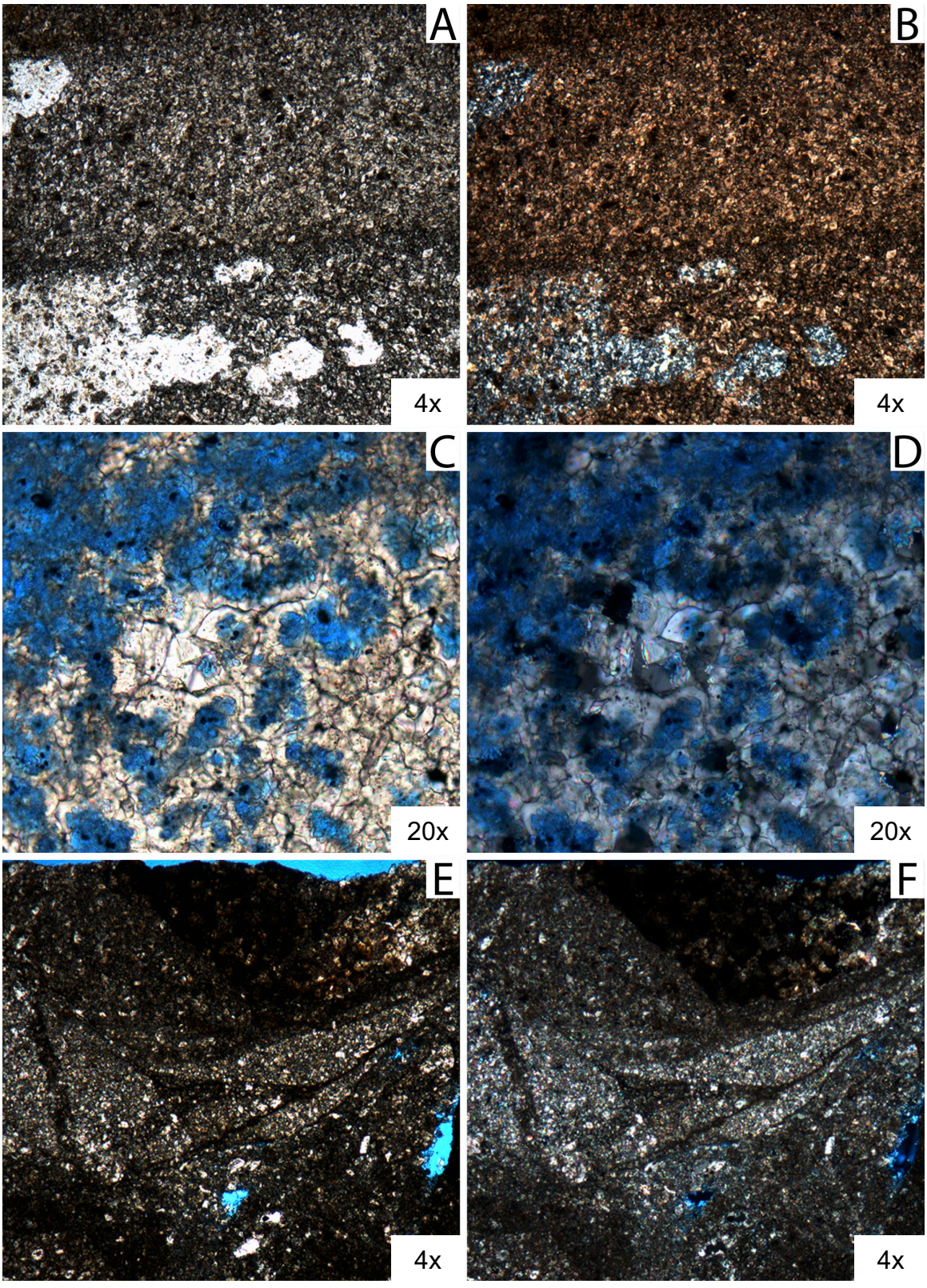
A
4x
B
4x
C
20x
D
20x
E
4x
F
4x

FIGURE 21. Microfabrics within the main body of dolomite breccia. A) Multiple zones of rhombohedral dolomite cement defined by thin lateral line of very fine-crystalline dolomite cement crossing near center of image. Some dolomite rhombohedra have dark cores. Lower cement zone has area with globular clear cement. Field of view is 3 mm. B) Clear globular cement in lower dolomite cement zone is composed of microcrystalline quartz. Field of view is 3 mm. C) Dolomite rhombohedra with high intracrystaline porosity formed from dissolution of crystals from the inside out. Some crystal boundaries are preserved. Field of view is 0.5 mm. D) Image in C with cross-polarized light. Field of view is 0.5 mm. E) Complex fabric of dolomite cements with angular fragments of first-generation cement reincorporated into breccia fabric. Field of view is 3 mm. F) Image in E with cross-polarized light. Field of view is 3 mm.

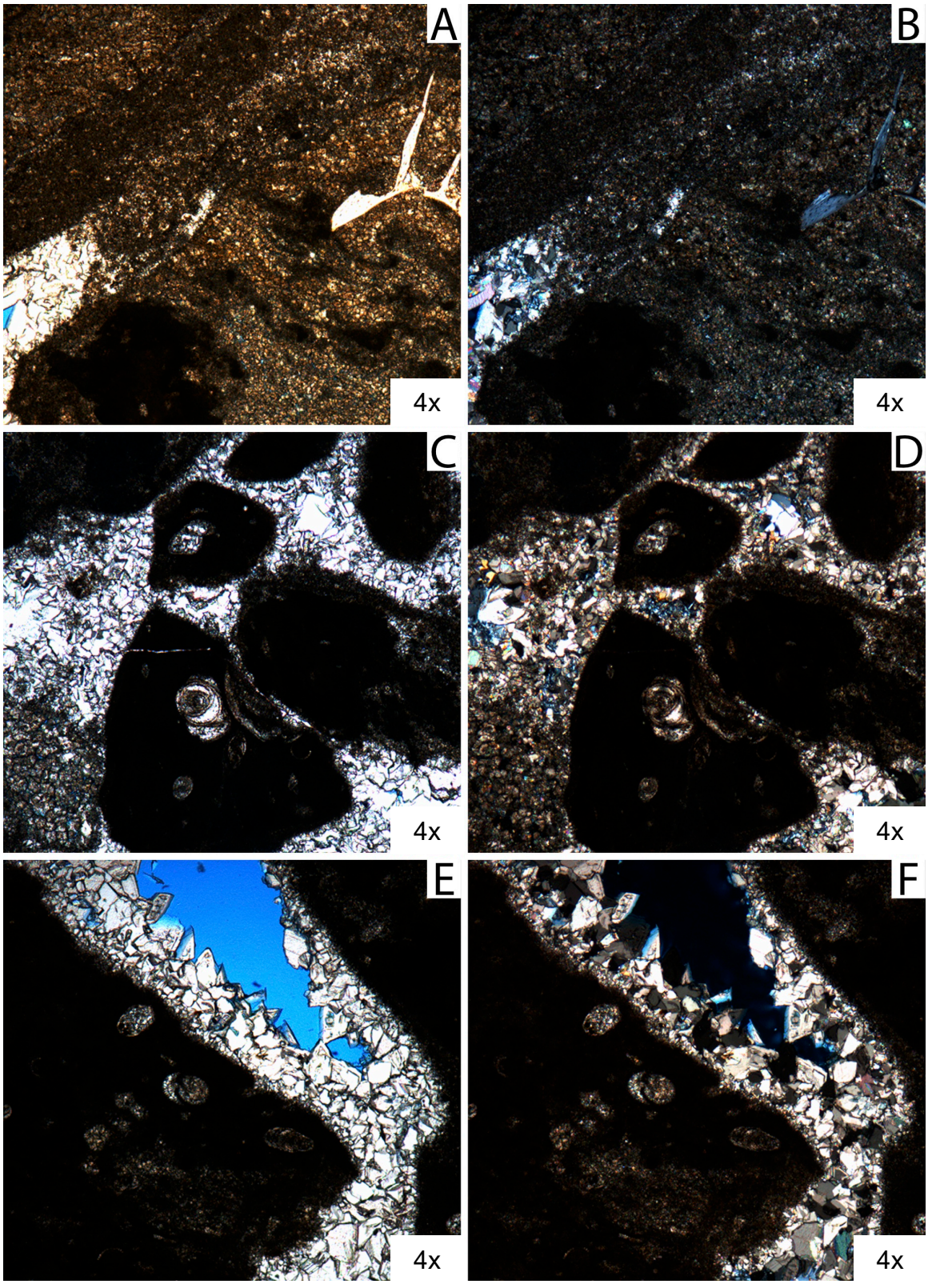
A
4x
B
4x
C
4x
D
4x
E
4x
F
4x

FIGURE 22. Microfabrics of dolomite breccia at upper contact. A) Very fine-crystalline (micritic) dolomite cement with two directions of aligned fabric, zone of clear cement on left side of image, and small bone fragment on right side of image. Field of view is 3 mm. B) Cross-polarization reveals clear cement at left is composed of coarse-crystalline dolomite cement. Voids between crystals are filled with chalcedonic cement. Field of view is 3 mm. C) Sub-angular fossiliferous Monterey clasts supported by multiple cementation fabrics. Cement at bottom left is comprised with rhombohedral crystals with dark cores. Cement in the rest of the image is clearer with coarser crystals. Field of view is 3 mm. D) Cross-polarized light reveals cement is predominantly dolomitic. Dolomite crystals in contact with clasts are radially oriented into coarse-crystalline dolomite cement and void-filling chalcedony and quartz cement. Field of view is 3 mm. E) Coarse-crystalline fracture-lining dolomite cement. Field of view is 3 mm. F) Image in E with cross-polarized light. Field of view is 3 mm.

sample had a composition of –6.5 and –7.6‰ for $\delta^{13}C$ and $\delta^{18}O$, respectively. Stratigraphic dolomite $\delta^{13}C$ values range between +1.5 and 4.5‰ VPDB and $\delta^{18}O$ between –0.2 and +4.7 ‰ for $\delta^{18}O$.

Trace Elements

Twenty-three trace elements were analyzed in twelve samples to better constrain the source of dolomitizing fluids. The value ranges and average concentrations for each element are presented in Table 5, and a complete table of results is in Appendix C.

TABLE 4. Isotopic Values From Grefco Road Dolomite Breccia and Dolomite Concretions From the Lompoc Area

Location on Transect B-B'	Figure No.	Location on Slab	Sample Name	$\delta^{13}C$ (‰ VPDB)	$\delta^{18}O$ (‰ VPDB)	Breccia Component Sampled
9	10	1	072615-08-JULGREF 1	–6.54	–7.66	translucent gray cement
		2	072615-08-JULGREF 2	–11.88	–1.09	white cement
		3	072615-08-JULGREF 3	–11.87	–0.83	beige cement
		4	072615-08-JULGREF 4.1	–11.96	–1.70	brown cement
		5	072615-08-JULGREF 5	–11.93	–0.17	gray cement
10	11	1	072815-20B-CMT6	–11.96	0.22	cement
		6	072815-20B-CMT2	–10.08	–0.37	cement
	12	1	072815-20C-1	–9.95	–1.37	cement
		2	072815-20C-17	–12.85	0.04	clast
		3	072815-20C-18	–10.78	–1.10	clast
		4	072815-20C-11	–14.29	0.60	micro breccia
		5	072815-20C-14	–11.75	0.28	micro breccia
11	13	1	072615-15A-1	–11.72	–0.15	white cement
		3	072615-15A-3	–12.35	–0.25	clast
12	14	1	102117-01-JULGREF 6	–11.12	0.28	buff-brown-pink cement
		2	102117-01-JULGREF 7.1	–13.43	1.11	clast
		3	102117-01-JULGREF 5	–9.83	1.20	pink-white cement
		4	102117-01-JULGREF 4	–13.37	1.77	clast
		5	102117-01-JULGREF 2	–11.17	1.14	clast
		6	102117-01-JULGREF 3.1	–11.49	1.91	white cement
		7	102117-01-JULGREF 1	–9.17	0.89	pink cement
15	17	1	011116-10-10	–8.70	1.01	white clast
		3	011116-10-5	–9.18	1.36	brown cement

TABLE 4. Continued

Location on Transect B-B'	Figure No.	Location on Slab	Sample Name	$\delta^{13}C$ (‰ VPDB)	$\delta^{18}O$ (‰ VPDB)	Breccia Component Sampled
15	17	4	011116-10-7	–11.47	0.79	cement vein
		5	011116-10-2	–12.55	2.20	white cement
		6	011116-10-1	–10.12	1.78	brown cement
16	18	2	011116-09-2	–10.58	0.47	micro breccia
		3	011116-09-1	–10.30	0.73	micro breccia
17	19	1	011116-7A-1	–11.64	1.90	white clast
		2	011116-7A-2	–8.84	0.56	brown cement
		3	011116-7A-3	–11.56	1.95	buff clast
		4	011116-7A-6	–10.35	0.49	gray cement
	NA	1	011116-7B-1	–10.71	0.58	white cement
		3	011116-7B-3	–9.95	0.79	ground mass
		4	011116-7B-4	–9.44	0.05	clast
NA	NA	NA	SWYRD 1	1.58	4.75	concretion - Sweeney Road
NA	NA	NA	LHD	4.46	–0.16	concretion - Lion's Head

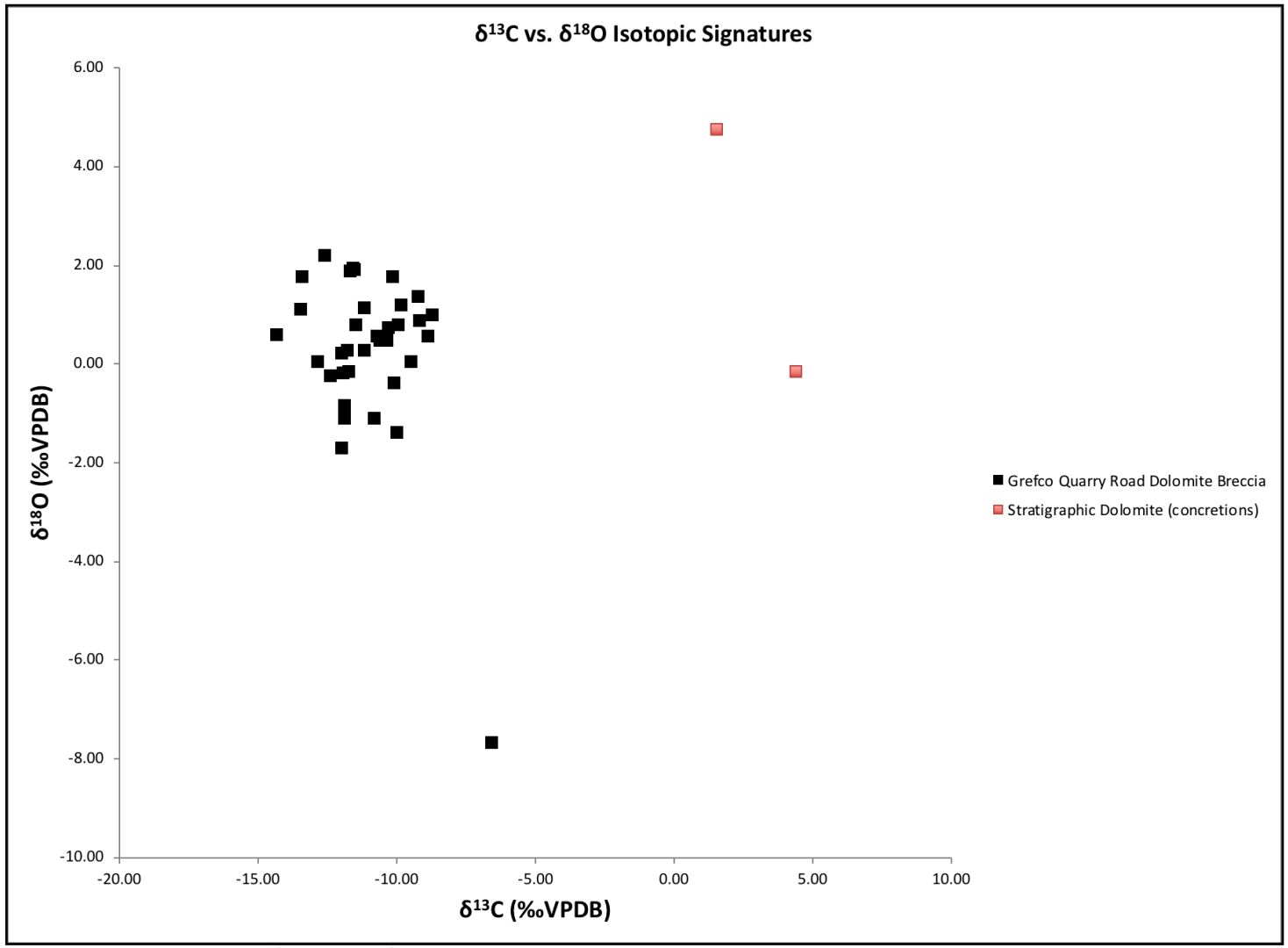

FIGURE 23. Plot of $\delta^{13}C$ and $\delta^{18}O$ values of dolomite breccia at Grefco Quarry Road compared to stratigraphic concretions from the greater Lompoc area. Black squares represent samples taken from B-B' transect. Red squares represent samples taken from Sweeney Road in Lompoc and Lion's Head on Vandenberg Air Force Base.

TABLE 5. Trace Elements Analyzed to Augment Fluid Provenance Determination

Trace Element	Conc. μg/g		
	Min.	Max.	Avg.
Be	0.13	0.28	0.20
B	2.71	12.04	6.19
Al	539.39	2196.41	1150.59
Ti	44.20	153.47	74.35
V	70.33	140.93	97.57
Cr	16.66	42.08	26.92
Mn	39.94	133.39	94.69
Fe	1514.13	3158.57	2026.80
Co	0.31	0.98	0.51
Ni	4.52	37.18	12.24
Cu	2.43	17.21	8.12
Zn	11.39	48.72	19.80
As	0.22	2.28	0.84
Se	0.00	0.28	0.06
Sr	180.19	334.69	247.52
Mo	0.00	1.42	0.45
Ag	0.13	2.45	0.51
Cd	1.14	4.79	2.27
Sn	0.11	0.31	0.17
Sb	0.00	0.34	0.11
Ba	69.43	199.70	134.2
Tl	0.00	0.12	0.02
Pb	0.19	6.00	0.93

CHAPTER 4

DISCUSSION

Deformational style, rock fabric, and stable isotopic composition of fragments and cement provide key constraints on the origin of an enigmatic map-scale brecciated dolomite at Grefco Quarry Road in the southern Santa Maria Basin. The results have implications for regional tectonics and fluid migration.

Interpretation of Deformation and Dolomitization

Deformation was analyzed along transect A-A' and along the basal contact of the dolomite breccia exposed along transect B-B' (Fig. 5). Brecciation at the basal contact between the dolomite breccia and an underlying sandstone includes angular clasts that are composed of both Monterey Formation-type rocks and the subjacent sandstone. Rather than an unconformity as previously interpreted, brecciated rock fabric with angular inclusions of underlying rocks in a cement-supported matrix indicate that the contact between the two units is faulted. Dolomitic breccias are confined to fold cores, exist sporadically along bedding planes, and define the basal contact of the Monterey Formation with underlying strata. Fold-core breccias along transect A-A' generally increase in size and degree of dolomitization from north to south, culminating with the large exposure of the dolomite breccia at the southern end of the transect. Deformation that includes brecciation in fold cores and along bedding planes (or other lateral planes of weakness, such as unconformable lithologic contacts) are consistent with fold and thrust belts studied elsewhere (e.g. Fisher and Jackson, 1998). Namson and Davis (1990) interpret much surface and subsurface data within the SMB as a fold and thrust belt developed over a deep detachment in a contractive tectonic regime. Based on strain analysis of the Monterey and Sisquoc formations in the SMB, Wirtz (2017) introduced a tectonic wedge model that ties higher amounts of shortening

recorded in the Monterey Formation relative to older strata to the deep thrust faults modeled by Namson and Davis (1990). Wirtz's model proposes a regional detachment surface along the base of the Monterey Formation in the southern region of the SMB. The faulted contact at the base of the Grefco Quarry dolomite may be part of that modeled detachment surface. Figure 24 is an interpretive cross-section derived from a combination of published geologic maps and the findings of this study. The section covers a small portion of the Lompoc Hills and Point Conception quadrangle (Dibblee and Ehrenspeck, 1988b) along C-C', which runs north-south. Note that this interpreted cross-section differs from others (c.f., Dibblee, 1950) because it includes a detachment surface that links the mapped occurrences of the dolomite breccia (Tmls) in the Lompoc Hills area. The detachment surface is inferred to be marked by the Tmls, undulating from below the lower member of the Monterey (Tml) to within the upper member of the Monterey (Tm), in some cases placing Tml above Tm. Excess folding in the Monterey Formation requires a detachment surface below. This detachment has a spatially heterogeneous expression and may or may not have locally produced thick, mappable breccias, like the Tmls unit, that were dolomitized or dolomite cemented. Development of a Tmls dolomite breccia is likely controlled by the brittleness of the rock types transected and the geometry of the faulted surface. The geometry interpreted in Figure 24 allows for extra tight, high-frequency folding within Monterey strata and enables Tmls to exist below and within Tm strata and below and throughout the Monterey Formation.

The predominant rock types exposed along transect A-A' are muddy diatomite, porcelanite and chert. These rocks, especially porcelanite and chert, have low matrix permeability that is typically less than one millidarcy, thus requiring increased fracture-related permeability for fluid transmittal (Eichhubl and Behl, 1998; Eichhubl and Boles, 2000b).

Because dolomitization is confined to brecciated zones at the Grefco Quarry location, it is inferred that brecciation in this area not only created secondary porosity within the Monterey Formation, but also created conduits for fluid flow along layer-parallel slip surfaces and the faulted contact at or near the base of the Monterey Formation. Preferred pathways for large volumes of fluid migration along bedding-parallel breccia zones in the Monterey Formation have been previously documented in the SMB (Redwine, 1981; Roehl, 1981; Behl, 1998; Eichhubl and Boles, 2000). Multiple cross-cutting breccia zones recorded in hand-sample slabs in this study indicate repeated episodes of brecciation associated with pulses of fluid and cementation. XRD shows that cements are primarily composed of dolomite with a secondary quartz component. Micritic dolomite crystals observed in thin section suggest that these cements precipitated relatively rapidly, not allowing enough time for large crystal growth. Microfabric relationships in thin section indicate that dolomite precipitated before quartz cement, as dolomite is either partially replaced by quartz, or quartz fills voids left after the dissolution of dolomite. Based on fluid inclusion data from Bodnar (1990), late-stage quartz cement at Jalama Beach was determined to form at lower temperatures than associated dolomite cements, and at Lion's Head, late-stage quartz cement within dolomite veins is interpreted to form during cementation that occurred in post-hydrothermal cooling phases. Based on the similarities between the dolomite-quartz relationships at the above locations, the quartz cement at Grefco Quarry Road likely precipitated at lower temperatures than dolomite cements.

The dolomite breccia in this area exhibits characteristics that are similar to what Davies and Smith (2006) have described as hydrothermal dolomite (HTD). Their research indicates that wrench and normal faults associated with releasing bends or step-overs in strike-slip fault systems created conduits for hydrothermal brines stored in sandstones to travel upward into

finer-grained, lower-permeability rocks (carbonates in their case) and lead to the precipitation of HTD. Central California is presently characterized by both compressional and extensional structures formed during the initiation and continued 90° clockwise rotation of the western Transverse Ranges in the early Miocene (Hornafius et al., 1986; Nicholson et al., 1994). Reverse and normal faults in the SMB and SBB act as conduits for fluid migration and Eichhubl and Boles (2000b) calculated rapid rates of fluid flow related to HTD in the Monterey Formation west of Santa Barbara. Behl (1998) calculated that 2,500-20,000 cm^3 of formation fluid per cm^3 of breccia volume had traveled through intraformational chert breccias in the Monterey Formation of SMB. Hence, large volumes of fluids have flowed through faults and breccias in the Monterey Formation. Evidence for HTD at this location includes faulted lithologic contacts, brecciation of Monterey strata, multiple episodes of cementation and rebrecciation, and the presence of saddle dolomite crystals. The sum of these features indicates that the Grefco Road (and related) dolomite breccia are of hydrothermal origin.

Discussion of Geochemistry and Implications for Fluid Source

To gain a better understanding of the environment of precipitation of dolomite and source of the fluids, stable isotopes of carbon and oxygen were measured on clasts and cements of the dolomite breccia. $\delta^{13}C$ was measured to gain insight into the origin of dissolved inorganic carbon in the fluids from which dolomites precipitated, and $\delta^{18}O$ was measured to estimate the temperatures of said fluids. The isotope results from this study are compared to previous isotopic studies conducted on stratigraphic dolomites and dolomite breccias in the Monterey Formation in the SMB and SBB (Fig. 25).

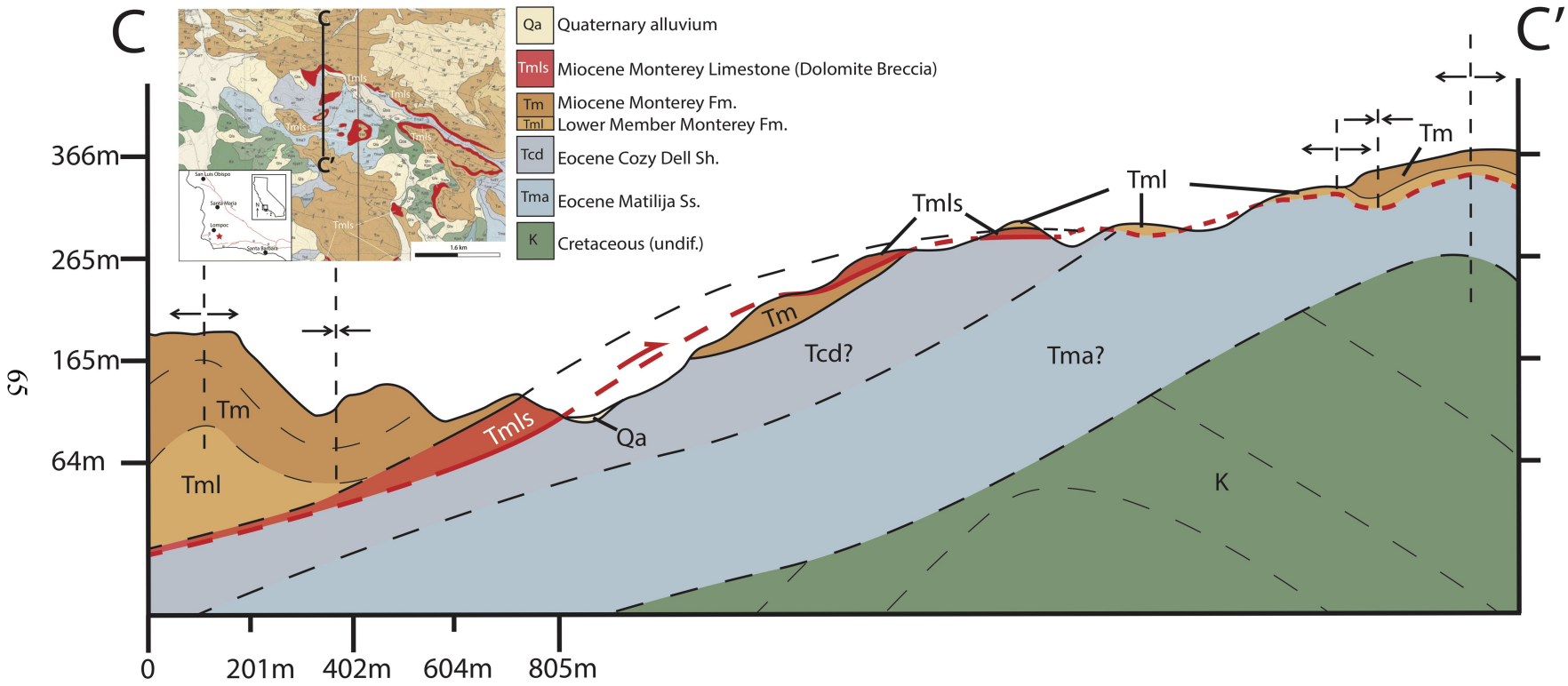

FIGURE 24. North-south cross section of select area of Lompoc hills. Detachment surface (red line) at base of Monterey Formation connects Tmls, jumps stratigraphically higher into Tm, and puts Tml above Tm near center of section. Map sourced from Dibblee and Ehrenspeck, 1988c.

Previous studies sampled stratigraphic or nodular dolomites south of Lompoc and Solvang, California (Murata et al., 1969), Montaña de Oro, Shell Beach, Naples Beach (Loyd et al., 2012a), Arroyo Seco, and Tepusquet Canyon (Kushnir and Kastner, 1984) (inset, Fig. 25). Previous studies also sampled fault-related dolomite breccias at Tepusquet Canyon (Malone et al., 1996; Martin and Rymerson, 2002), and Jalama Beach (Winter and Knauth, 1992; Eichhubl and Boles, 2000b; Martin and Rymerson, 2002) (inset, Fig. 25). Generally, isotopic signatures of stratigraphic/early diagenetic dolomites fall into discrete domains that are different from location to location, but isotopic data from each sample set are arranged in linear arrays of $\delta^{13}C$ and $\delta^{18}O$ values. $\delta^{13}C$ values are between –12.7‰ and +16.6‰ and are mostly positive, except for sample MNC2 from Naples Beach and samples from Shell Beach. $\delta^{18}O$ values are evenly distributed between –5.1‰ and +3.5‰. Isotopic signatures of dolomites from fault breccias also form different discrete domains, but within each, their distribution forms broad fields of $\delta^{13}C$ and $\delta^{18}O$ values. $\delta^{13}C$ values from Jalama Beach generally clump between –23.5‰ and –11.23‰ with $\delta^{18}O$ values from -9.65‰ to -5.1‰. Tepusquet Canyon $\delta^{13}C$ values are between –9.81‰ and –4.07‰ with $\delta^{18}O$ values nearly identical to those from Jalama Beach.

In comparison, the isotope signatures from the dolomite breccia at the Grefco Quarry road are mostly clumped between $\delta^{13}C$ values of –14.3‰ to –8.7‰ and $\delta^{18}O$ values –1.7‰ to +2.2‰, with the exception of one outlier with values that are similar to those of the dolomite breccia from Tepusquet Canyon.

For stratigraphic dolomites, $\delta^{13}C$ values are representative of the pore fluids where dolomites formed authigenically. In these environments, $\delta^{13}C$ is generally related to the degradation of organic matter. Light, or negative, values of $\delta^{13}C$ are the result of aerobic respiration (Kushnir and Kastner, 1984), microbial sulfate reduction, and/or thermal

decarboxylation (Kushnir and Kastner, 1984; Loyd et al., 2012a). Lighter values of $\delta^{13}C$ (~ –35 to –8‰) are also related to organic substances like organic matter, coal, and oil (Murata et al. 1969). Heavy, or positive, values of $\delta^{13}C$ are characteristic of methanogenesis (Kushnir and Kastner, 1984; Loyd et al., 2012a). For dolomite breccias, $\delta^{13}C$ values are likely controlled by the carbon pool from which the cement or replacing fluids were sourced, including both organic and inorganic carbon (Eichhubl and Boles, 2000b). For stratigraphic dolomite and dolomite breccias, the $\delta^{18}O$ compositions reflect the fluid isotope composition and temperature at which the dolomite formed (Pisciotto, 1981; Roehl, 1981; Kushnir and Kastner, 1984).

Trace elemental data were compared with other dolomites analyzed in the Monterey Formation from breccias at Jalama Beach and Tepusquet Canyon, as well stratigraphic dolomite from the SMB (across Highway 1 from Grefco Quarry road, Montaña de Oro, Shell Beach, Lion's Head) and the SBB (Naples Beach). No unique geochemical characteristics were observed that could provide any information on the genesis of the dolomite breccia at the Grefco Quarry road.

Initially, the dolomite breccia at the Grefco Quarry road was expected to have a stable isotopic signature resembling those of the dolomite breccias at Tepusquet Canyon and Jalama Beach. However, the $\delta^{13}C$ values are at the extreme light end of the stratigraphic dolomites and in between the $\delta^{13}C$ values of the other two dolomite breccias while $\delta^{18}O$ values are similar to stratigraphic dolomites. An important question arises: how does a fault-associated dolomite breccia have $\delta^{18}O$ values that are so enriched in ^{18}O compared to other fault-associated dolomites? Two scenarios are possible when considering the answer to this question: 1) the fluids associated with dolomites at Grefco Quarry road were formation fluids from the Monterey

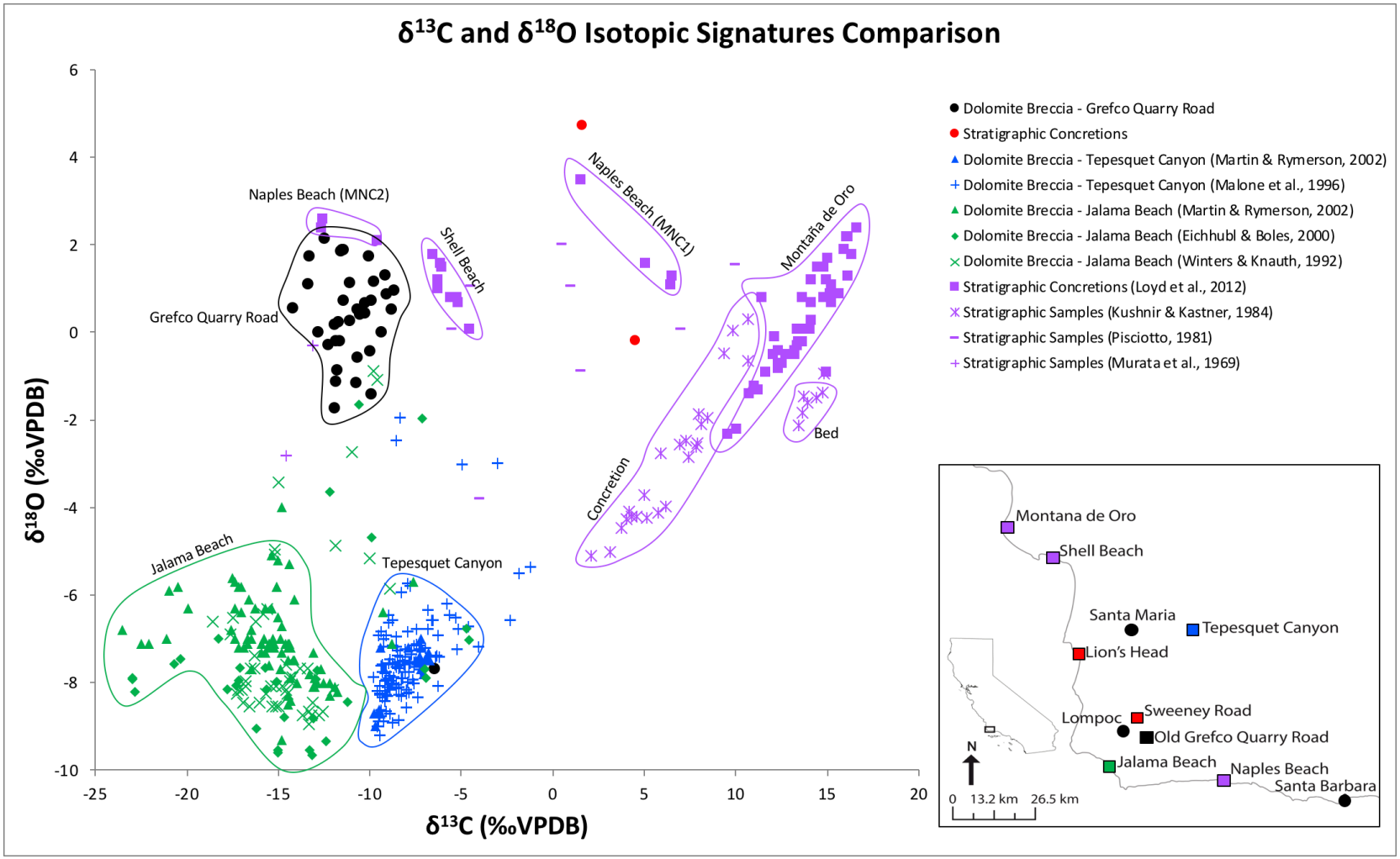

FIGURE 25. Isotopic values for dolomite breccias and stratigraphic dolomite in the SMB. Black and red solid circles are data from this study. Stratigraphic dolomites are represented by purple markers. Dolomite breccia at Jalama Beach is represented by green markers. Dolomite breccia at Tepusquet Canyon is represented by blue markers. Comparison data are from Murata et al. (1969), Pisciotto (1981), Kushnir and Kastner (1984), Winter and Knauth (1992), Malone et al. (1996), Eichhubl and Boles (2000), Maritn and Rymerson (2002), Loyd et al. (2012a).

Formation itself, and fluid flow was an intraformational closed-system (as in the findings form Eichhubl and Boles, 2000a); 2) the dolomite formed from Franciscan- or ophiolite-derived fluids associated with the Mesozoic Franciscan Assemblage, which underlies most of the SMB. Both hypotheses are discussed individually below, but both are conditional on the assumption that the detachment surface, evident in the brecciated basal contact of the dolomite breccia, is a fluid conduit that cross-cuts Monterey strata, connecting upper members to lower members of the Monterey Formation, or connecting the Monterey Formation to Mesozoic section.

Monterey-Sourced Fluids

In previous studies of the Monterey, the isotopic signatures of stratigraphic dolomite differ significantly from the isotopic signatures of fault-related dolomite breccias. Stratigraphic dolomites at Naples and Shell Beach formed at shallow burial depths where pore waters are expected to have a $\delta^{18}O$ signature similar to Miocene seawater between –30.0‰ and –29.0‰. By deep burial into the quartz phase, both Winter and Knauth (1992) and Behl (1992) modeled the pore water to be ~ 2.91‰ to 3.88‰ more positive than Miocene seawater in the lower members of the Monterey (~ 0.97 to 1.94‰ more positive if the fluid source is from the opal-CT phase of upper members of the Monterey). $\delta^{18}O$ values between –27.0‰ and –26.1‰ are the best estimate of what the isotopic composition of water sourced from the lower Monterey would be.

In addition to $\delta^{18}O$ values representing evolved pore waters from the lower Monterey members, the $\delta^{13}C$ values also suggest dolomitizing fluids were derived from Monterey pore waters. The light $\delta^{13}C$ values (–14.3‰ to –8.7‰) of the dolomite at the Grefco Quarry road indicate the carbon pool was sourced from either a deeper environment of thermal, abiotic degradation of organic matter (decarboxylation) or from a shallower environment of microbial oxidation of organic matter or methane (Loyd et al., 2012a). The lower members of the Monterey

Formation are rich in organic matter (Compton and Siever, 1984; MacKinnon, 1989), and methane and hydrocarbon seeps in the Monterey Formation have been documented in the SMB and SBB (Tennyson and Isaacs, 2001; Boles et al., 2004). These factors indicate that environments required to produce the composition of $\delta^{13}C$ measured at Grefco Road likely existed within the Monterey Formation. Temperatures calculated from $\delta^{18}O$ values and the considerable amounts of fluid required to precipitate dolomite at this location (discussed in detail below) suggest the fluids were derived from the deeper environment of thermal decarboxylation.

The dolomite breccias at Jalama Beach and Tepusquet Canyon are examples of such Monterey-sourced, "closed-system" type of fluid flow. For the dolomite breccia at Jalama Beach, Eichhubl and Boles (2000a) believe the source for the dolomitizing fluids is derived from within the Monterey Formation. In his discussion of the formation of the dolomite breccia at Tepusquet Canyon, Roehl (1981) suggests that there was enough mobile pore water with enough available magnesium in Monterey pore fluids to support the precipitation of dolomite if kinetics and other chemical conditions were satisfied. These findings coupled with the data from this study indicate that the breccia at Grefco Road is likely derived from Monterey-sourced fluids.

Basement-Derived Fluids

The influence on Cenozoic sediments of the serpentinization of ultramafic rocks in the SMB is an interesting topic to consider. The serpentinization reaction generates a significant amount of heat ($6.6x10^8$ joules/ft^3), produces extremely basic fluids (pH ~9-11) that are enriched in magnesium, and can increase the volume of the rock up to 40% (Früh-Green, 2005), providing a mechanism for fracturing and fluid release. Remnant metamorphosing fluids from serpentinization are ^{18}O-enriched (Magaritz and Taylor, 1976) and alkaline. Since mélange of the Franciscan Assemblage, likely containing lenses of peridotites, underlies most of the SMB

(McLean, 1995), this scenario provides a heat source for hydrothermal fluids and increased concentrations of magnesium, thus explaining the emplacement of HTD. $\delta^{18}O$ values of seawater associated with serpentinization evolved to become more enriched in ^{18}O; however, the $\delta^{18}O$ values of such evolved fluids are not estimated to exceed –15‰ (Magaritz and Taylor, 1976; Brown, 2014). The lowest value of $\delta^{18}O$ measured at the Grefco Quarry road location is –7.7‰, and that measurement is of an outlying sample. The more reasonable lowest value of $\delta^{18}O$ for this study area is –1.7‰. In order to precipitate dolomite with a $\delta^{18}O$ value of –1.7‰ from a fluid with a $\delta^{18}O$ value of –15‰, the temperature of the environment would have to be ~159˚C, which is much higher than temperature of formation estimates for the Grefco Road dolomite breccia (see discussion below). Estimated temperature of formation required if using $\delta^{18}O$ values of evolved connate waters of the lower members of the Monterey Formation (–27‰ to –26.1‰) falls between 55-61˚C, which is more consistent with temperatures calculated for the dolomite at Grefco Road. Because the temperatures required for dolomite precipitation from a pore fluid with $\delta^{18}O$ values of less than –15‰ are higher than estimated formation temperatures of the dolomite at Grefco Road, the scenario of HTD forming from serpentinization fluids is not favored.

Discussion of Temperature of Formation of HTD

The benchmark definition of hydrothermal fluid pertains to fluid that is at least 5˚C warmer than surrounding environment (White, 1957). Herein, I follow the definition of Davies and Smith (2006) for HTD, where the term “hydrothermal” refers to any fluid or precipitate that is introduced to or emplaced in a host that is warmer by any degree than the ambient temperature of the host. In order to determine if the dolomite at the Grefco Quarry road site is HTD, the temperature of formation for brecciated dolomite and stratigraphic dolomite from the SMB were

compared. Temperatures of HTD emplacement in comparative studies were determined from fluid inclusions (Bodnar, 1990; Eichuubl and Boles, 2000b) and $\delta^{18}O$ (Pisciotto, 1981; Kushnir and Kastner, 1984; Malone et al., 1996).

There are numerous expressions of calculations for temperatures at which dolomite forms. For dolomite precipitation at the Grefco Quarry road, temperatures were derived from $\delta^{18}O$ values of the dolomite breccia, using two equations for dolomite fractionation, 1) for low-temperature, microbe-facilitated precipitation (Vasconcelos et al., 2005):

$$1000 \ln \alpha_{\text{dolomite-water}} = 2.73 \times 10^{6} T^{-2} + 0.26,$$

and 2) for hydrothermal dolomite formation (Horita, 2014):

$$1000 \ln \alpha_{\text{dolomite-water}} = 3.14 \times 10^{6} T^{-2} - 3.14.$$

Because clasts of Monterey porcelanites and cherts are present in the dolomite breccia, it is known that diagenesis of upper Monterey members preceded dolomitization/brecciation; therefore, diagenesis in lower Monterey strata had certainly occurred. In the structural model presented earlier (Fig. 24) the lower members of the Monterey are interpreted to connect to the dolomite breccia; therefore, the modeled $\delta^{18}O_{water}$ value of –26.6‰ of evolved connate waters associated with quartz-phase rocks from the lower Monterey (Behl, 1992) is used for temperature calculations. Results of these equations are in Table 6. There is some uncertainty with this method of temperature calculation (Davies and Smith, 2006; Loyd et al., 2012b); however, using $\delta^{18}O_{water}$ values for modified pore waters instead of seawater values reduces that error. Because the dolomite breccia at Grefco Quarry Road is believed to be of hydrothermal origin, the dolomite fractionation equation presented by Horita (2014) better represents the conditions of dolomitization for this study. Consequently, the temperature range of dolomite precipitation is

taken to be 36.6-95.5˚C. These temperatures are then compared to temperatures of dolomite precipitation in the SMB derived from other studies (Table 7).

TABLE 6. Derived Dolomitization Temperature Ranges

Equation	Temp. (˚C) ($\delta^{18}O_{water}$ = –26.6‰)
Vasconcelos et al. (2005)	32-104
Horita (2014)	37-96

Pisciotto (1981) presented dolomite precipitation temperatures for stratigraphic dolomite from the "Santa Ynez River Area" in the SMB that were derived from data collected by Murata et al. (1969). The latitude and longitude specified in that study show that data were collected from the dolomite breccia upon which this study focuses, and from within the Cretaceous Espada Formation (according to Dibblee and Ehrenspeck, 1988a). The temperature derivations in Piscotto's study are thus skewed to represent temperature of formation of HTD and non-Monterey rocks.

With these considerations in mind, some conclusions can be made when comparing the temperatures calculated in this study with temperatures from other studies. The precipitation temperatures for the dolomite breccia at Grefco Quarry road are likely lower than the temperatures of the dolomite breccias at Jalama Beach and Tepusquet Canyon. When compared to temperatures for stratigraphic dolomite, the temperature range of the Grefco breccia is similar to, but generally warmer than, the full range of temperatures of stratigraphic dolomite occurrences.

TABLE 7. Temperature of Precipitation of Various Dolomite Occurrences in SMB

Occurrence Type	Temp. (C)	Location	Source
Breccia	37– 96	Grefco Quarry Rd.	This study
Breccia	65 – 100	Jalama Beach	Eichhubl and Boles, 2000b
Breccia	70 – 105	Tepusquet Canyon	Malone et al., 1996
Stratigraphic	10 – 78	Southern SMB	Pisciotto, 1981[1]
Stratigraphic	25 – 60	Northeast SMB	Kushnir and Kastner, 1984
Stratigraphic	4*	Sweeney Rd. (Tm)	This study
Stratigraphic	23 *	Lion's Head (Tml)	This study

Note: [1] Data points used for temperature determinations are not representative of stratigraphic dolomite in SMB. See text for further discussion. * Calculated using dolomite fractionation eqn. from Vasconcelos et al. (2005).

Work done by Behl (1992) shows that quartz-phase cherts in the Grefco Quarry road area formed at about 40˚C. The mixed silica phases of the rocks described in transect A-A' (diatomite, porcelanite, and chert) indicate the temperature range of bulk diagenesis at this location is approximately 45˚C to 48˚C, and likely did not exceed temperatures of 50˚C (Behl, 1998). These findings indicate that the temperatures calculated for the dolomite breccia likely reached higher temperatures than stratigraphic dolomite precipitation and silica diagenetic temperatures, indicating that the dolomite breccia formed in a focused area of greater temperature and is therefore of hydrothermal origin.

Using a method derived from Behl (1998), an estimate was made of the minimum fluid required to flow through the breccia zone in order to precipitate the amount of cement observed in hand-samples. Dolomite cements make up approximately 35% of the rock volume of the breccia. Between temperatures of 37˚C to 95˚C, dolomite ranges in solubility from roughly 4.25 ppm to 7.65 ppm (Morey, 1962). Assuming all of the dissolved reactant ions for dolomite in a fluid volume flowing through breccia fractures were consumed to form the cements, a minimum

of 128,000 cm^3 to 231,000 cm^3 of fluid per cm^3 of breccia volume would be required to precipitate the amount of cement present in this breccia.

Consideration of Development of Faulting and Fluid Pathways

Deformation and the style of brecciation observed at Grefco Quarry road support the idea that a detachment surface, evident in the brecciated contact between the dolomite breccia and underlying sandstone, exists at the base of the Monterey Formation, allowing for higher levels of shortening to be accommodated in the Monterey. Preferred dolomitization within fold-core and intrastratal breccias indicate that the fractured rocks along the fault acted as conduits for concentrated fluid migration. The detachment surface interpreted in cross section (Fig. 24) undulates throughout the Monterey Formation, creating cross-cutting fluid pathways. Figure 26 shows a step-by-step model of how this detachment surface may have developed.

Parts of the Monterey Formation may have been deposited in relatively shallow basins with uneven topography (Isaacs, 2001; observations at La Salle and Sudden Canyons, Appendix A) (Fig. 26-1), similar to the "Pecten Reef" in Orange County, California, where fine-grained deposits of the Monterey Formation unconformably overlie the Vaqueros Formation (Fife, 1979; Finger, 1988). During initial shortening, faulting may have developed along the unconformable contact between the Monterey Formation and Eocene strata (Fig. 26-2). Continued shortening and weakness along thin beds of Monterey Strata allowed the detachment to not only continue to grow, but to "step" into higher stratigraphic sections of the Monterey (Fig. 26-3). This provides a mechanism to advect fluids from the lower to upper Monterey, and in some locations to the south, puts lower Monterey above upper Monterey members.

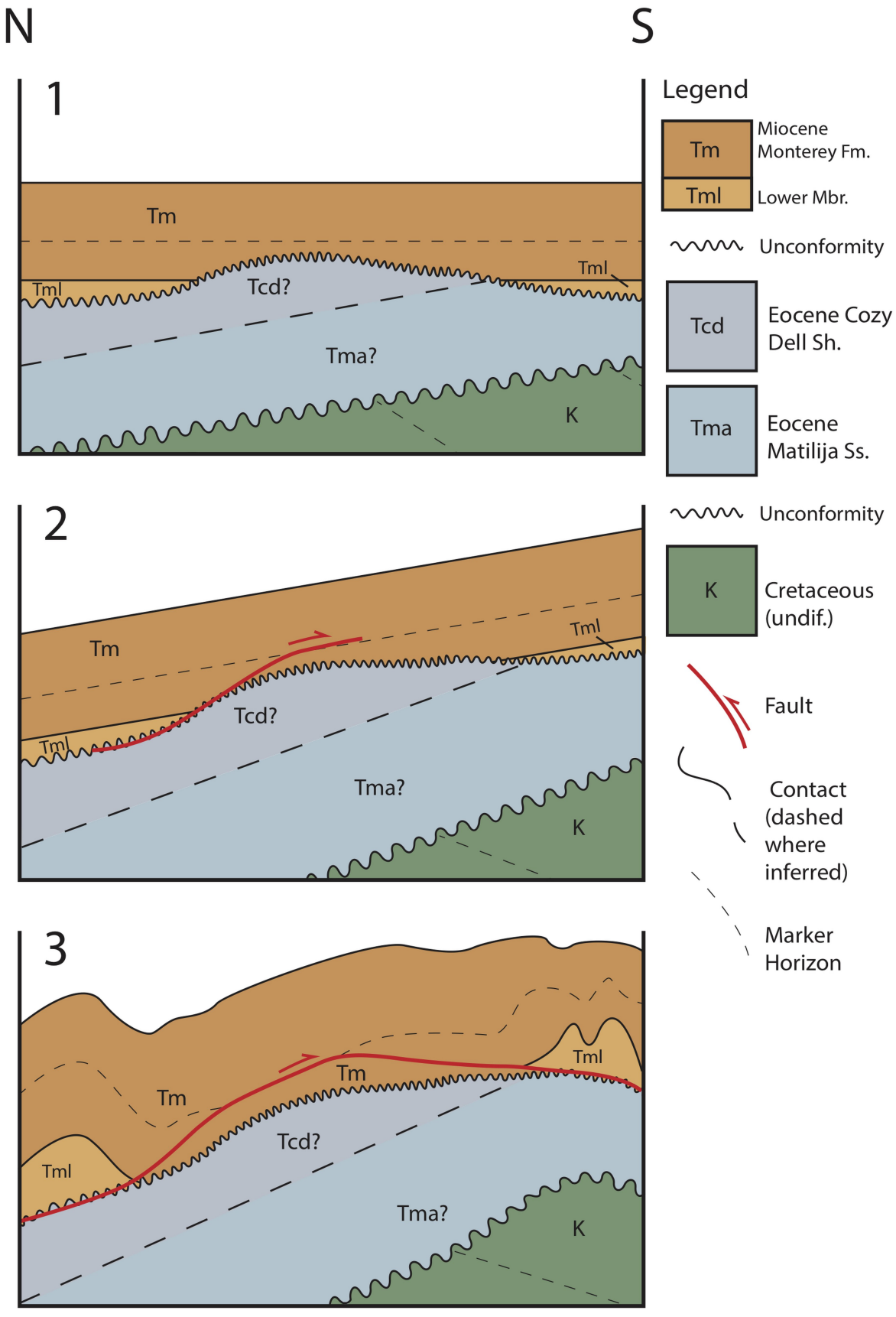
N
S
1
Tm
Tml
Tml
Tcd?
Tma?
K
2
Tm
Tml
Tml
Tcd?
Tma?
K
3
Tml
Tm
Tm
Tml
Tcd?
Tma?
K
Legend
Tm
Miocene Monterey Fm.
Tml
Lower Mbr.
Unconformity
Tcd
Eocene Cozy Dell Sh.
Tma
Eocene Matilija Ss.
Unconformity
K
Cretaceous (undif.)
Fault
Contact (dashed where inferred)
Marker Horizon

FIGURE 26. Step-by-step development of detachment fault at the base of the Monterey Formation. Step 1 – Unconformable deposition of Monterey strata onto unevenly-eroded Eocene strata. Local high of Eocene strata allows for deposition of Tm directly onto Eocene rocks. Tml deposited on either side of high. Step 2 – Initial shortening and initiation of detachment surface at the base of the Monterey Formation. Detachment surface jumps into Tm along weak bedding surfaces. Step 3 – Continued shortening and development of detachment surface. Detachment surface returns to unconformable surface at the base of the Monterey Formation, allowing for higher levels of shortening in the Monterey Formation relative to underlying strata.

CHAPTER 5

CONCLUSIONS

Several key conclusions are drawn from the analysis of the Grefco Quarry road dolomite breccia:

1. The brecciated contact between the dolomite breccia and an underlying sandstone at this location indicates a faulted contact between the Monterey Formation and older strata rather than an unconformable contact as previously interpreted by Dibblee and Ehrenspeck (1988b, 1988c).
2. Deformation patterns are consistent with a fold-thrust belt compression regime. Brecciation along bedding planes and within fold cores is consistent with layer-parallel shortening.
3. Brecciated basal contact of dolomite breccia with underlying strata is evidence for a detachment surface at base of the Monterey Formation, consistent with findings from Wirtz (2017).
4. Brecciation provides secondary porosity along layer-parallel slip surfaces and detachment surface at the base of the Monterey Formation, creating conduits for focused fluid migration.
5. The dolomite breccia is interpreted to be of hydrothermal origin based on faulted lithologic contacts, brecciation of Monterey strata, episodes of cementation and continued re-brecciation, and the presence of saddle dolomite.
6. $\delta^{13}C$ and $\delta^{18}O$ isotope data reveal that isotopic signatures at this location are more similar to isotopic signatures of stratigraphic dolomites within the lower members of the Monterey Formation, indicating hydrothermal dolomitizing fluids are likely derived from

the lower members of the Monterey. Conduits created by brecciation associated with the detachment surface at the base of and within the Monterey Formation allowed fluids to reach higher stratigraphic levels.

7. An estimated range of 128,000 cm^3 to 231,000 cm^3 of fluid per cm^3 of breccia volume was calculated as a minimum fluid volume required for the amount of cement observed at this location, indicating vast volumes of fluids were channeled through the breccia conduit.

CHAPTER 6

FUTURE WORK

Based on the findings of this research, several ideas for potential future work arise.

1. Isotopic analysis of quartz $\delta^{18}O$ to determine source of depositing fluids.
2. Fluid inclusion analysis of dolomite and quartz crystals to verify temperature and salinity of fluids that deposited dolomite and to determine the temperature of fluids that deposited quartz cements.
3. Isotopic analysis of dolomite-included strontium to better constrain the age of the stratigraphic source of dolomitizing fluid.
4. Radiogenic isotope analysis of dolomite to determine age/timing of brecciation and dolomitization.
5. In-depth investigation of the outcrop at Sudden Canyon, South Vandenberg Air Force Base. This outcrop has large bivalve molds in the host rock of a dolomite breccia with a complex series of cementation events and cement fabrics that include dolomite and quartz cements. Preliminary examination of thin sections of samples collected from this area shows mysterious elongate quartz crystals with length-slow extinction properties – something that is commonly a characteristic of chalcedony, but rarely of monocrystalline quartz. These features have implications for paleogeography, depositional environment, diagenetic and chemical history, and tectonic deformation of the Monterey Formation along the modern margin of the SMB and SBB.

APPENDICES

APPENDIX A

OUTCROP DESCRIPTIONS OF OTHER MAP-SCALE CARBONATES IN THE SANTA MARIA AND SANTA BARBARA BASINS

APPENDIX A: Outcrop Descriptions of Other Map-Scale Carbonates in the Santa Maria and Santa Barbara Basins

Tepusquet and Colson Canyons

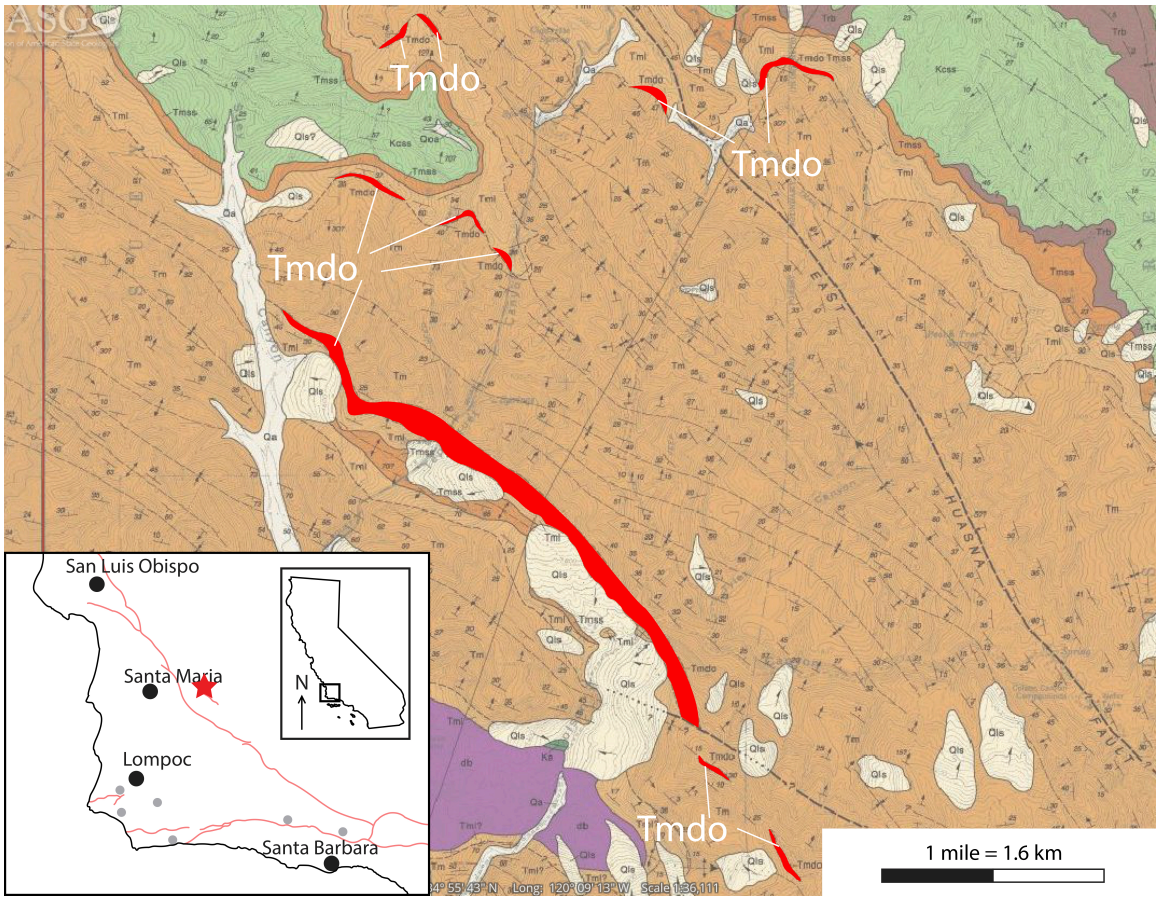

This exposure is a resistant, ridge-forming outcrop that exhibits three distinct zones of brecciation. The first zone is near vertical, dolomitized, insipiently fractured Monterey strata with some open fracture voids sub-perpendicular to bedding that are lined with saddle dolomite crystals. The second zone consists of fractured dolomitized Monterey strata with dolomite cement, and the third zone is brecciated dolomite cements further cemented by dolomite, and in some cases with hydrocarbons present in voids often lined with euhedral dolomite crystals.

Gibraltar and Paradise Roads

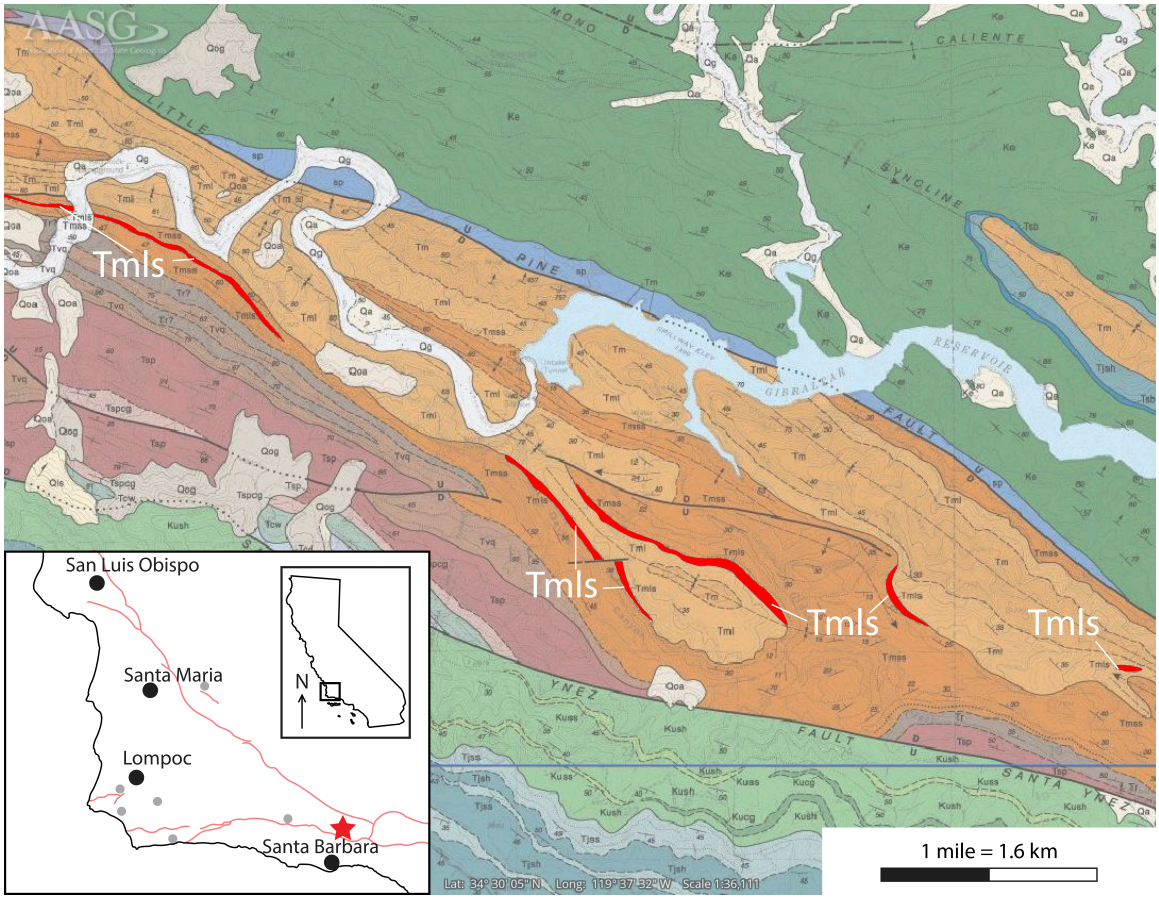

Dibblee and Ehrenspeck (1986) mapped the carbonate occurrence that spans Gibraltar Road and Paradise Road in conformable contact with the subjacent Miocene Temblor Formation (Dibblee, 1966) and the superjacent lower member of the Miocene Monterey Formation. The exposure discontinuously extends for roughly ten kilometers from the northwest to the southeast, two kilometers from the southwest to the northeast, and reaches thicknesses of around nine meters. The carbonate in this location is a resistant, gray, fossiliferous, algal limestone. This unit is not brecciated and displays no outcrop-scale zonation as seen at Tepusquet/Colson Canyon.

Hollister Ranch

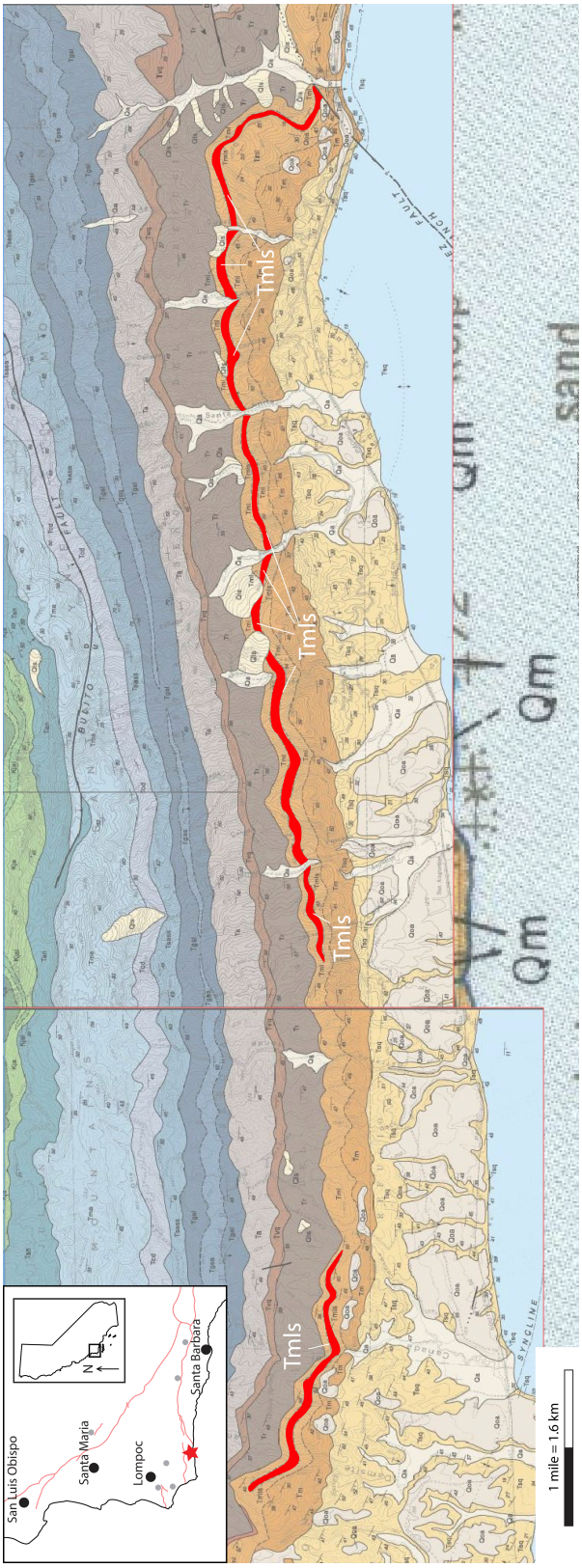

The carbonate body on Hollister Ranch has been mapped within the lower member of the Monterey Formation, roughly thirteen kilometers long and 85 meters wide (Dibblee and Ehrenspeck, 1988b, 1988c). Field investigation of this unit revealed a thickness of roughly eleven to fourteen meters. The carbonate is a continuous bed of white, non-resistant foraminiferite that locally contains interstitial hydrocarbon (oil or heavier) and chert lenses. This unit is actually thinner than what was previously mapped, and may be too thin to be represented in a 1:24,000 scale. This unit is not brecciated, and it displays no outcrop-scale zonation.

La Salle Canyon (Vandenberg Air Force Base)

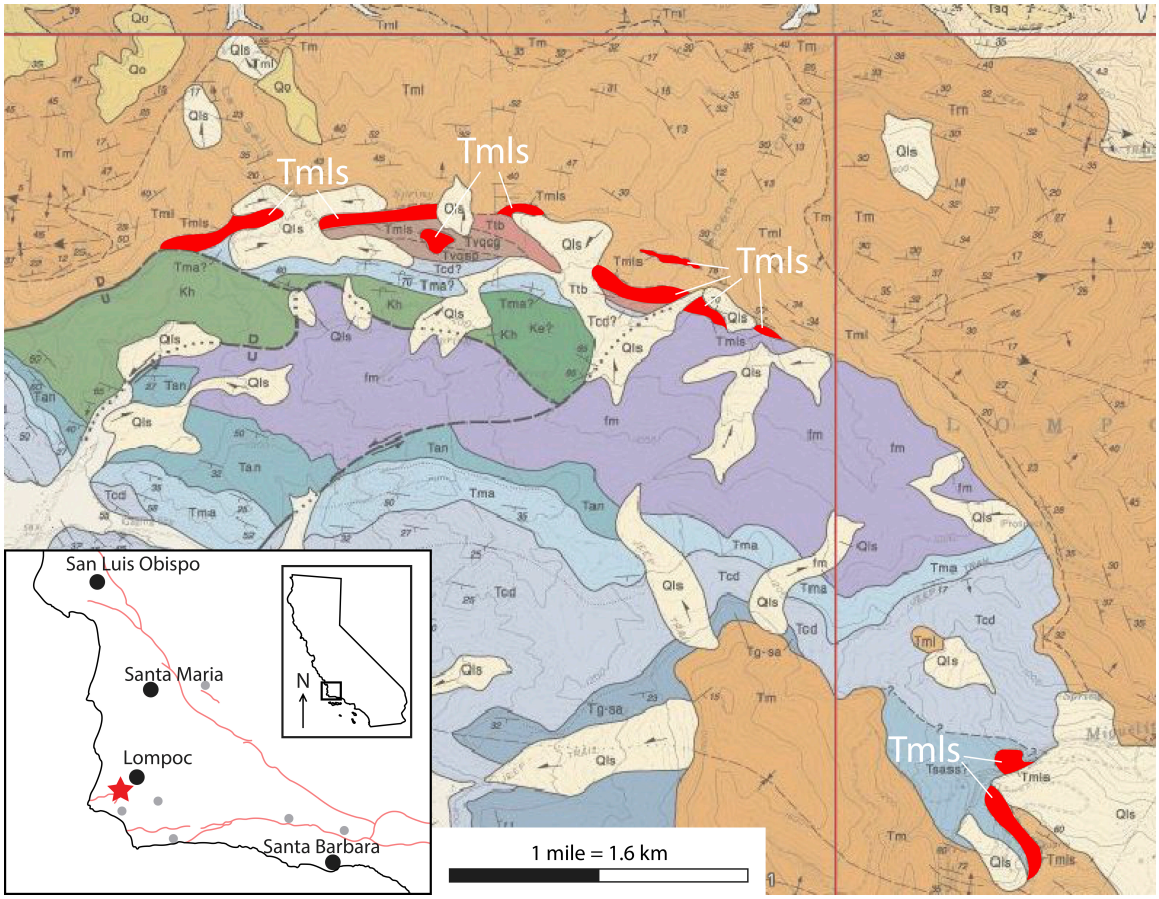

The carbonate mapped by Dibblee and Ehrenspeck (1988d) at La Salle Canyon is composed of resistant, dolomitized, fossiliferous limestone that extends roughly three kilometers from west to east, and is about 85 meters wide. The carbonate is mapped along the unconformable contact between the base of the Monterey Formation and Neogene and Cretaceous strata. Outcrops are surrounded by non-resistant rocks and create prominent ridges where exposed. The unit is brecciated on the north edge. Clasts and cements are dolomitic. The breccia is on an apparent fault contact. Brecciation within the unit increases from south to north. Fossil molds of bivalves create pores exceeding two centimeters in diameter that are lined or nearly filled with quartz cement and euhedral quartz crystals on the centimeter scale.

Sudden Canyon (Vandenberg Air Force Base)

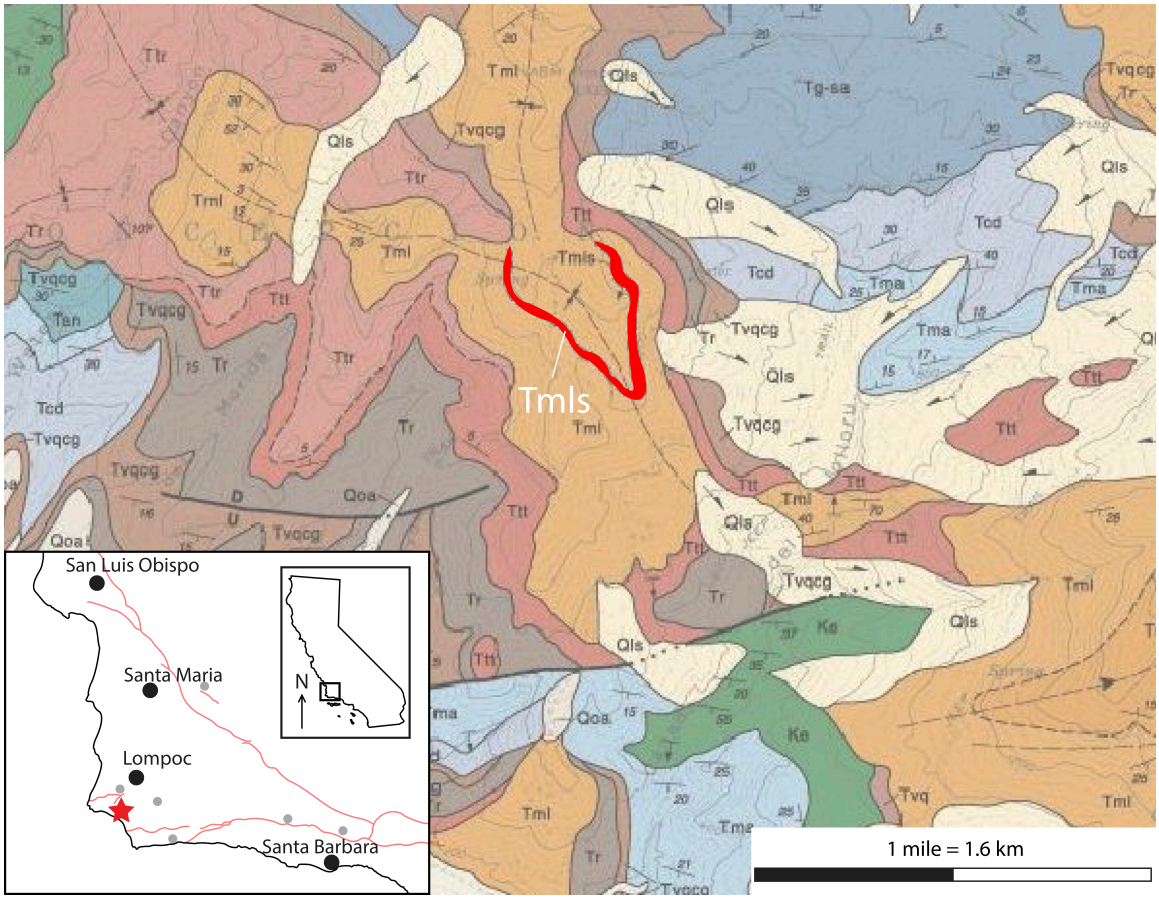

The carbonate occurrence mapped by Dibblee and Ehrenspeck (1988d) at Sudden Canyon is composed of resistant, dolomitized, fossiliferous limestone with quartz-lined bivalve fossil molds, similar to La Salle Canyon. This exposure is underlain by Tertiary strata and volcanic rocks, covers approximately 0.65 square kilometers, and was mapped as a lenticular unit within the lower member of the Monterey Formation that conforms to a local structural syncline. Two distinct zones of brecciation exist at this location – a breccia zone along the basal contact of the dolomitic unit, and the main body of the carbonate. The basal zone is characterized by fractured and brecciated dolomitized Monterey strata. The main body of the carbonate is characterized by fractured and rebrecciated dolomitic breccias with veins and void-filling dolomite and quartz cement.

APPENDIX B

X-RAY DIFFRACTION DATA

APPENDIX B: X-ray Diffraction Data

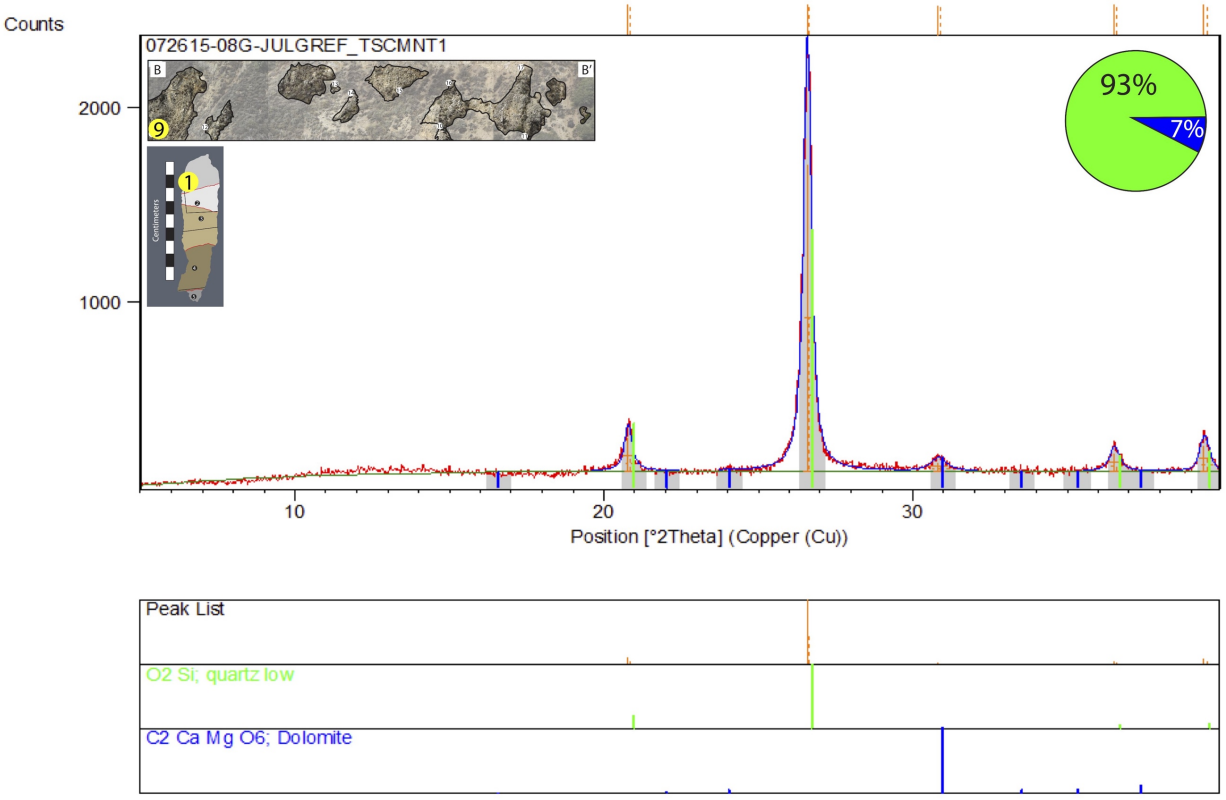

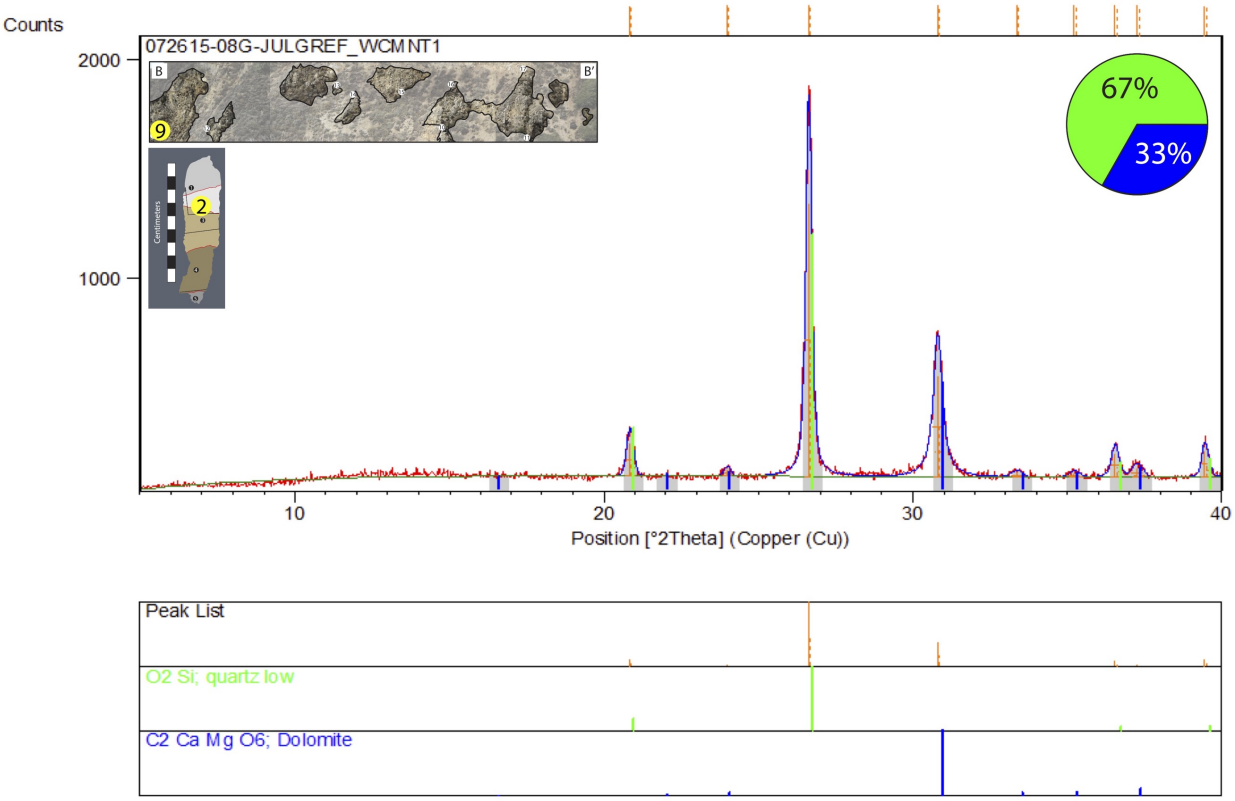

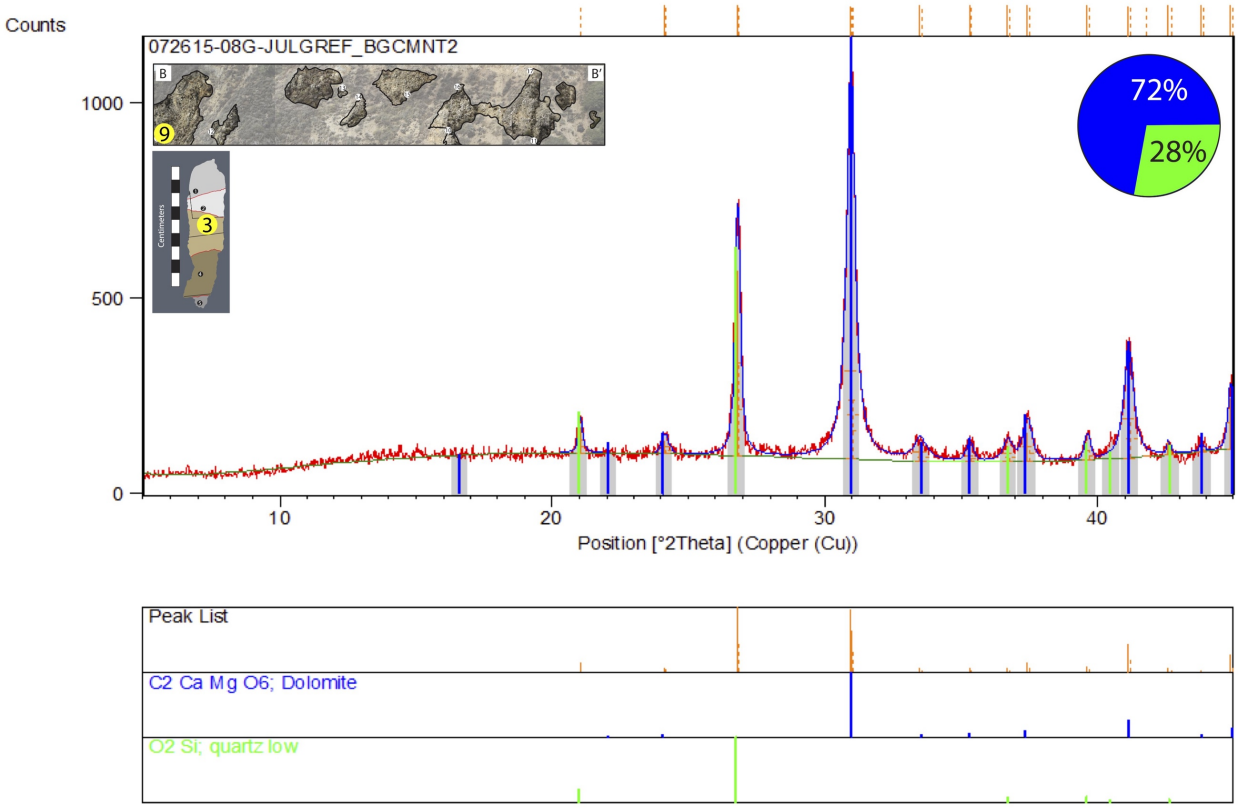
Counts
072615-08G-JULGREF_BGCMNT2
B
B'
9
3
Centimeters
72%
28%
1000
500
0
10
20
30
40
Position [°2Theta] (Copper (Cu))
Peak List
C2 Ca Mg O6; Dolomite
O2 Si; quartz low

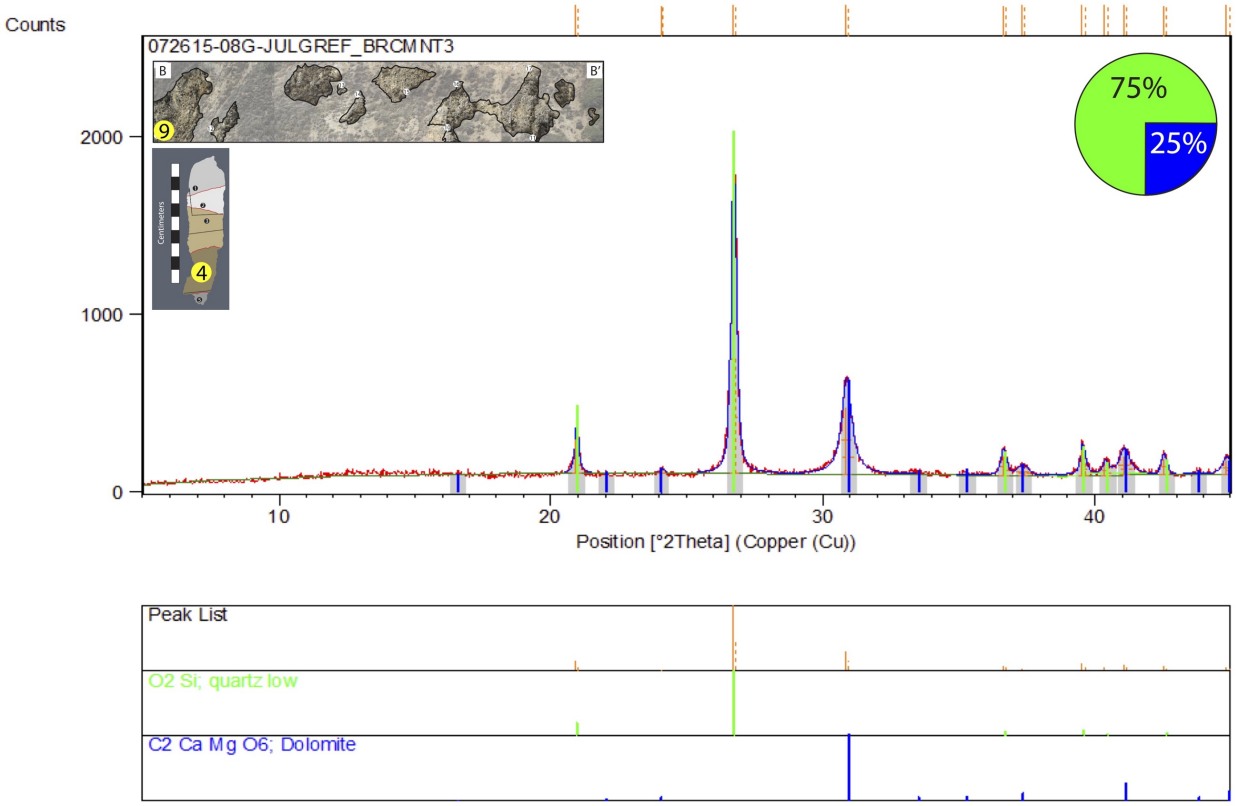
Counts
072615-08G-JULGREF_BRCMNT3
B
B'
9
4
Centimeters
75%
25%
2000
1000
0
10
20
30
40
Position [°2Theta] (Copper (Cu))
Peak List
O2 Si; quartz low
C2 Ca Mg O6; Dolomite

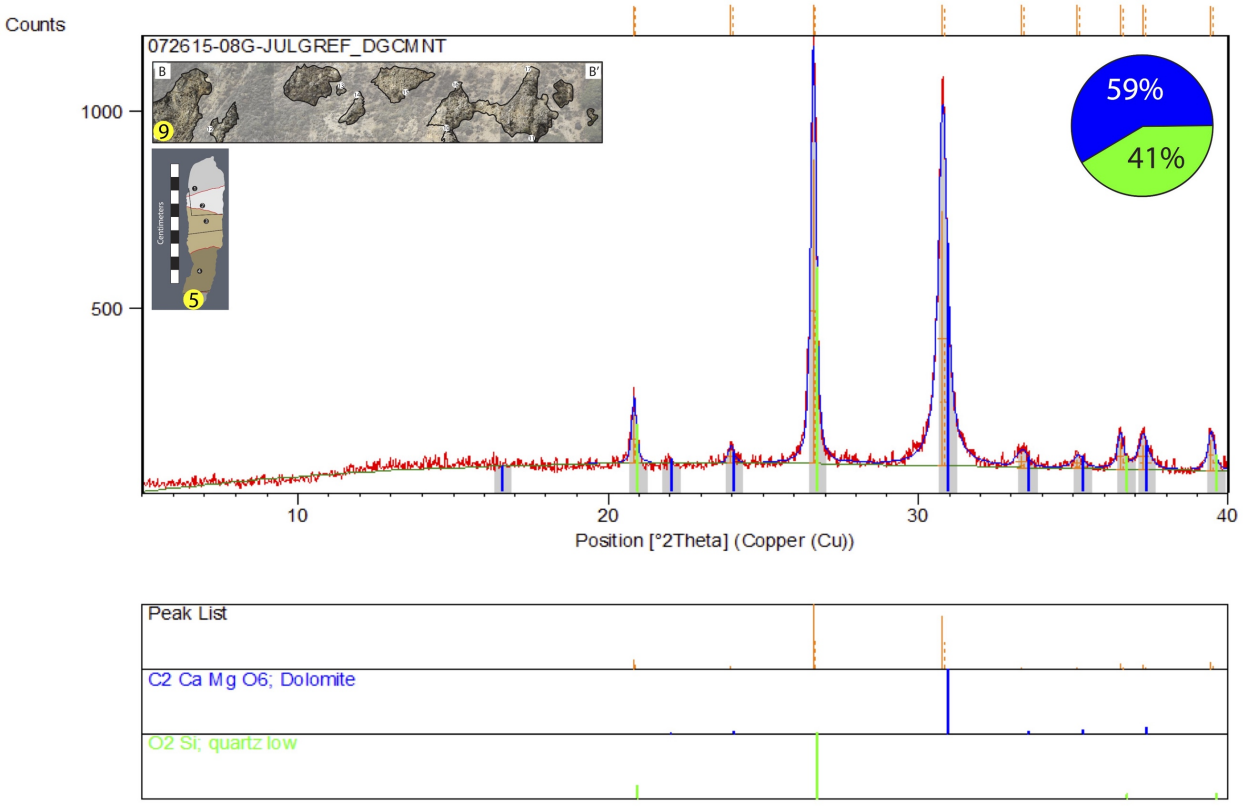
Counts
072615-08G-JULGREF_DGCMNT
B
B'
9
5
59%
41%
1000
500
10
20
30
40
Position [°2Theta] (Copper (Cu))
Peak List
C2 Ca Mg O6; Dolomite
O2 Si; quartz low

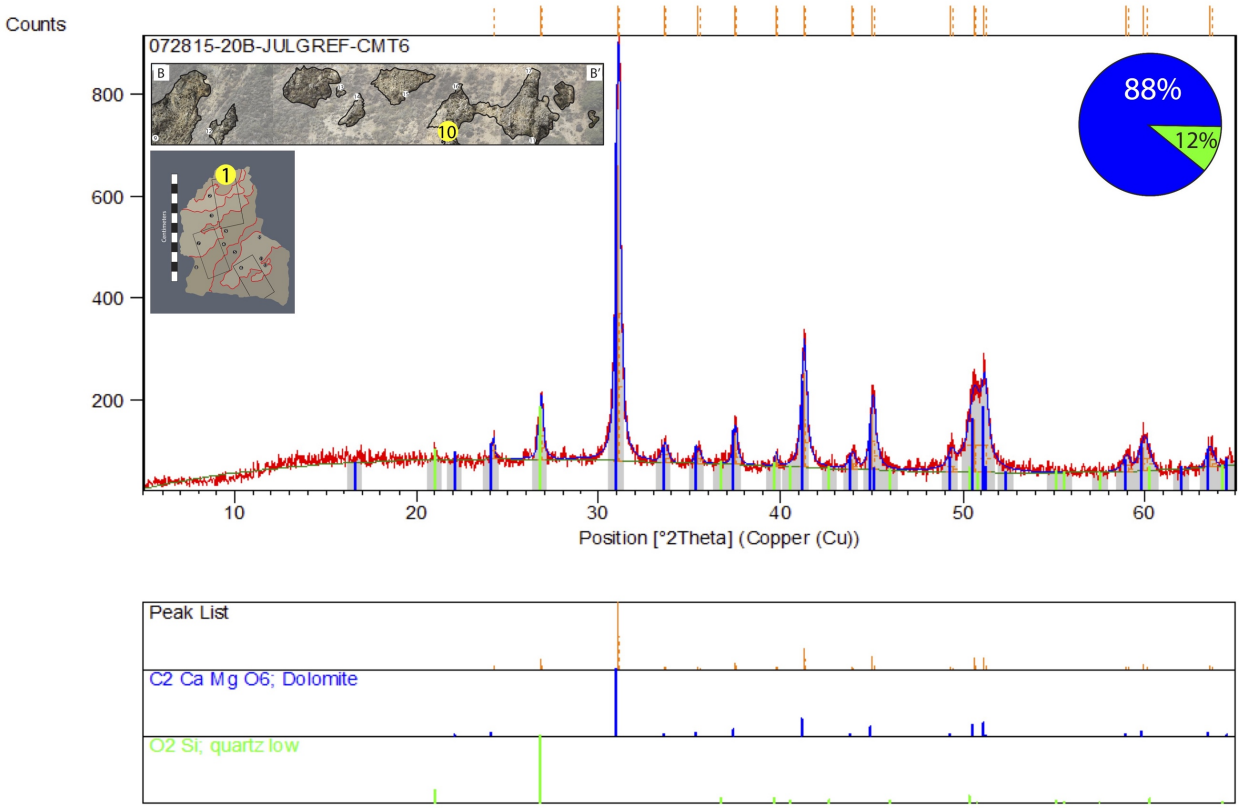
Counts
072815-20B-JULGREF-CMT6
B
B'
10
1
88%
12%
800
600
400
200
10
20
30
40
50
60
Position [°2Theta] (Copper (Cu))
Peak List
C2 Ca Mg O6; Dolomite
O2 Si; quartz low

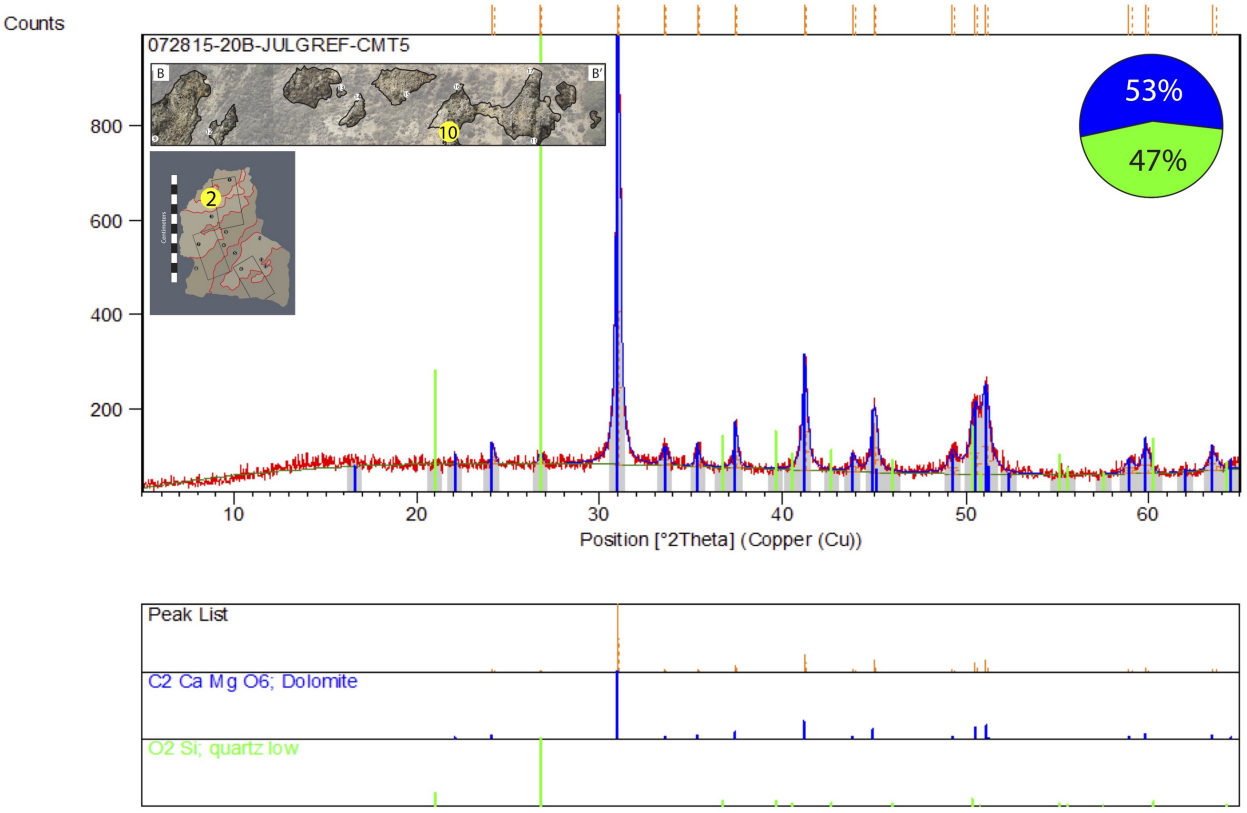
Counts
072815-20B-JULGREF-CMT5
B
B'
10
2
53%
47%
800
600
400
200
10
20
30
40
50
60
Position [°2Theta] (Copper (Cu))
Peak List
C2 Ca Mg O6; Dolomite
O2 Si; quartz low

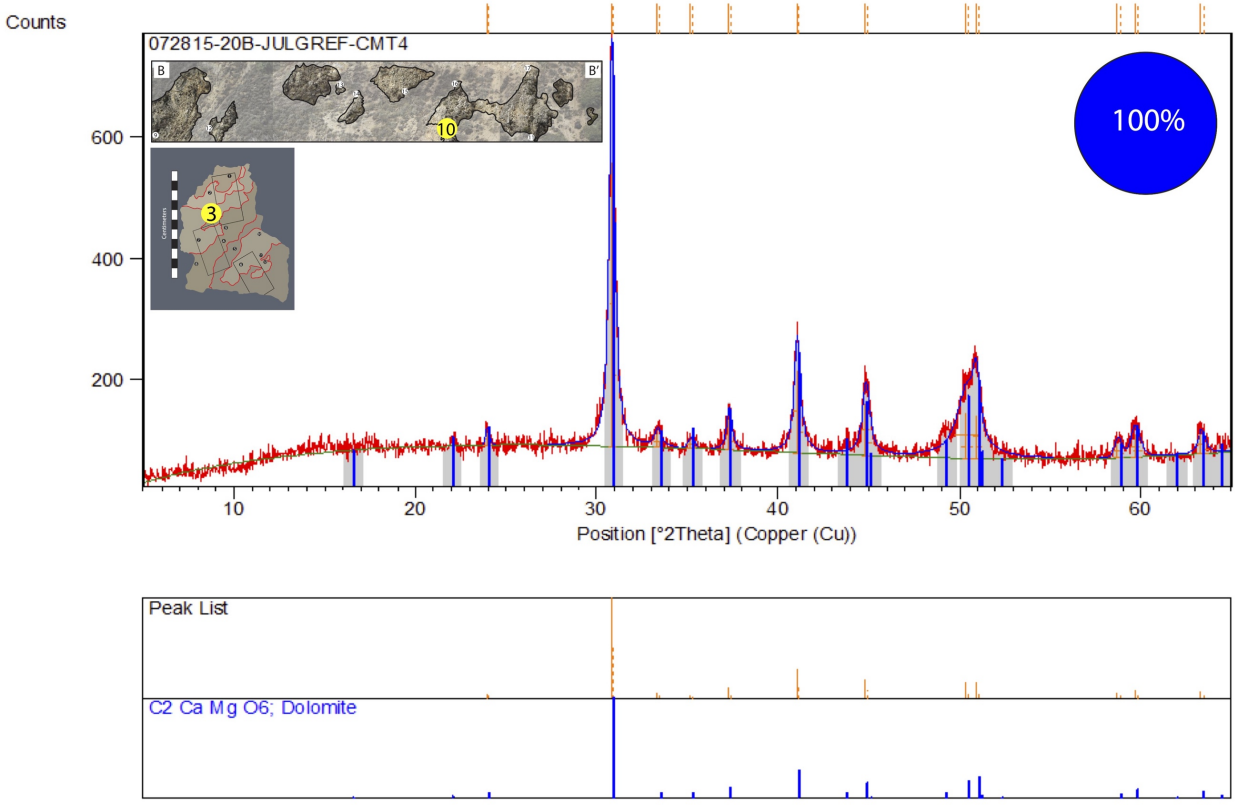
Counts
072815-20B-JULGREF-CMT4
B
B'
10
3
100%
600
400
200
10
20
30
40
50
60
Position [°2Theta] (Copper (Cu))
Peak List
C2 Ca Mg O6; Dolomite

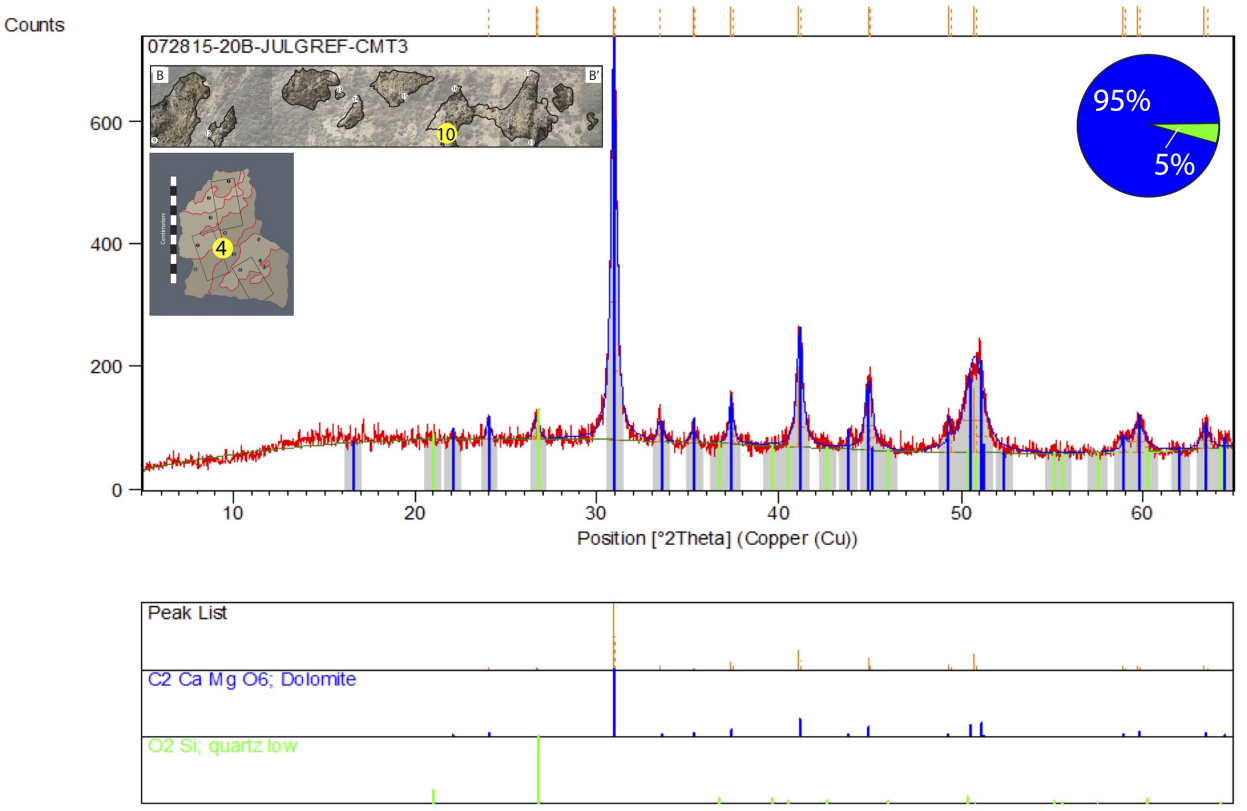
Counts
072815-20B-JULGREF-CMT3
B
B'
10
4
95%
5%
600
400
200
0
10
20
30
40
50
60
Position [°2Theta] (Copper (Cu))
Peak List
C2 Ca Mg O6; Dolomite
O2 Si; quartz low

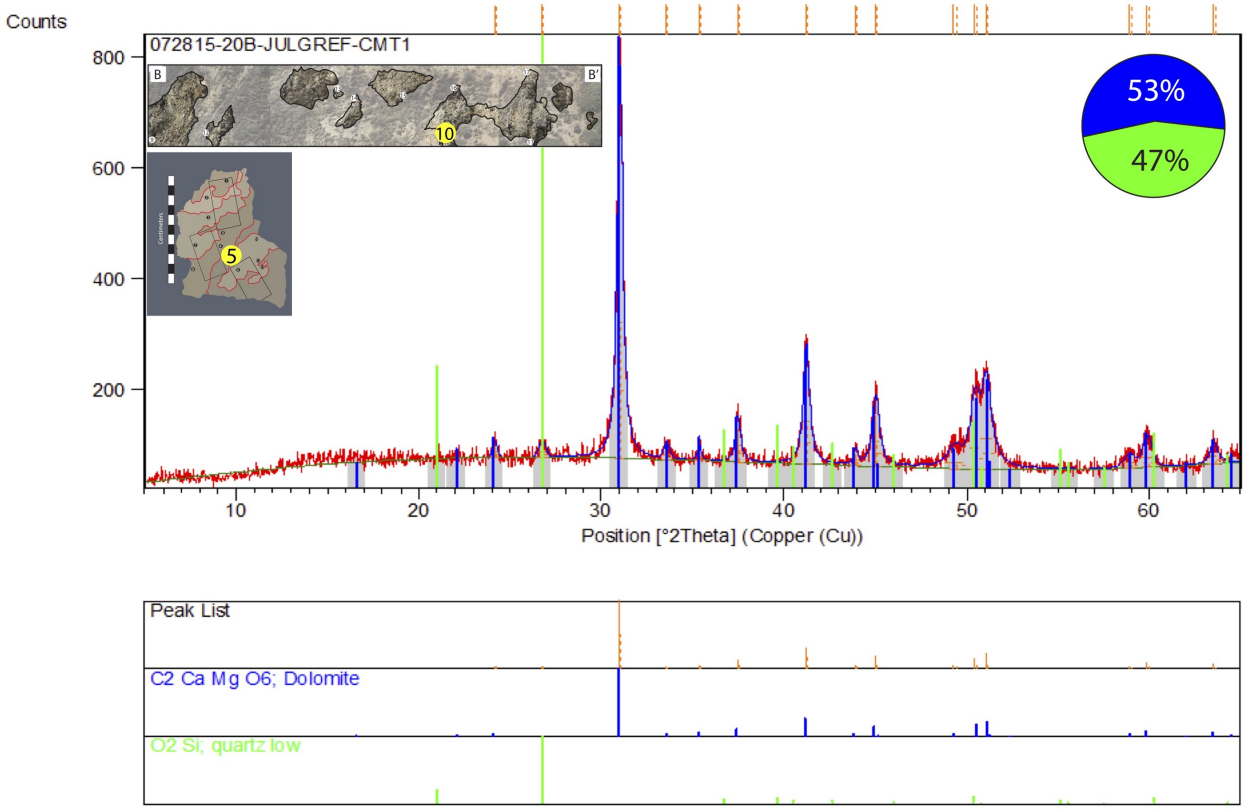
Counts
072815-20B-JULGREF-CMT1
B
B'
10
5
53%
47%
800
600
400
200
10
20
30
40
50
60
Position [°2Theta] (Copper (Cu))
Peak List
C2 Ca Mg O6; Dolomite
O2 Si; quartz low

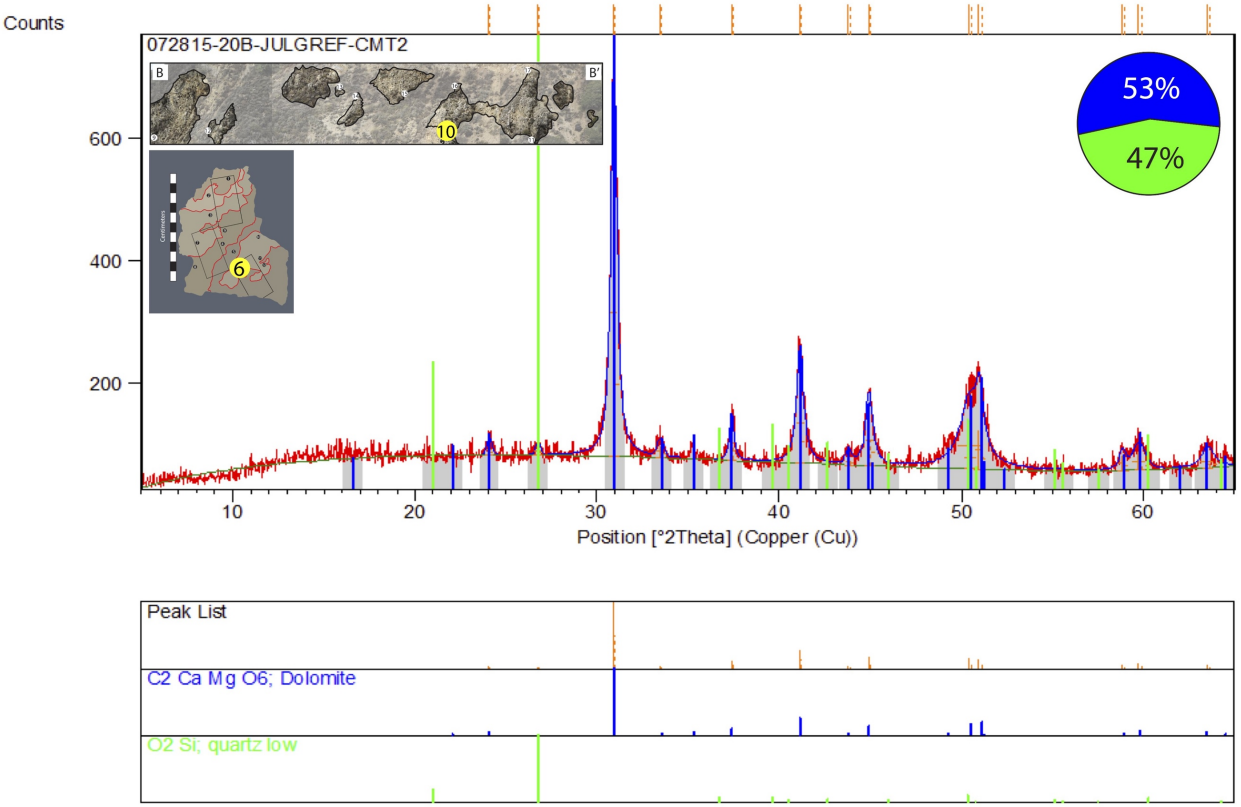
Counts
072815-20B-JULGREF-CMT2
B
B'
10
6
53%
47%
600
400
200
10
20
30
40
50
60
Position [°2Theta] (Copper (Cu))
Peak List
C2 Ca Mg O6; Dolomite
O2 Si; quartz low

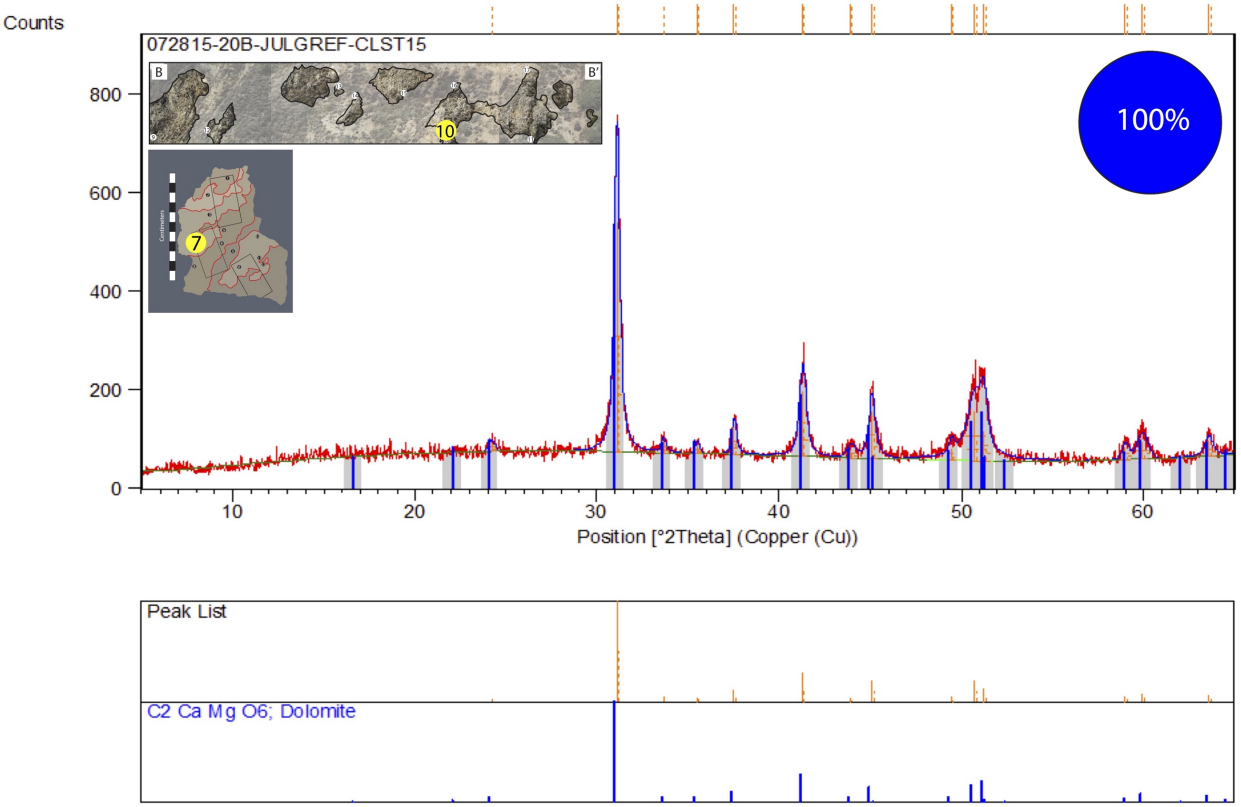
Counts
072815-20B-JULGREF-CLST15
B
B'
10
7
100%
800
600
400
200
0
10
20
30
40
50
60
Position [°2Theta] (Copper (Cu))
Peak List
C2 Ca Mg O6; Dolomite

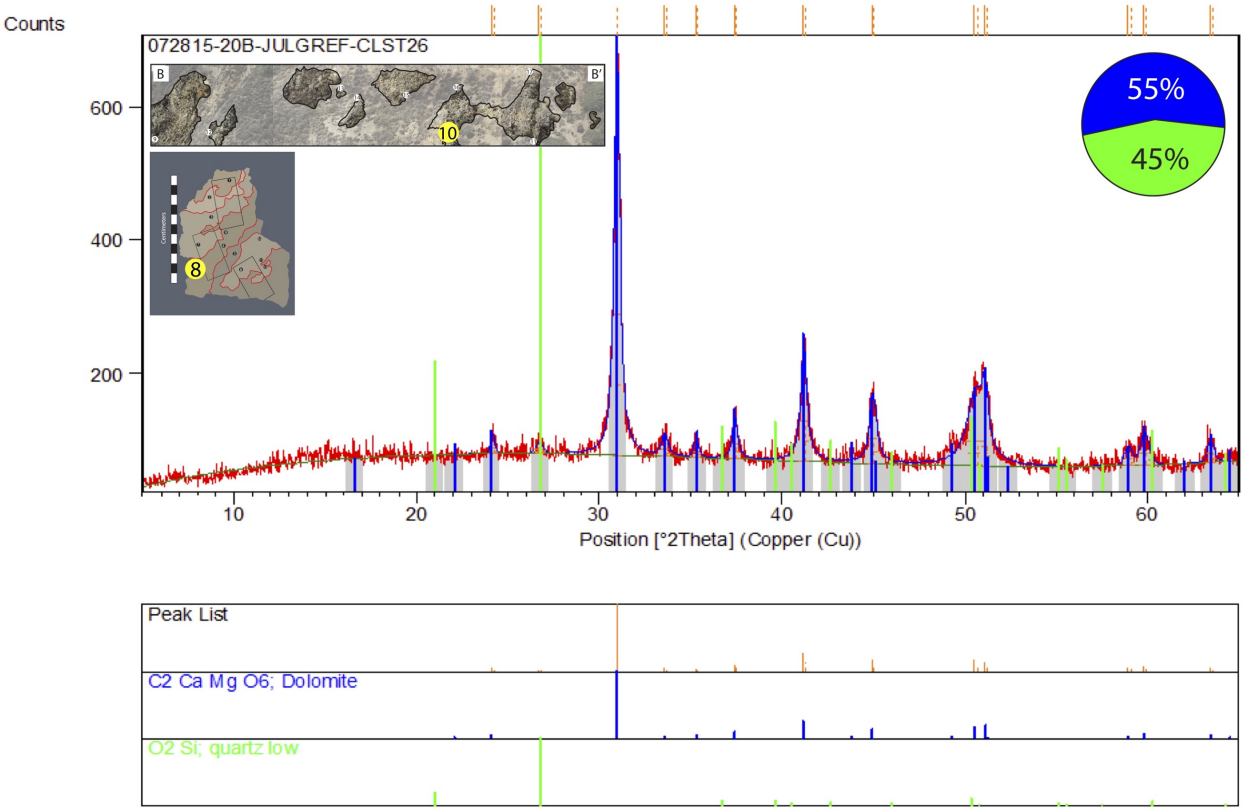
Counts
072815-20B-JULGREF-CLST26
B
B'
10
8
55%
45%
600
400
200
10
20
30
40
50
60
Position [°2Theta] (Copper (Cu))
Peak List
C2 Ca Mg O6; Dolomite
O2 Si; quartz low

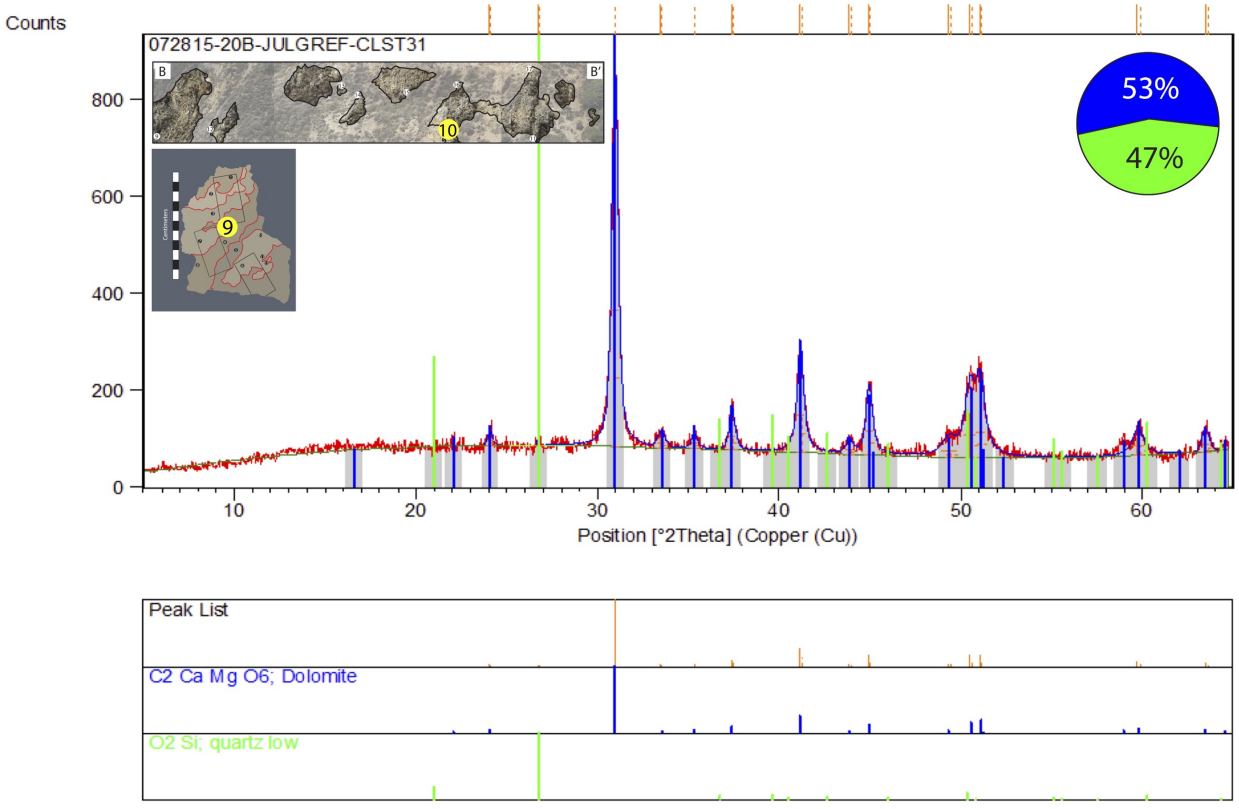
Counts
072815-20B-JULGREF-CLST31
B
B'
10
9
53%
47%
800
600
400
200
0
10
20
30
40
50
60
Position [°2Theta] (Copper (Cu))
Peak List
C2 Ca Mg O6; Dolomite
O2 Si; quartz low

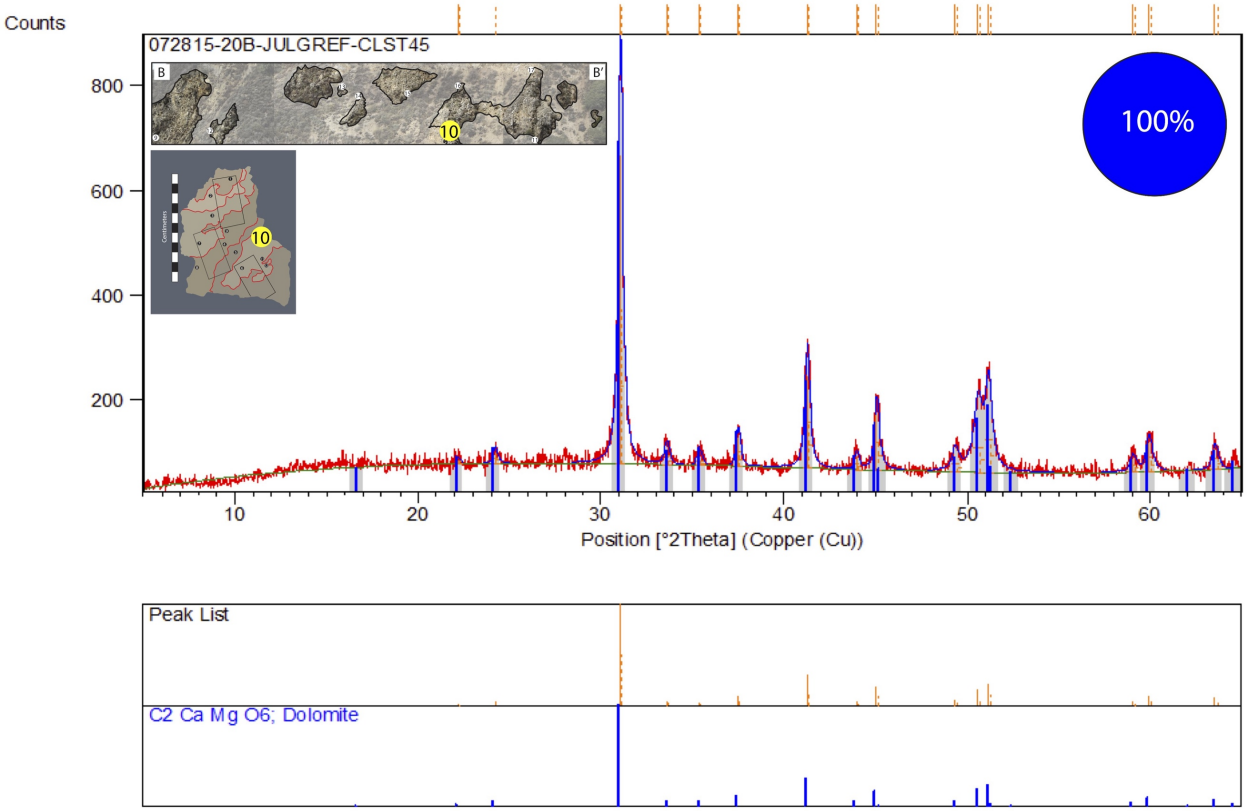
Counts
072815-20B-JULGREF-CLST45
B
B'
10
100%
800
600
400
200
10
20
30
40
50
60
Position [°2Theta] (Copper (Cu))
Peak List
C2 Ca Mg O6; Dolomite

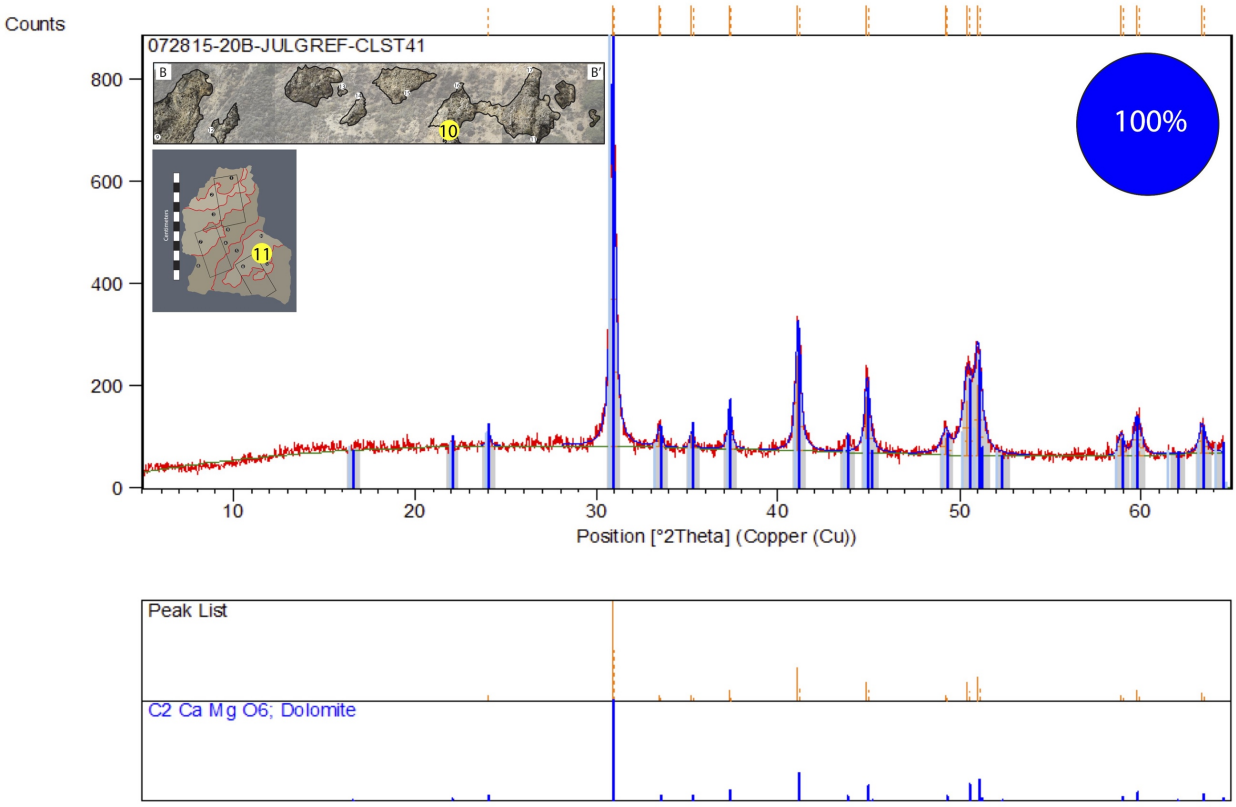
Counts
072815-20B-JULGREF-CLST41
B
B'
10
11
100%
800
600
400
200
0
10
20
30
40
50
60
Position [°2Theta] (Copper (Cu))
Peak List
C2 Ca Mg O6; Dolomite

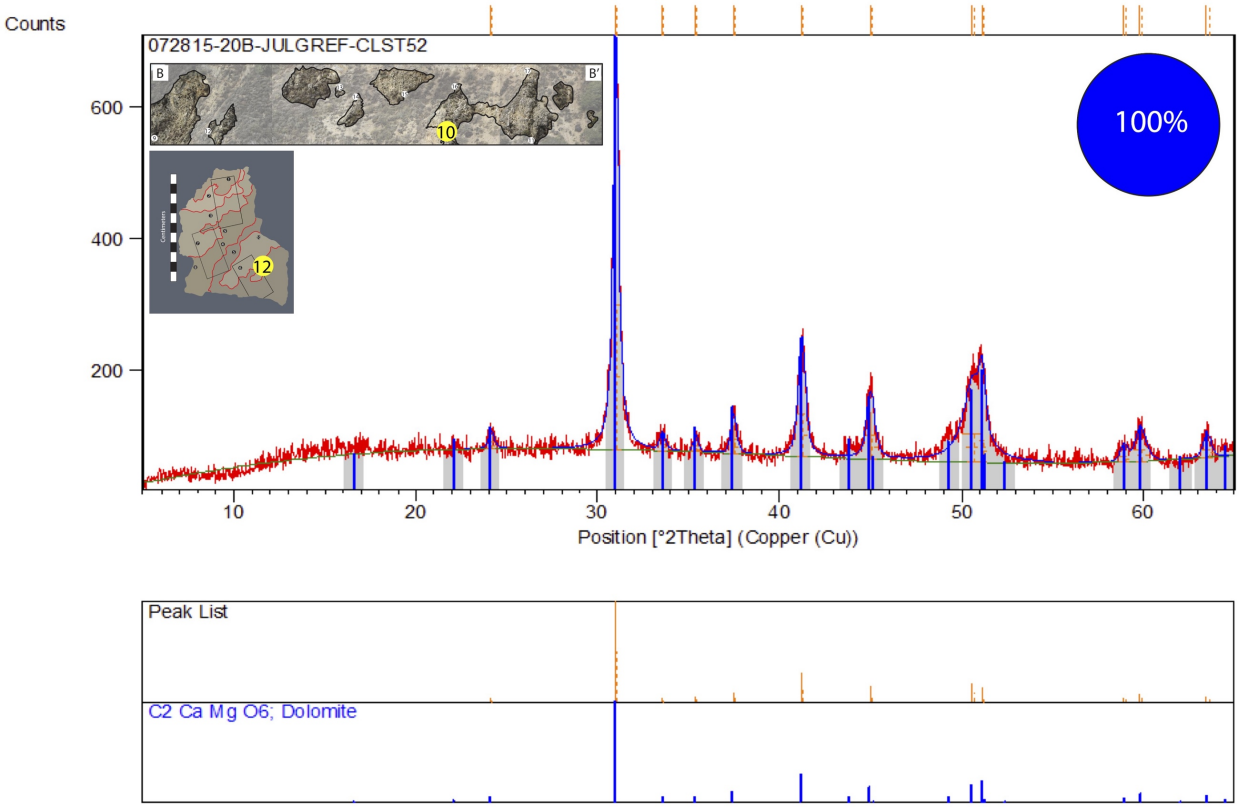
Counts
072815-20B-JULGREF-CLST52
B
B'
10
12
100%
600
400
200
10
20
30
40
50
60
Position [°2Theta] (Copper (Cu))
Peak List
C2 Ca Mg O6; Dolomite

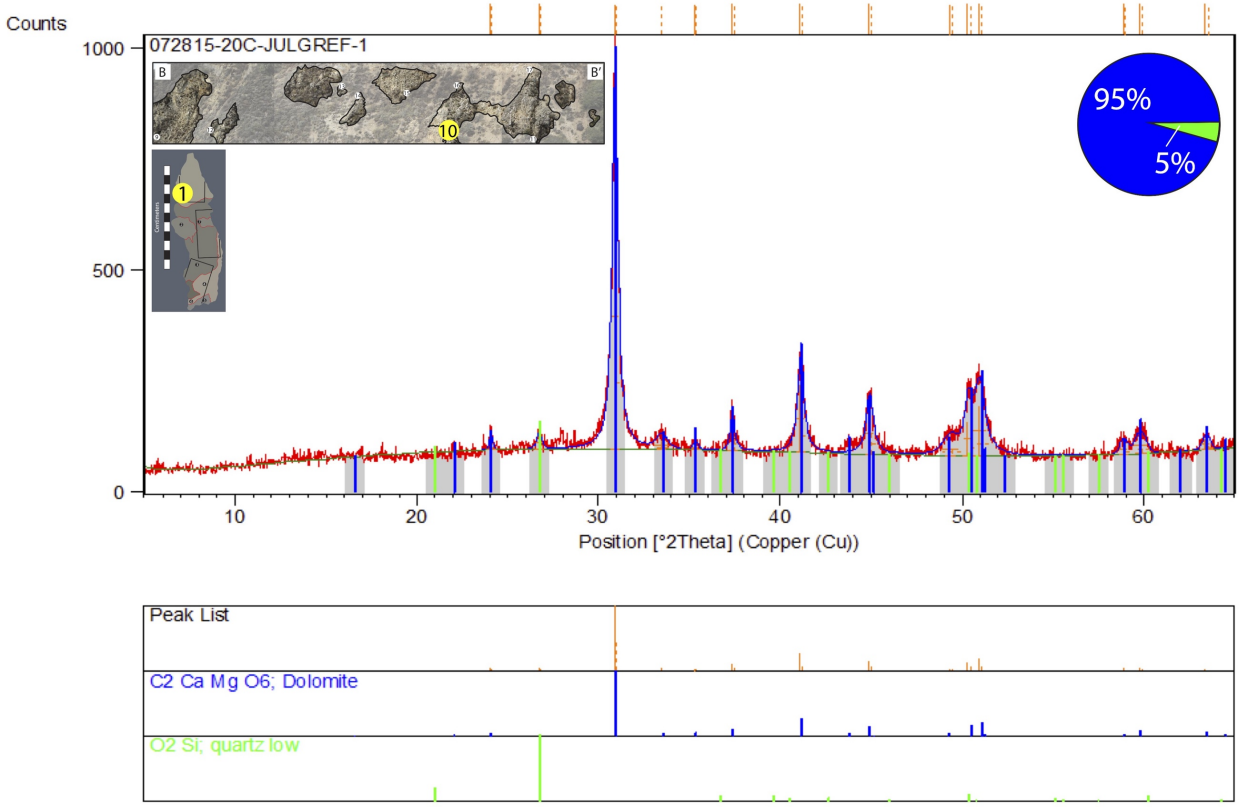
Counts
072815-20C-JULGREF-1
B
B'
10
1
95%
5%
1000
500
0
10
20
30
40
50
60
Position [°2Theta] (Copper (Cu))
Peak List
C2 Ca Mg O6; Dolomite
O2 Si; quartz low

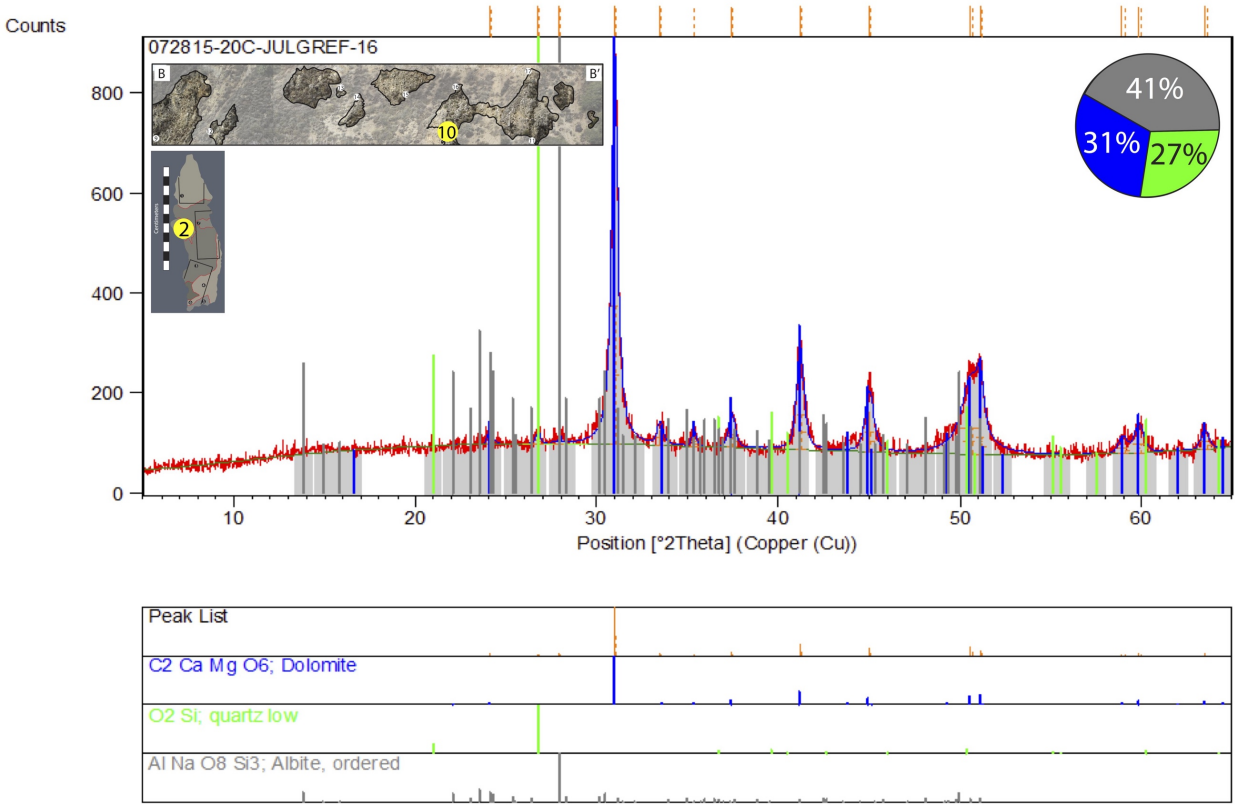
Counts
072815-20C-JULGREF-16
B
B'
10
2
41%
31%
27%
800
600
400
200
0
10
20
30
40
50
60
Position [°2Theta] (Copper (Cu))
Peak List
C2 Ca Mg O6; Dolomite
O2 Si; quartz low
Al Na O8 Si3; Albite, ordered

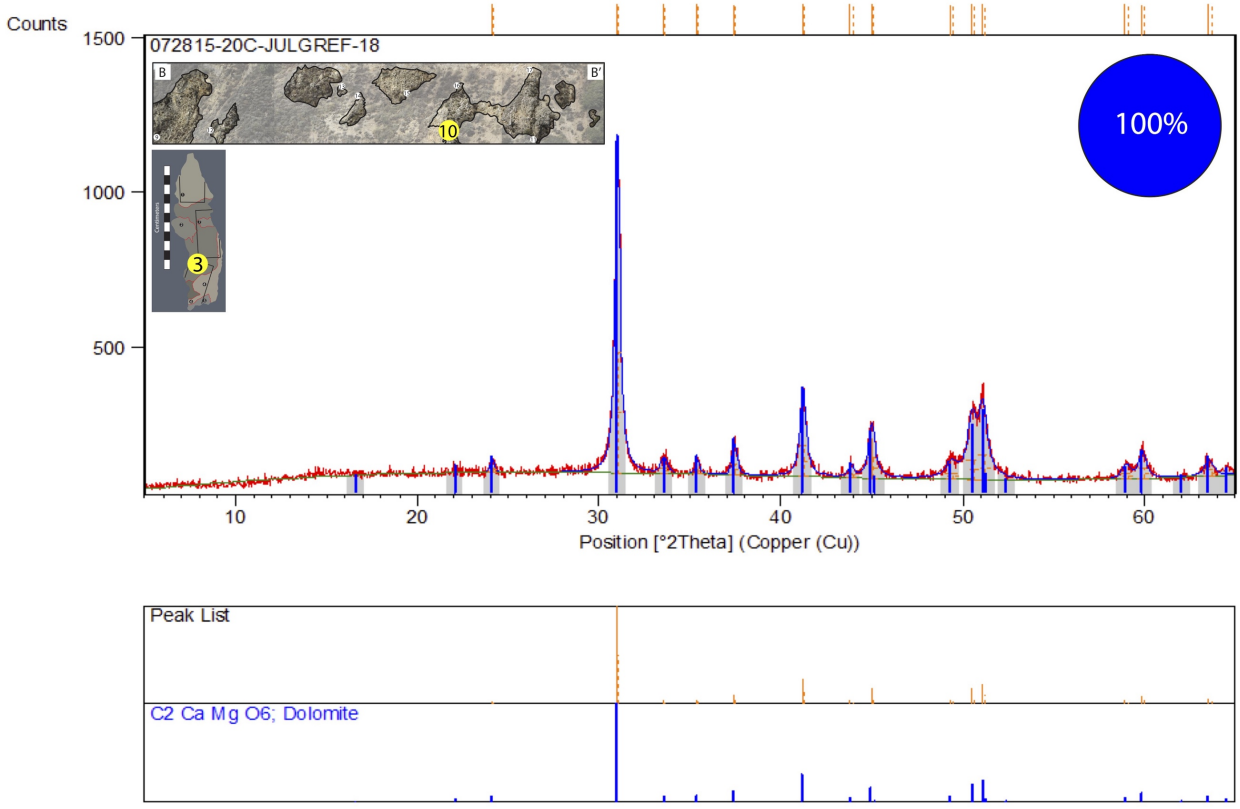
Counts
1500
1000
500
072815-20C-JULGREF-18
B
B'
10
3
100%
10
20
30
40
50
60
Position [°2Theta] (Copper (Cu))
Peak List
C2 Ca Mg O6; Dolomite

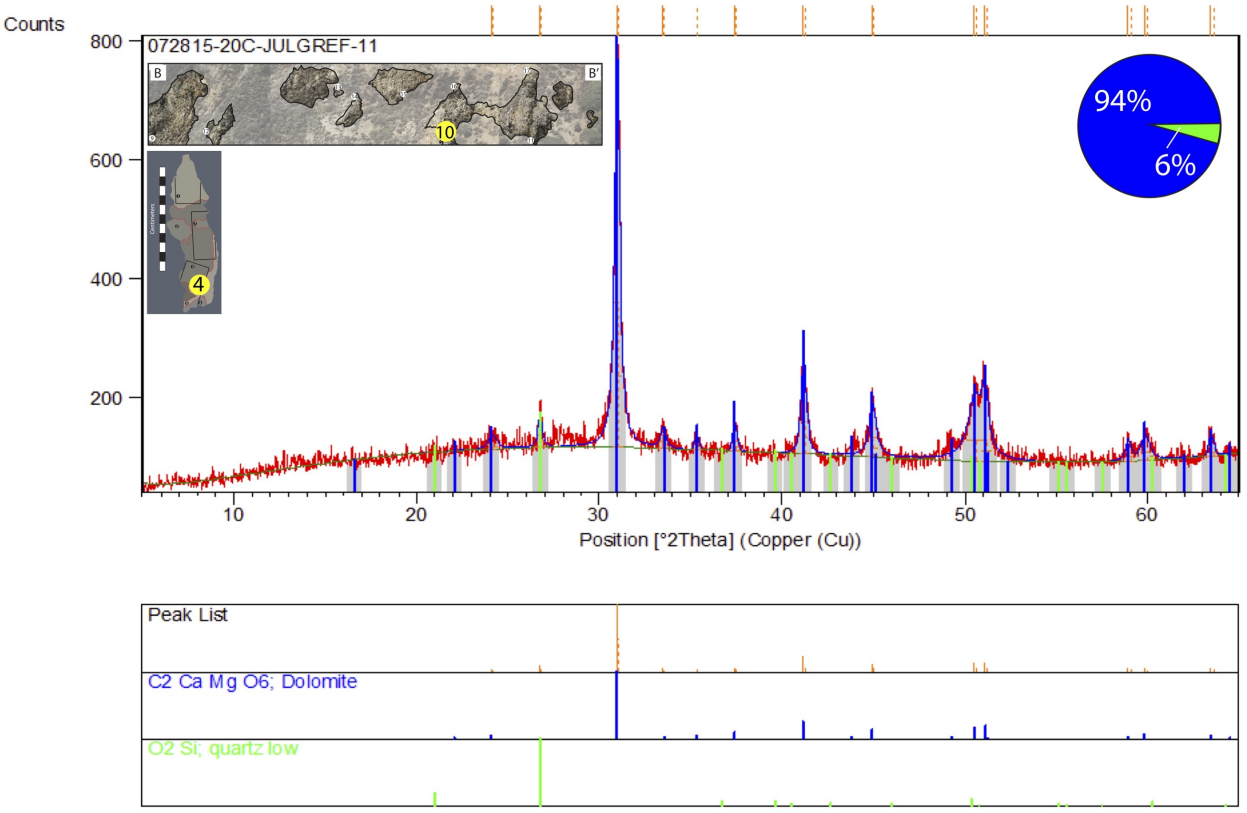
Counts
072815-20C-JULGREF-11
B
B'
10
4
94%
6%
800
600
400
200
10
20
30
40
50
60
Position [°2Theta] (Copper (Cu))
Peak List
C2 Ca Mg O6; Dolomite
O2 Si; quartz low

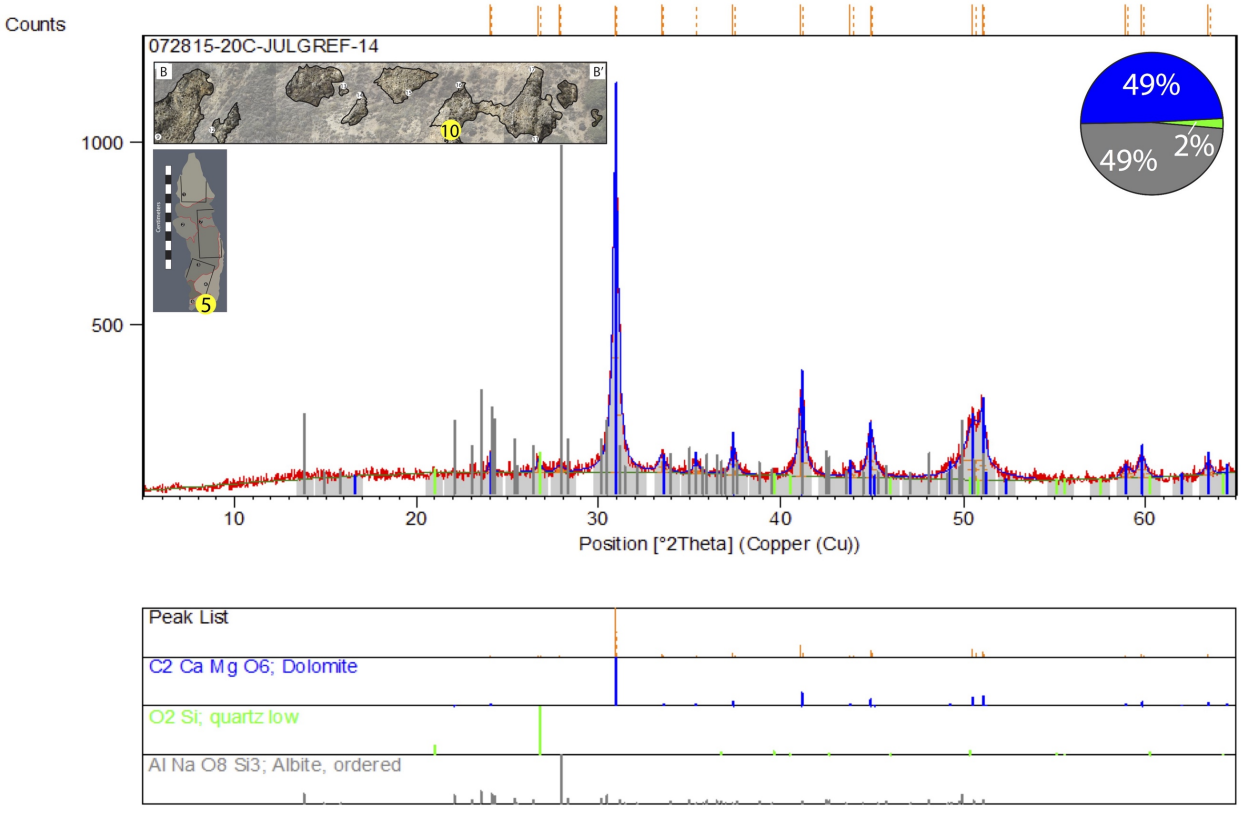
Counts
072815-20C-JULGREF-14
B
B'
10
5
49%
2%
49%
1000
500
10
20
30
40
50
60
Position [°2Theta] (Copper (Cu))
Peak List
C2 Ca Mg O6; Dolomite
O2 Si; quartz low
Al Na O8 Si3; Albite, ordered

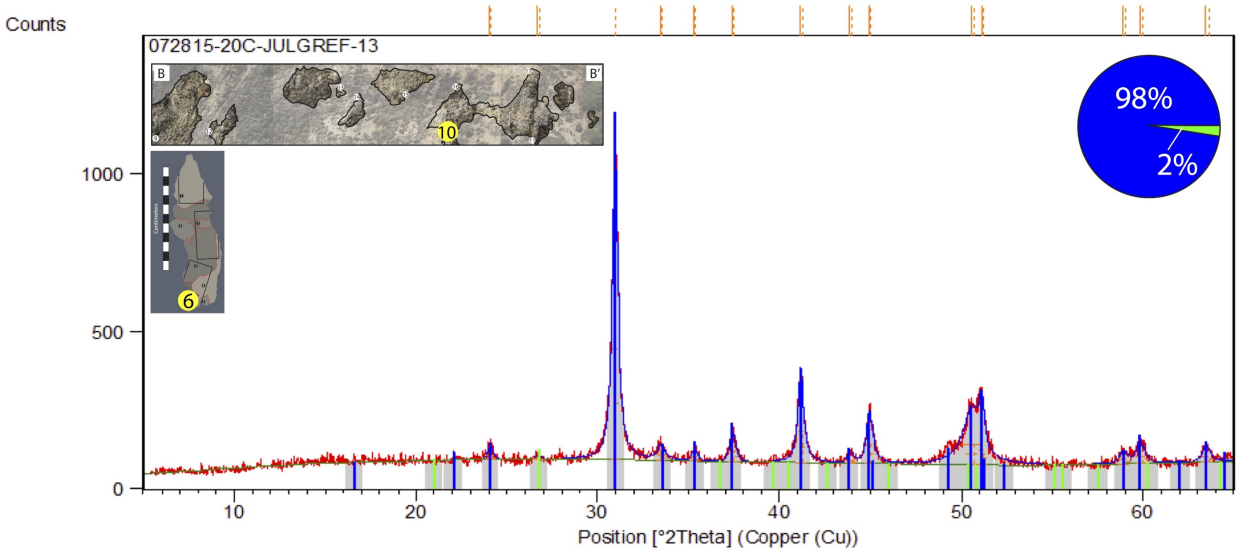
Counts
072815-20C-JULGREF-13
B
B'
10
6
98%
2%
1000
500
0
10
20
30
40
50
60
Position [°2Theta] (Copper (Cu))

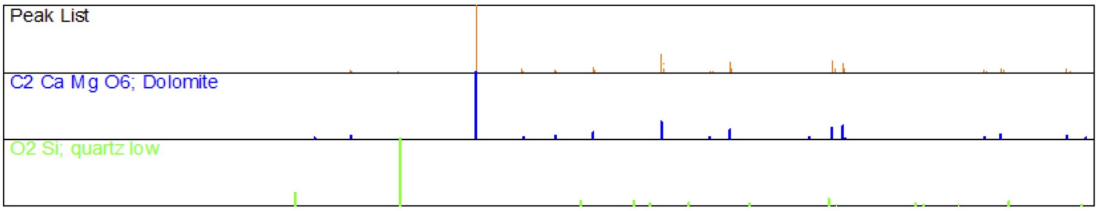
Peak List
C2 Ca Mg O6; Dolomite
O2 Si; quartz low

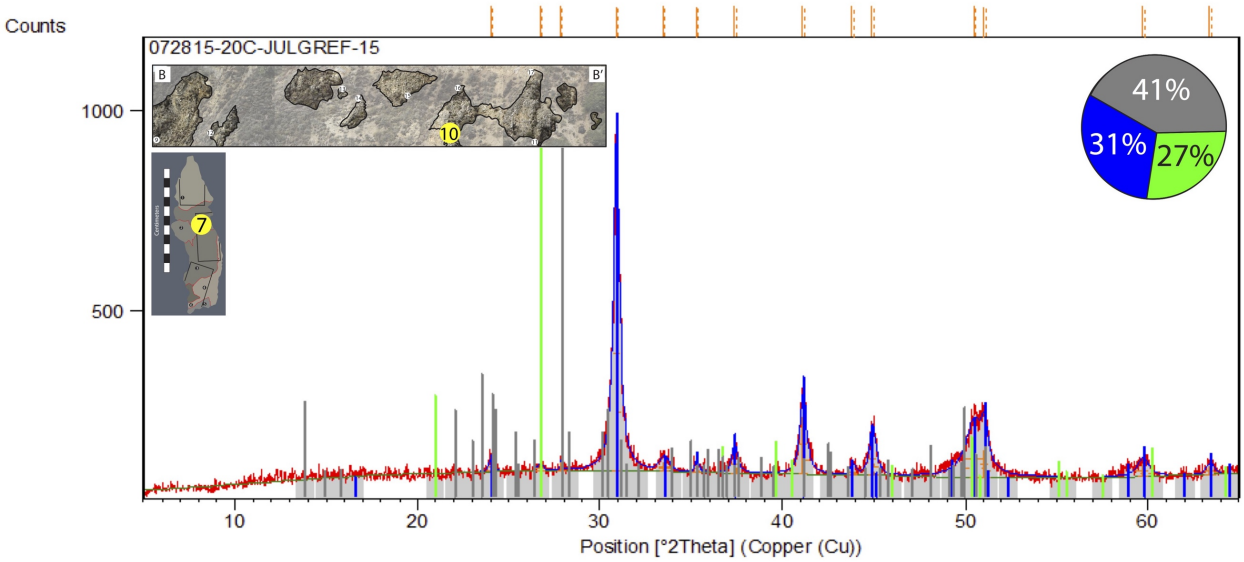
Counts
072815-20C-JULGREF-15
B
B'
10
7
41%
31%
27%
1000
500
10
20
30
40
50
60
Position [°2Theta] (Copper (Cu))

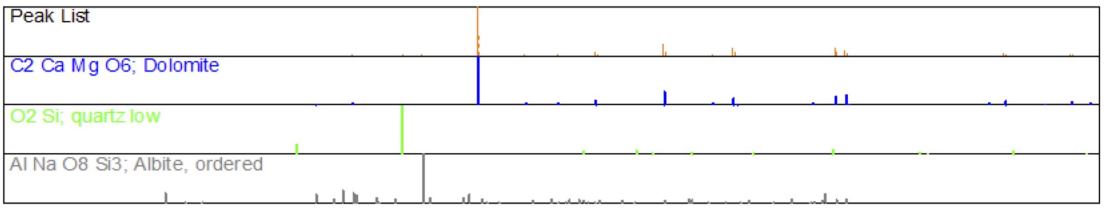
Peak List
C2 Ca Mg O6; Dolomite
O2 Si; quartz low
Al Na O8 Si3; Albite, ordered

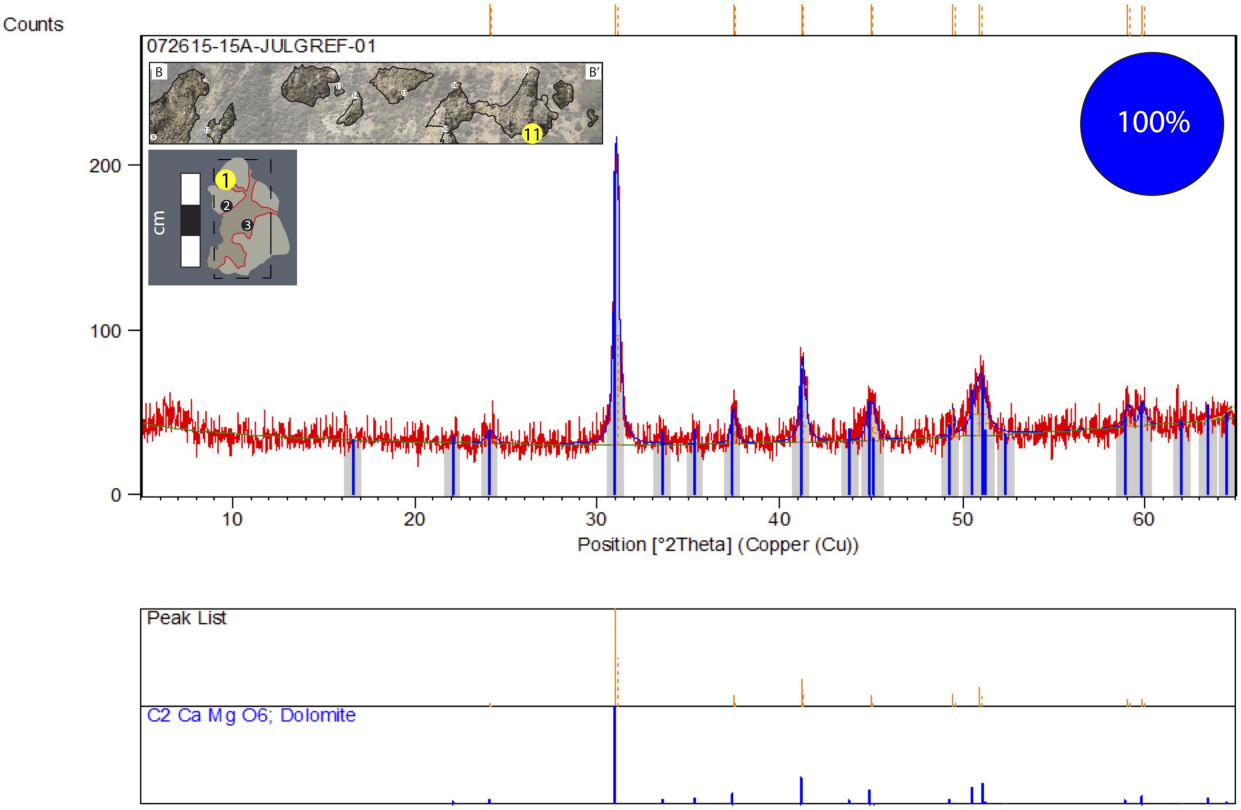
Counts
072615-15A-JULGREF-01
B
B'
11
100%
cm
1
2
3
200
100
0
10
20
30
40
50
60
Position [°2Theta] (Copper (Cu))
Peak List
C2 Ca Mg O6; Dolomite

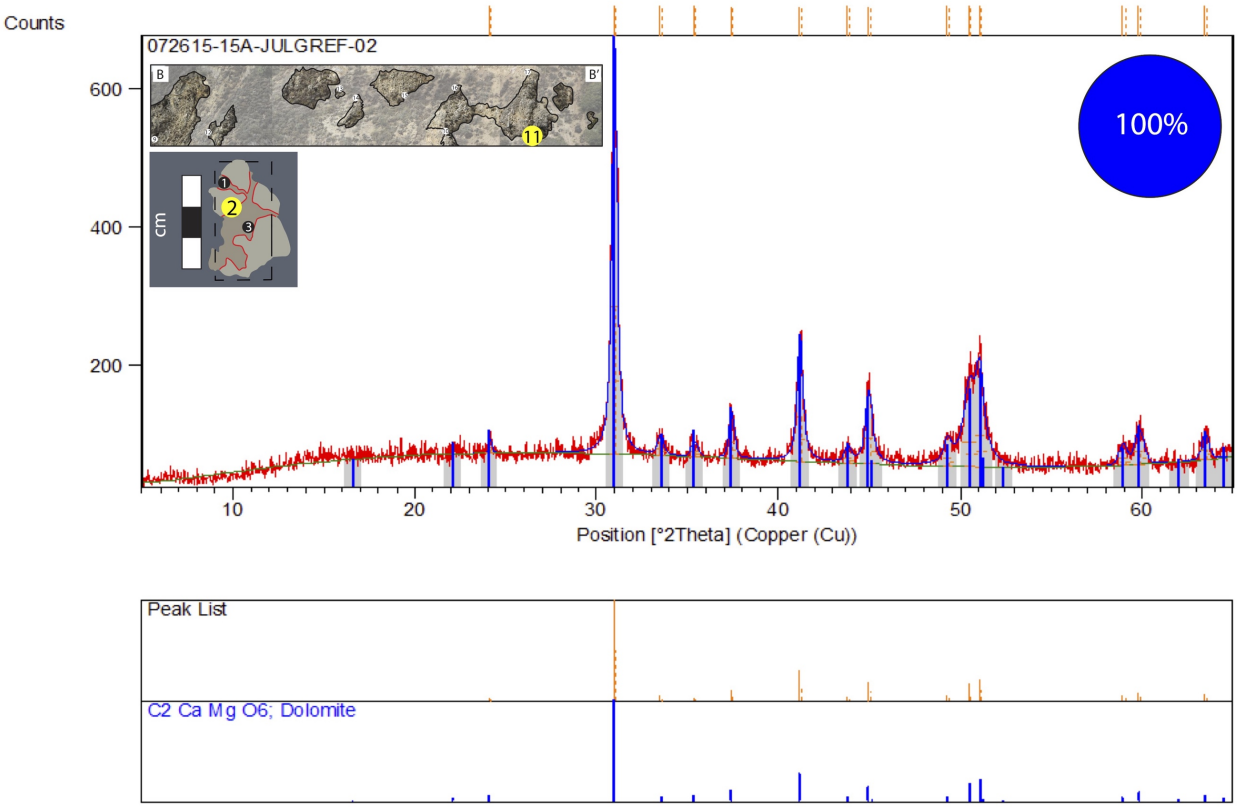
Counts
072615-15A-JULGREF-02
B
B'
11
100%
cm
1
2
3
600
400
200
10
20
30
40
50
60
Position [°2Theta] (Copper (Cu))
Peak List
C2 Ca Mg O6; Dolomite

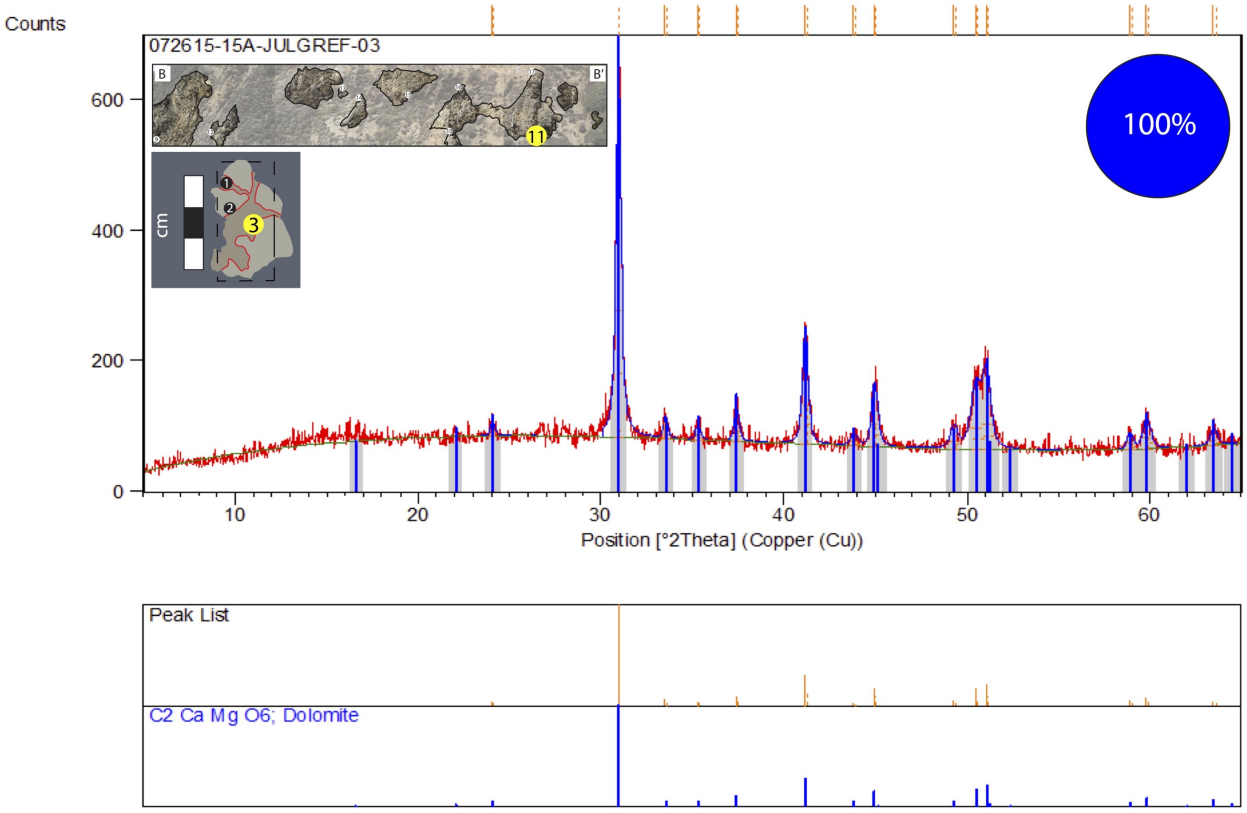
Counts
072615-15A-JULGREF-03
B
B'
11
cm
1
2
3
100%
600
400
200
0
10
20
30
40
50
60
Position [°2Theta] (Copper (Cu))
Peak List
C2 Ca Mg O6; Dolomite

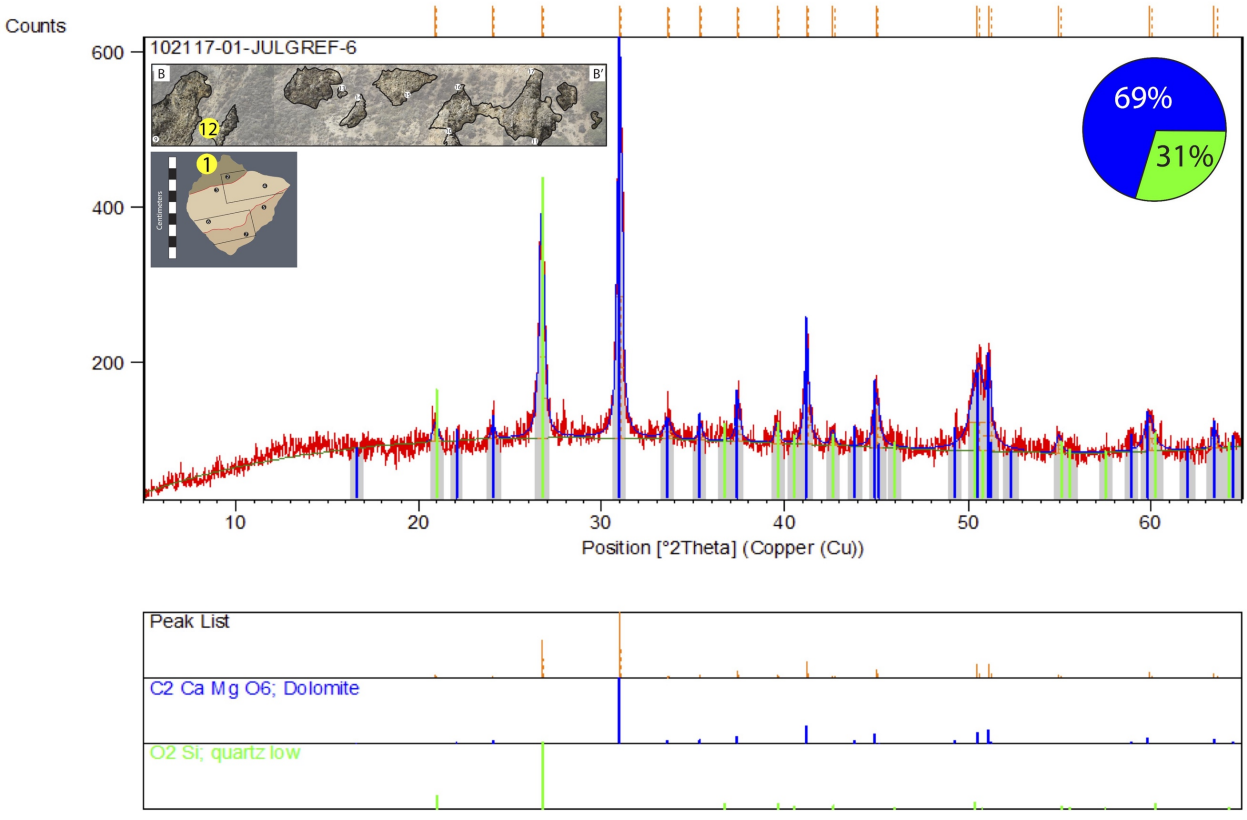
Counts
102117-01-JULGREF-6
B
B'
12
1
69%
31%
600
400
200
10
20
30
40
50
60
Position [°2Theta] (Copper (Cu))
Peak List
C2 Ca Mg O6; Dolomite
O2 Si; quartz low

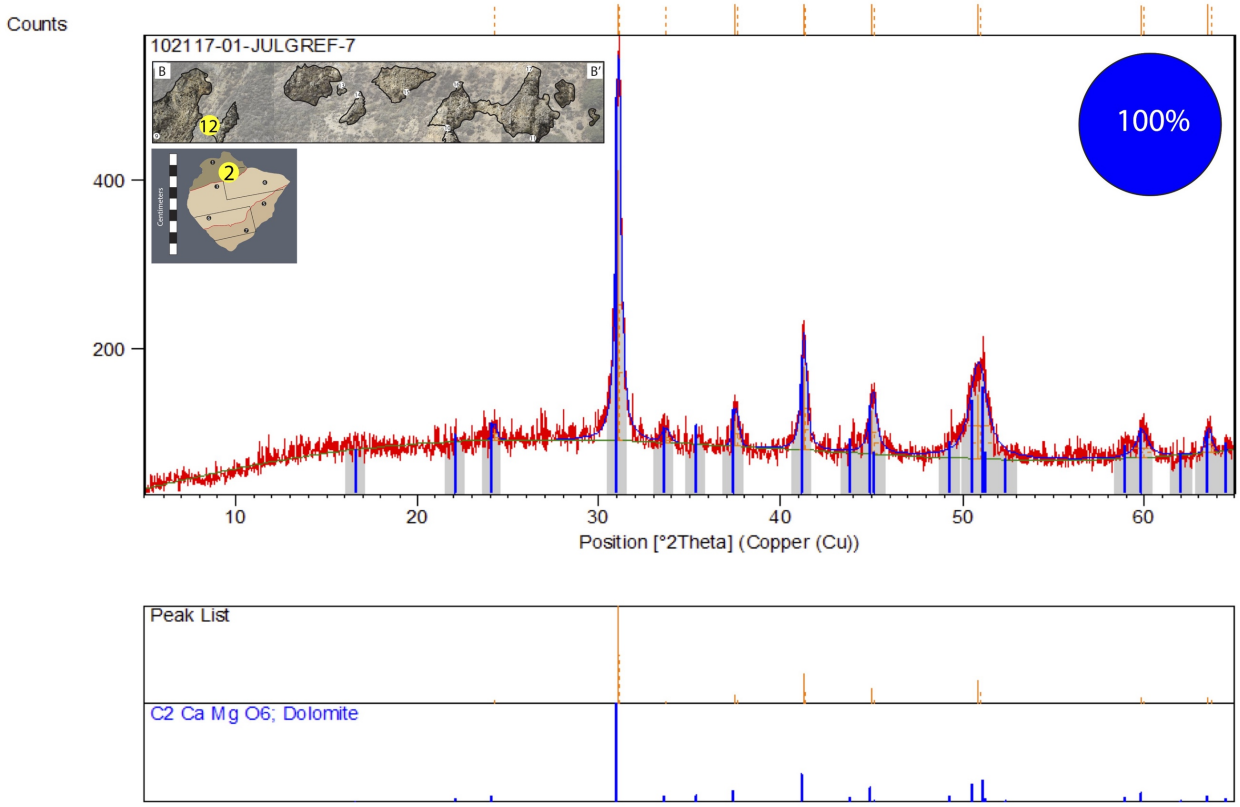
Counts
102117-01-JULGREF-7
B
B'
12
2
100%
400
200
10
20
30
40
50
60
Position [°2Theta] (Copper (Cu))
Peak List
C2 Ca Mg O6; Dolomite

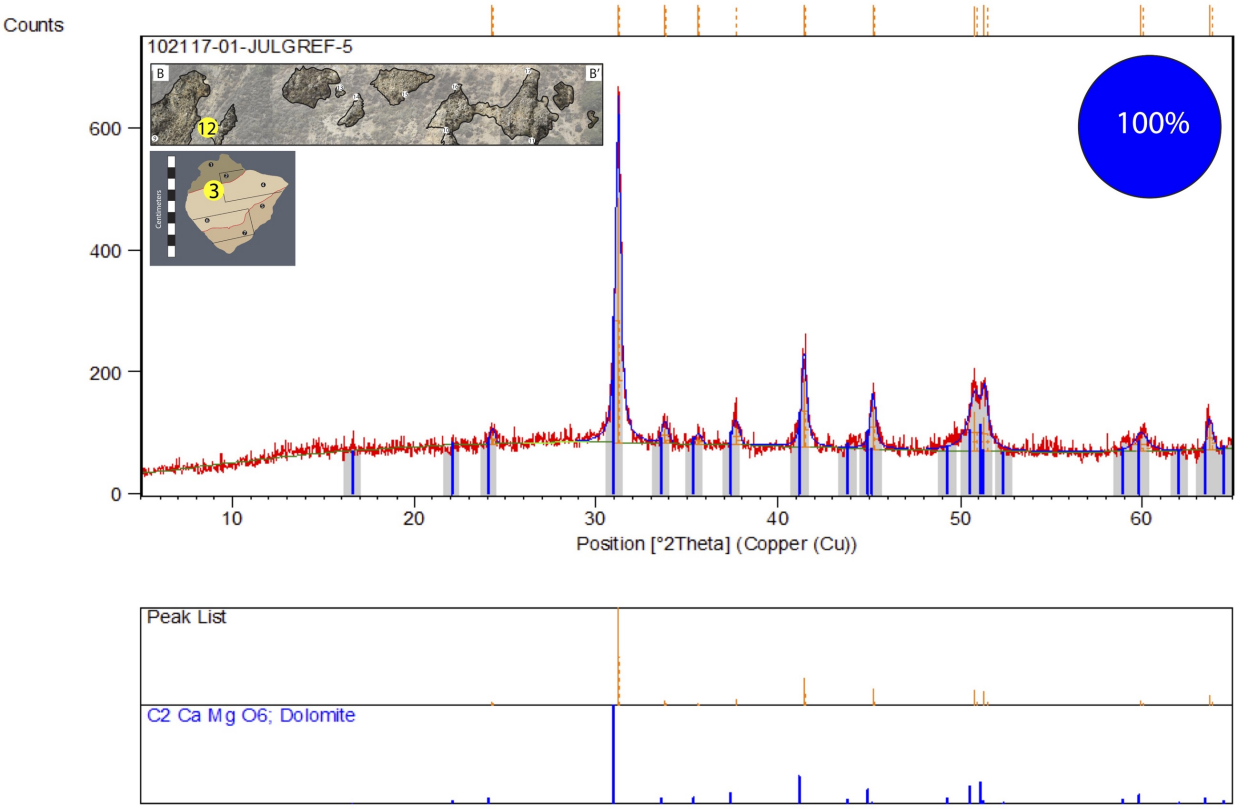
Counts
102117-01-JULGREF-5
B
B'
12
3
100%
600
400
200
0
10
20
30
40
50
60
Position [°2Theta] (Copper (Cu))
Peak List
C2 Ca Mg O6; Dolomite

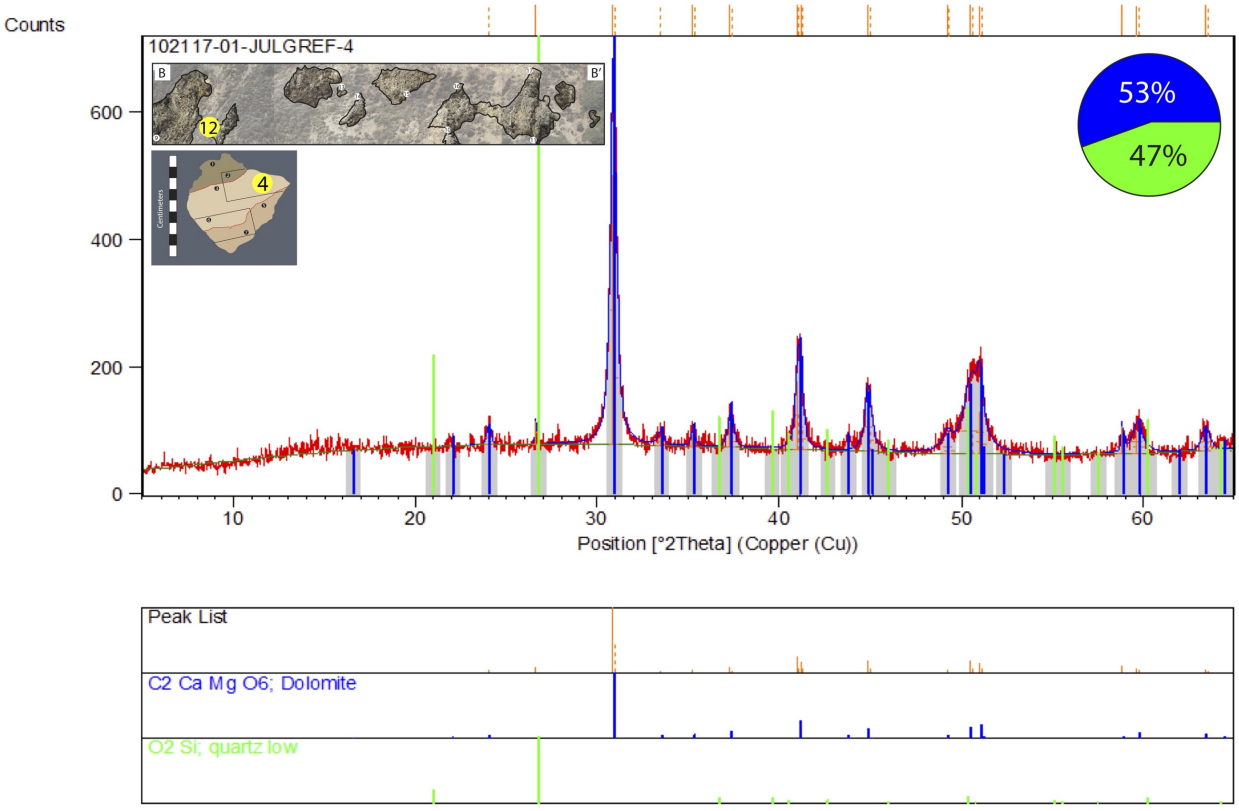
Counts
102117-01-JULGREF-4
B
B'
12
4
53%
47%
600
400
200
0
10
20
30
40
50
60
Position [°2Theta] (Copper (Cu))
Peak List
C2 Ca Mg O6; Dolomite
O2 Si; quartz low

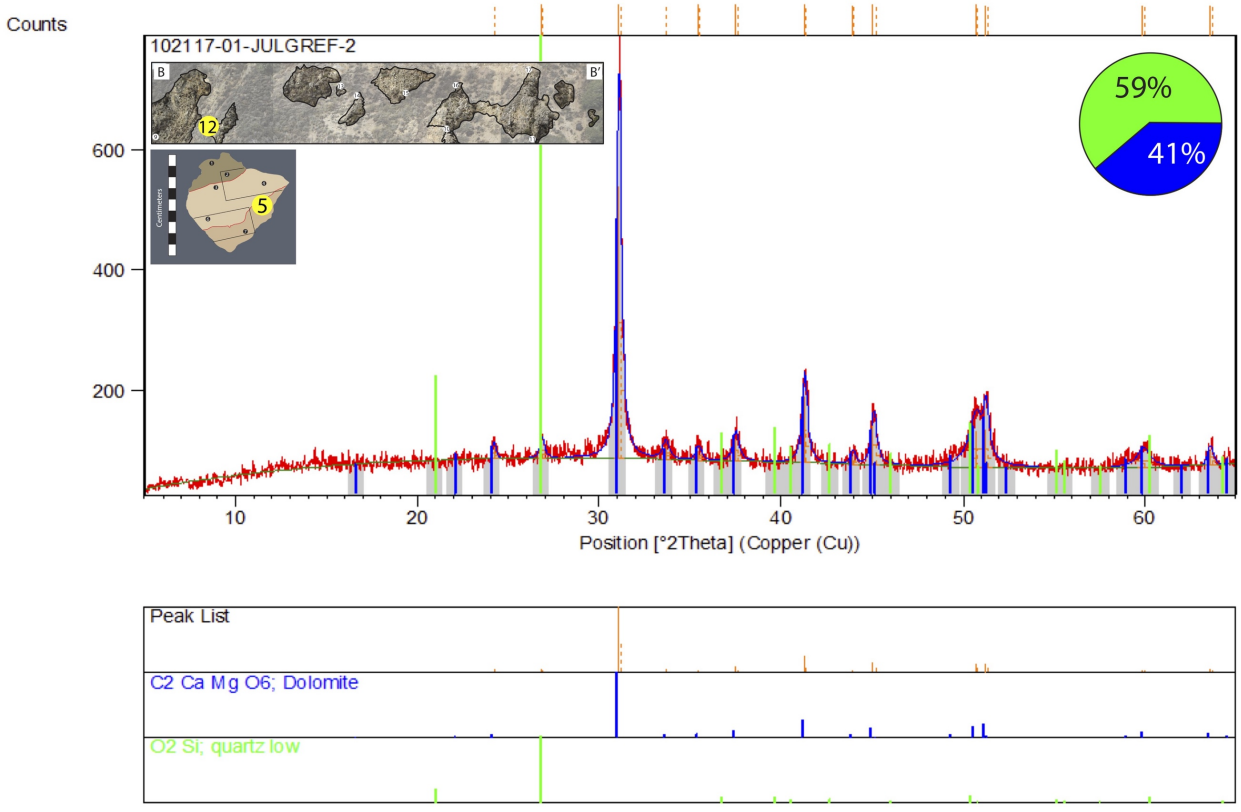
Counts
102117-01-JULGREF-2
B
B'
12
5
59%
41%
600
400
200
10
20
30
40
50
60
Position [°2Theta] (Copper (Cu))
Peak List
C2 Ca Mg O6; Dolomite
O2 Si; quartz low

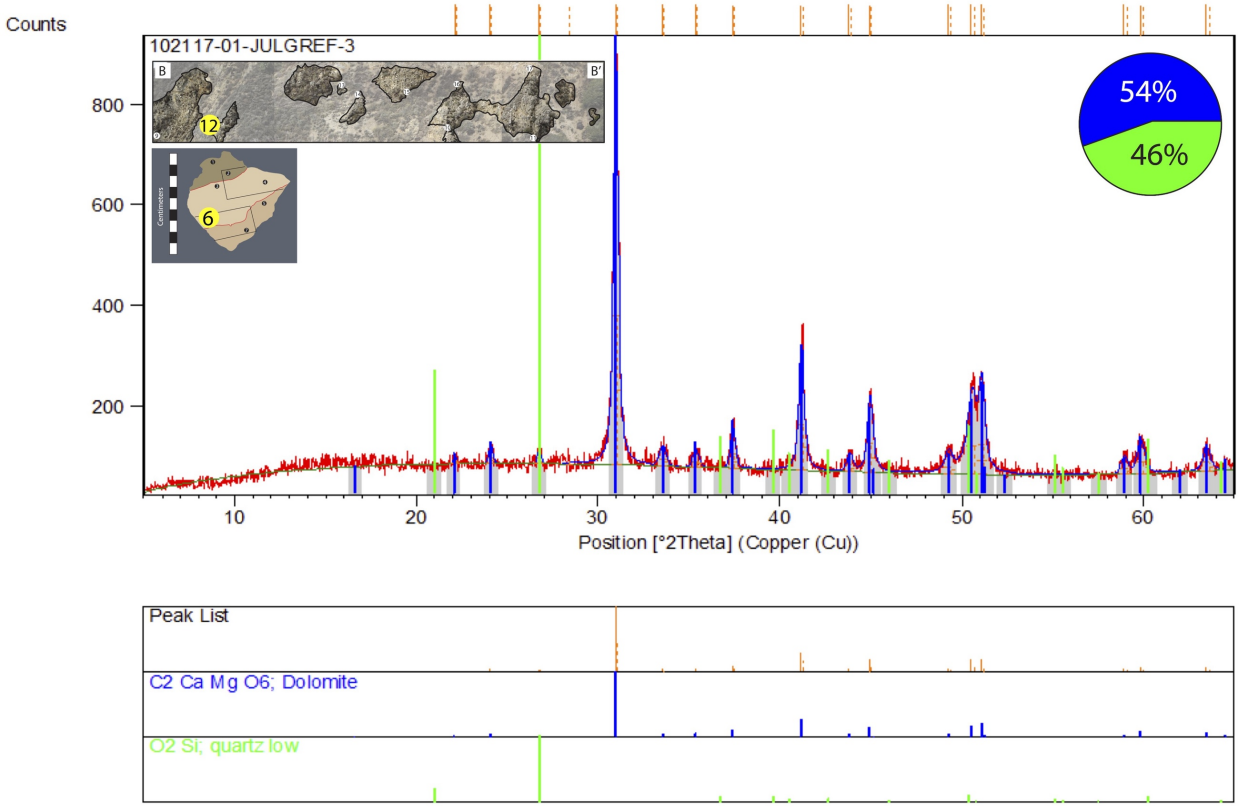
Counts
102117-01-JULGREF-3
B
B'
12
6
54%
46%
800
600
400
200
10
20
30
40
50
60
Position [°2Theta] (Copper (Cu))
Peak List
C2 Ca Mg O6; Dolomite
O2 Si; quartz low

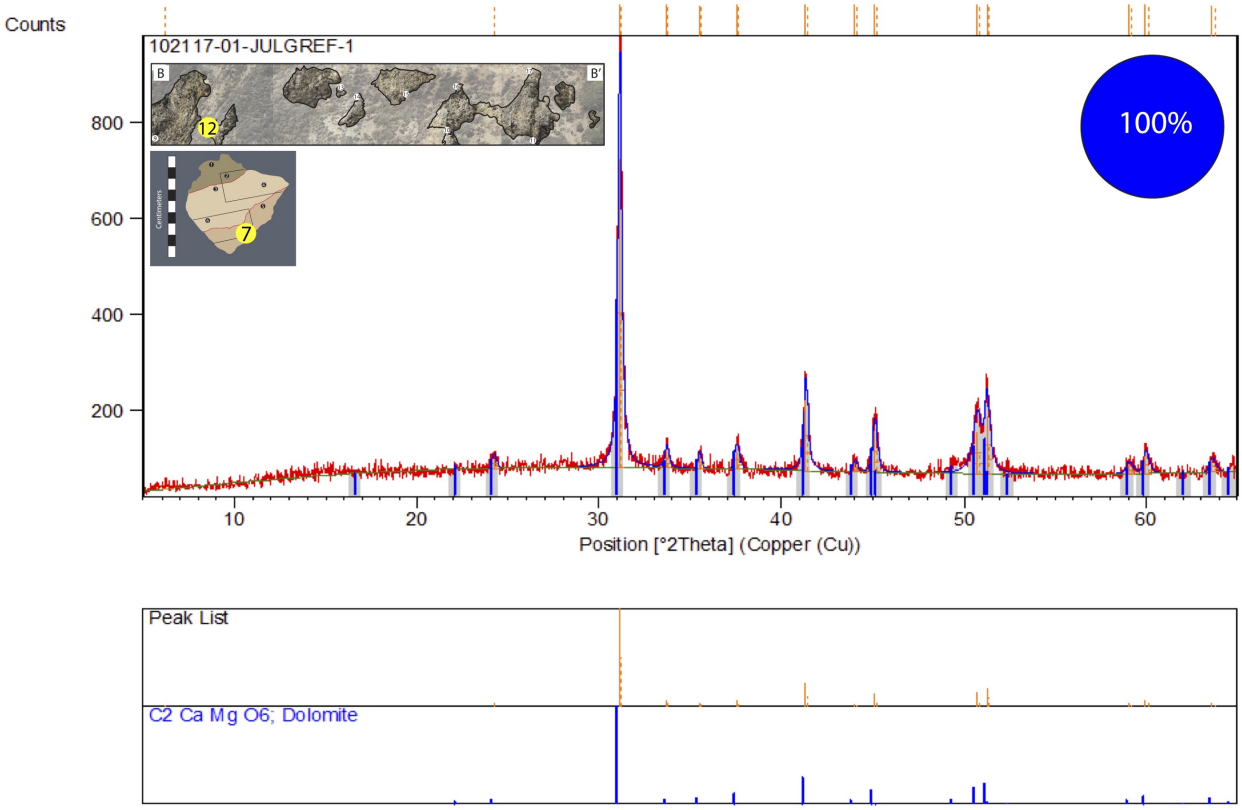
Counts
102117-01-JULGREF-1
B
B'
12
7
100%
800
600
400
200
10
20
30
40
50
60
Position [°2Theta] (Copper (Cu))
Peak List
C2 Ca Mg O6; Dolomite

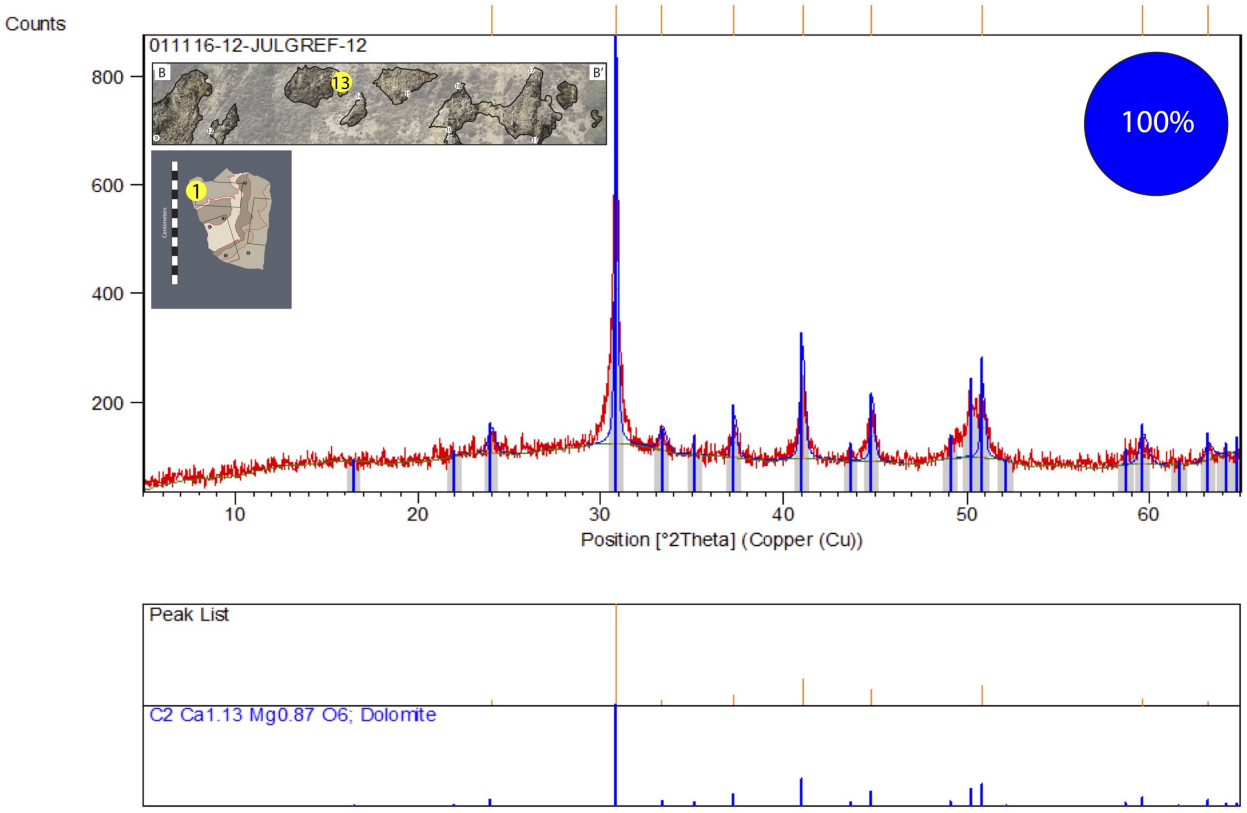
Counts
011116-12-JULGREF-12
B
B'
13
1
100%
800
600
400
200
10
20
30
40
50
60
Position [°2Theta] (Copper (Cu))
Peak List
C2 Ca1.13 Mg0.87 O6; Dolomite

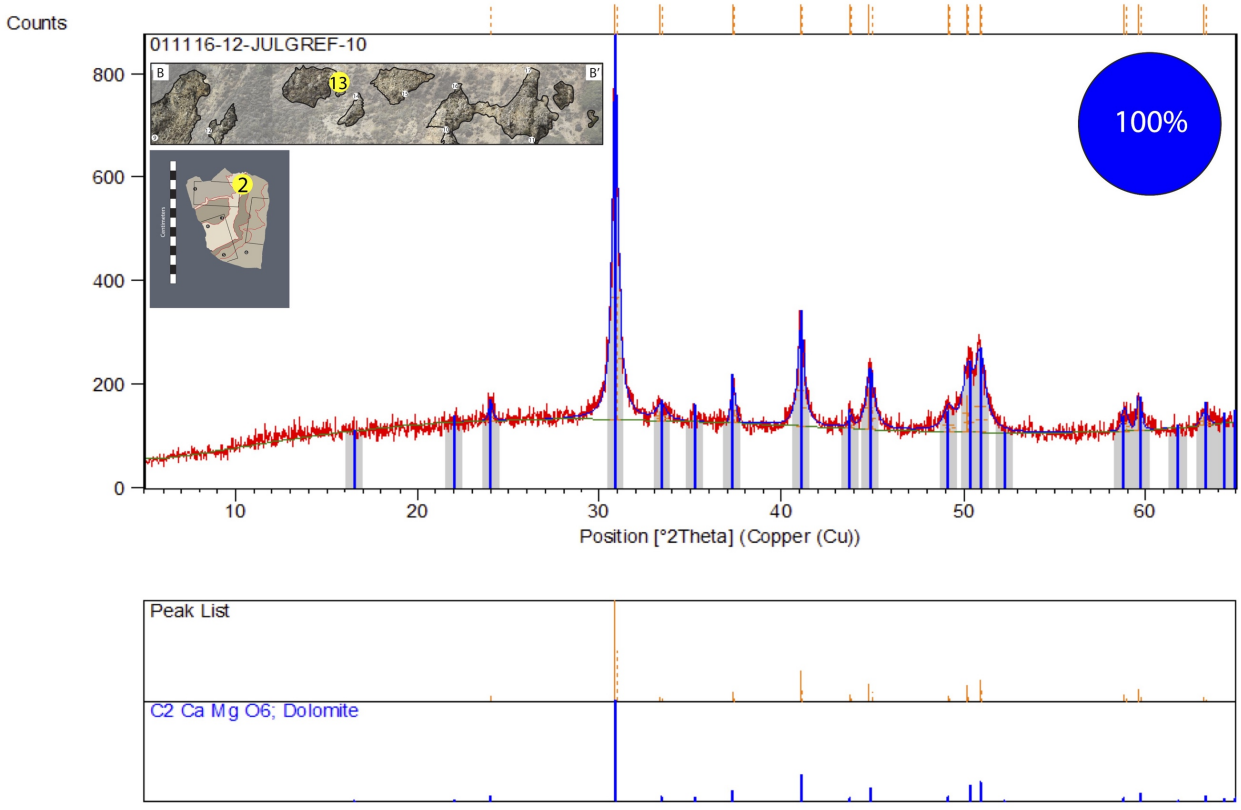
Counts
011116-12-JULGREF-10
B
B'
13
2
100%
800
600
400
200
0
10
20
30
40
50
60
Position [°2Theta] (Copper (Cu))
Peak List
C2 Ca Mg O6; Dolomite

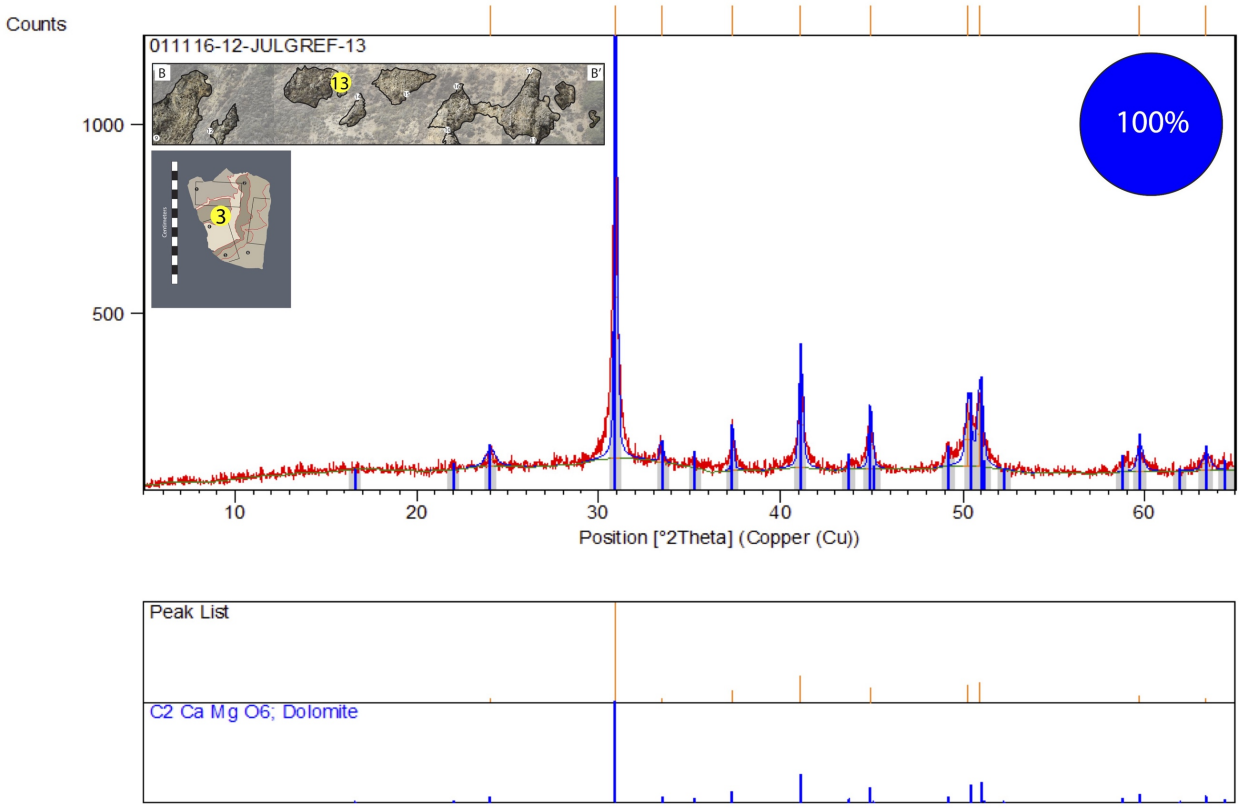
Counts
011116-12-JULGREF-13
B
B'
13
3
100%
1000
500
10
20
30
40
50
60
Position [°2Theta] (Copper (Cu))
Peak List
C2 Ca Mg O6; Dolomite

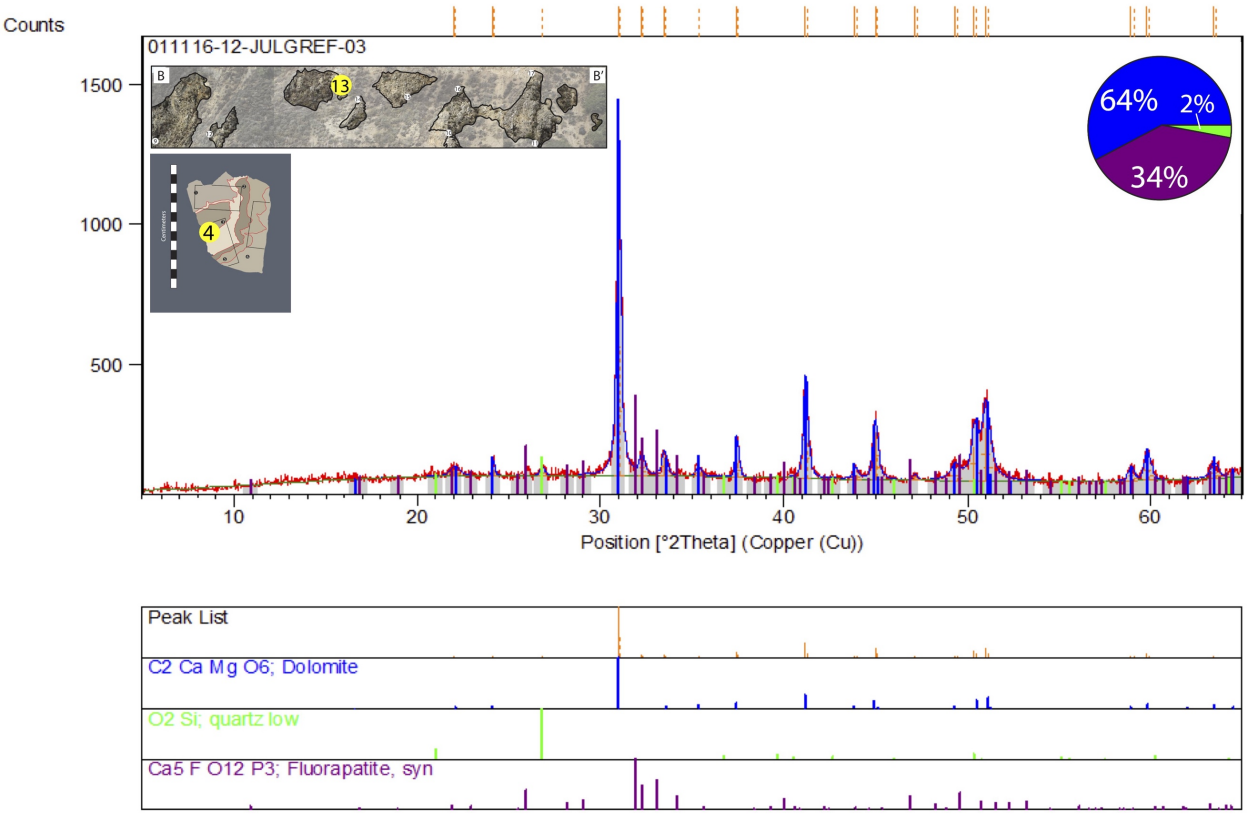
Counts
011116-12-JULGREF-03
B
B'
13
4
64%
2%
34%
1500
1000
500
10
20
30
40
50
60
Position [°2Theta] (Copper (Cu))
Peak List
C2 Ca Mg O6; Dolomite
O2 Si; quartz low
Ca5 F O12 P3; Fluorapatite, syn

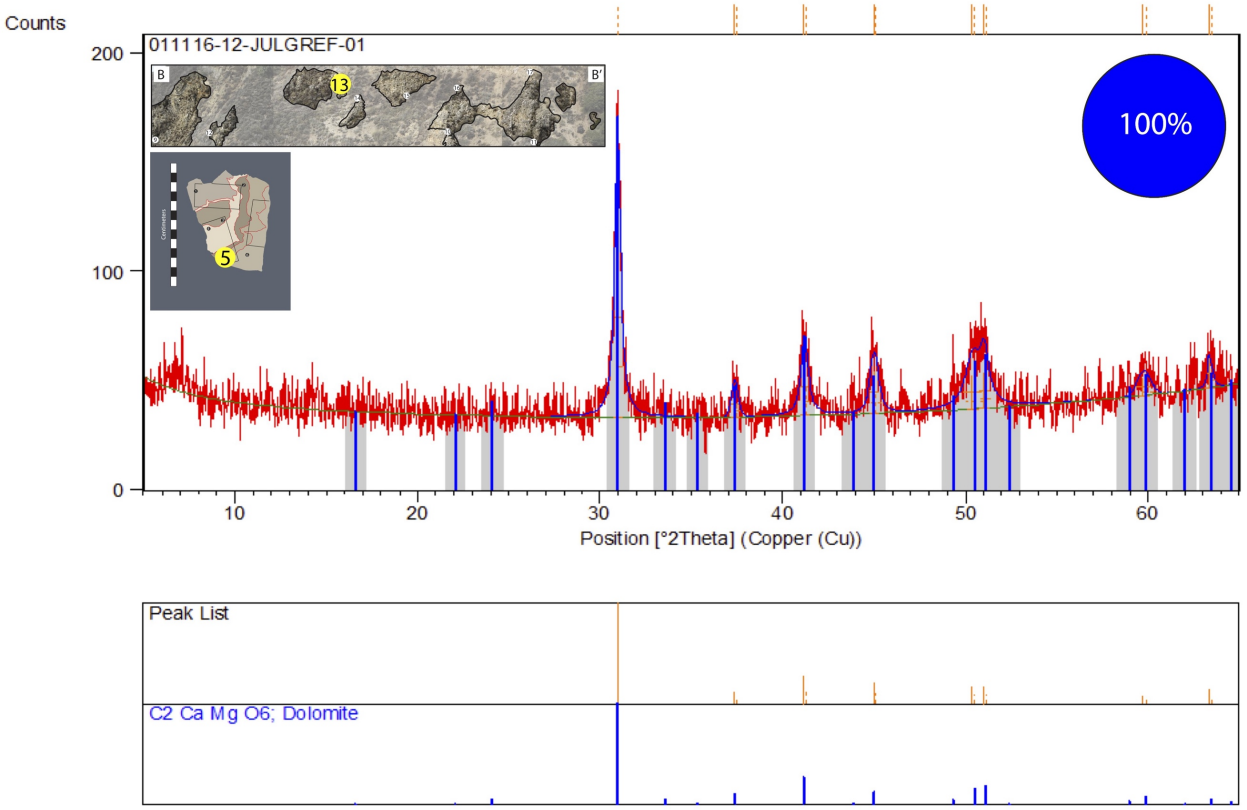
Counts
011116-12-JULGREF-01
B
B'
13
5
100%
200
100
0
10
20
30
40
50
60
Position [°2Theta] (Copper (Cu))
Peak List
C2 Ca Mg O6; Dolomite

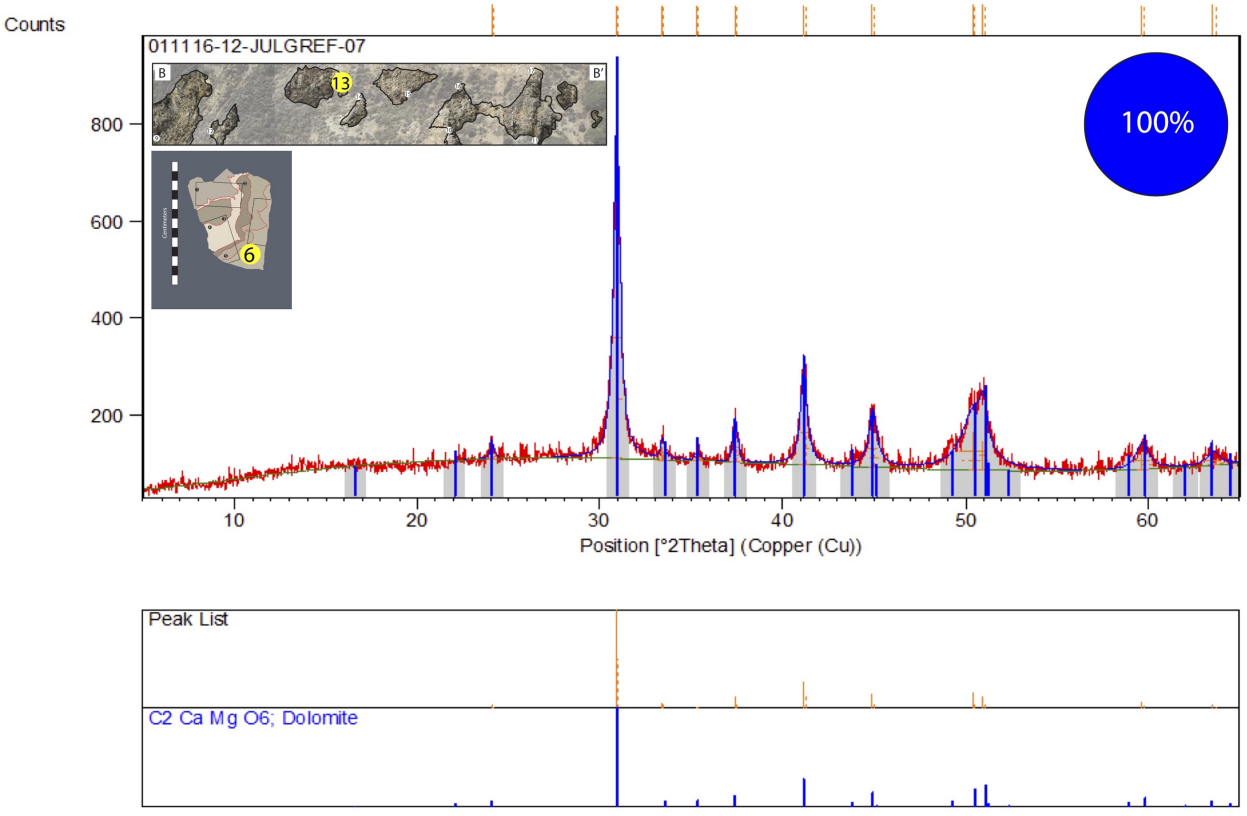
Counts
011116-12-JULGREF-07
B
B'
13
6
100%
800
600
400
200
10
20
30
40
50
60
Position [°2Theta] (Copper (Cu))
Peak List
C2 Ca Mg O6; Dolomite

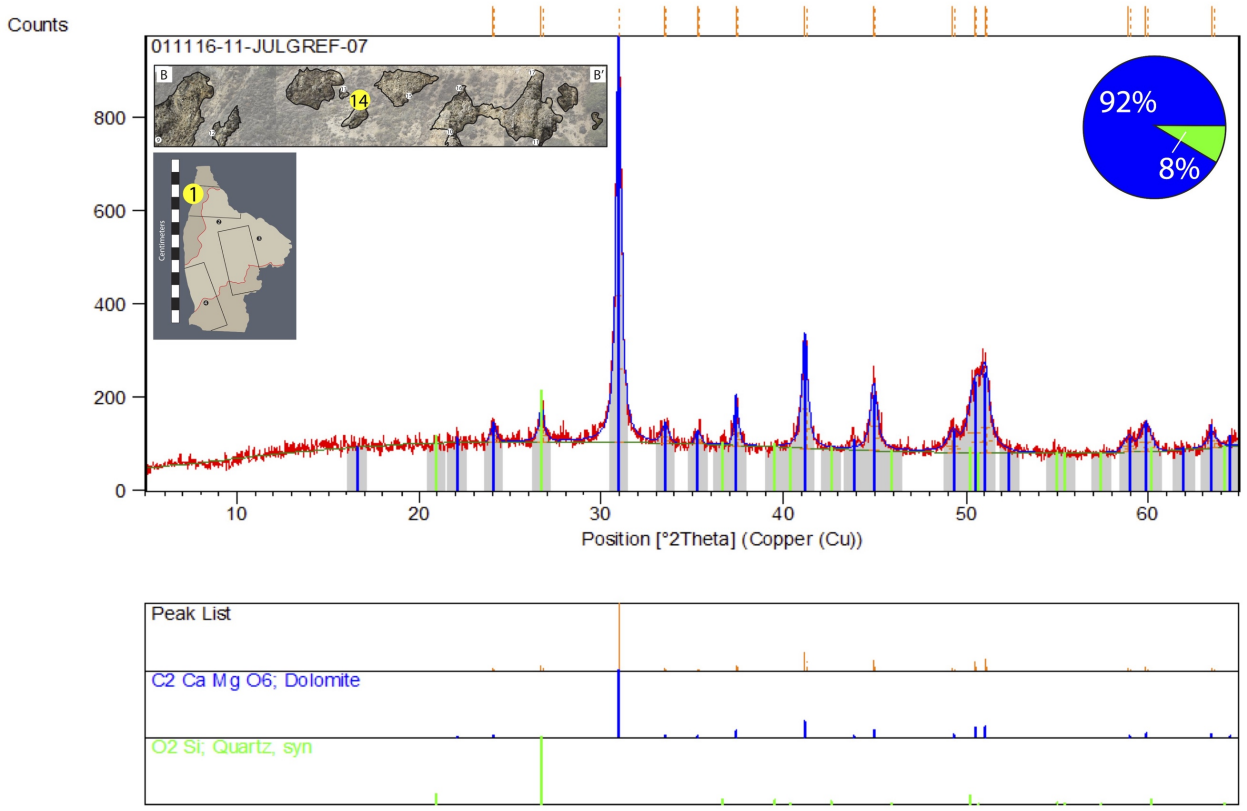
Counts
011116-11-JULGREF-07
B
B'
14
1
92%
8%
800
600
400
200
0
10
20
30
40
50
60
Position [°2Theta] (Copper (Cu))
Peak List
C2 Ca Mg O6; Dolomite
O2 Si; Quartz, syn

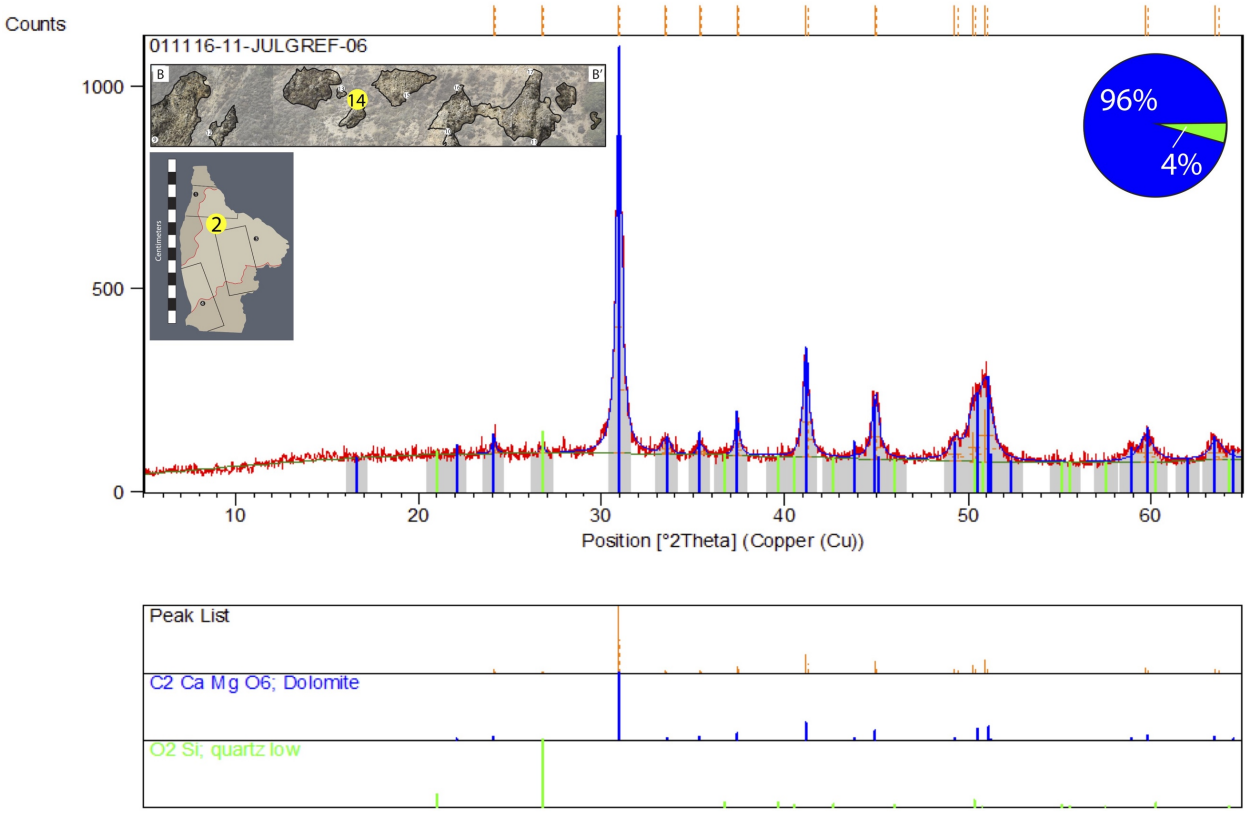
Counts
011116-11-JULGREF-06
B
B'
14
2
96%
4%
1000
500
0
10
20
30
40
50
60
Position [°2Theta] (Copper (Cu))
Peak List
C2 Ca Mg O6; Dolomite
O2 Si; quartz low

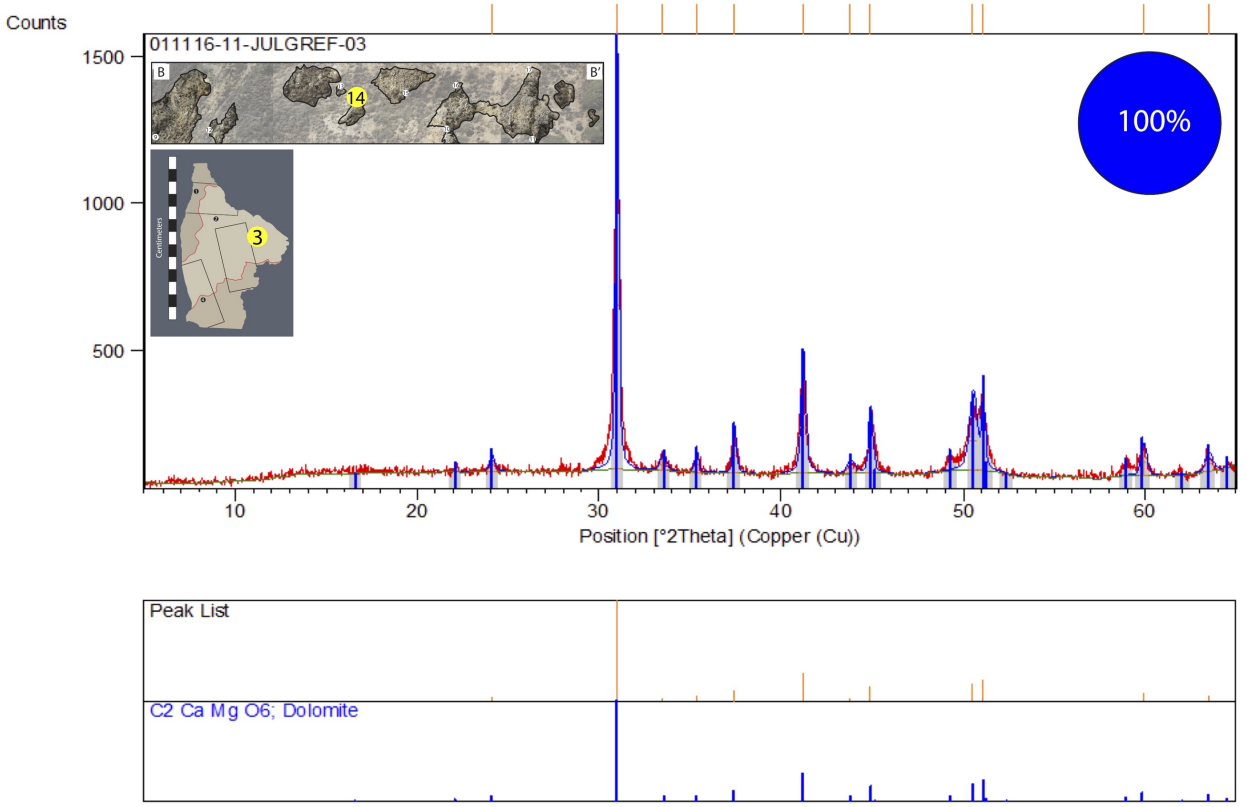
Counts
011116-11-JULGREF-03
B
B'
14
3
100%
1500
1000
500
10
20
30
40
50
60
Position [°2Theta] (Copper (Cu))
Peak List
C2 Ca Mg O6; Dolomite

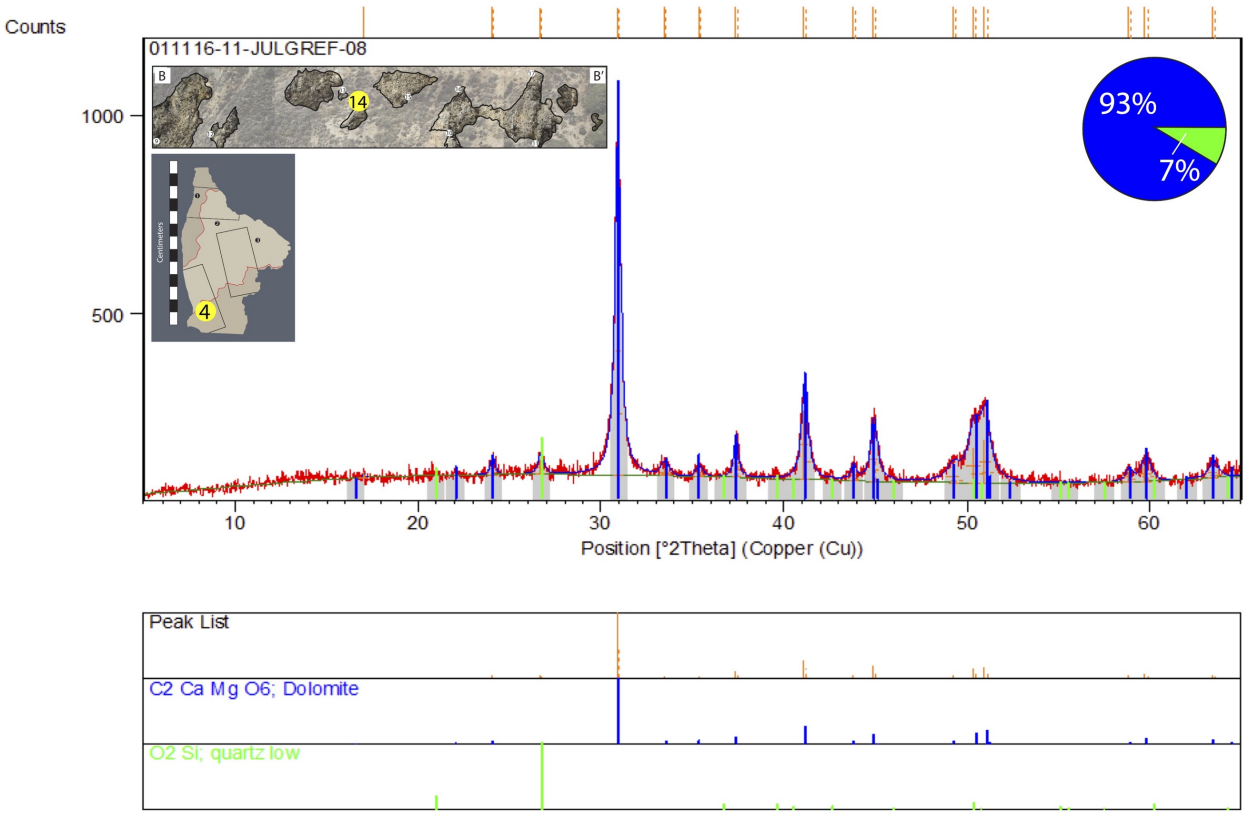
Counts
011116-11-JULGREF-08
B
B'
14
4
93%
7%
1000
500
10
20
30
40
50
60
Position [°2Theta] (Copper (Cu))
Peak List
C2 Ca Mg O6; Dolomite
O2 Si; quartz low

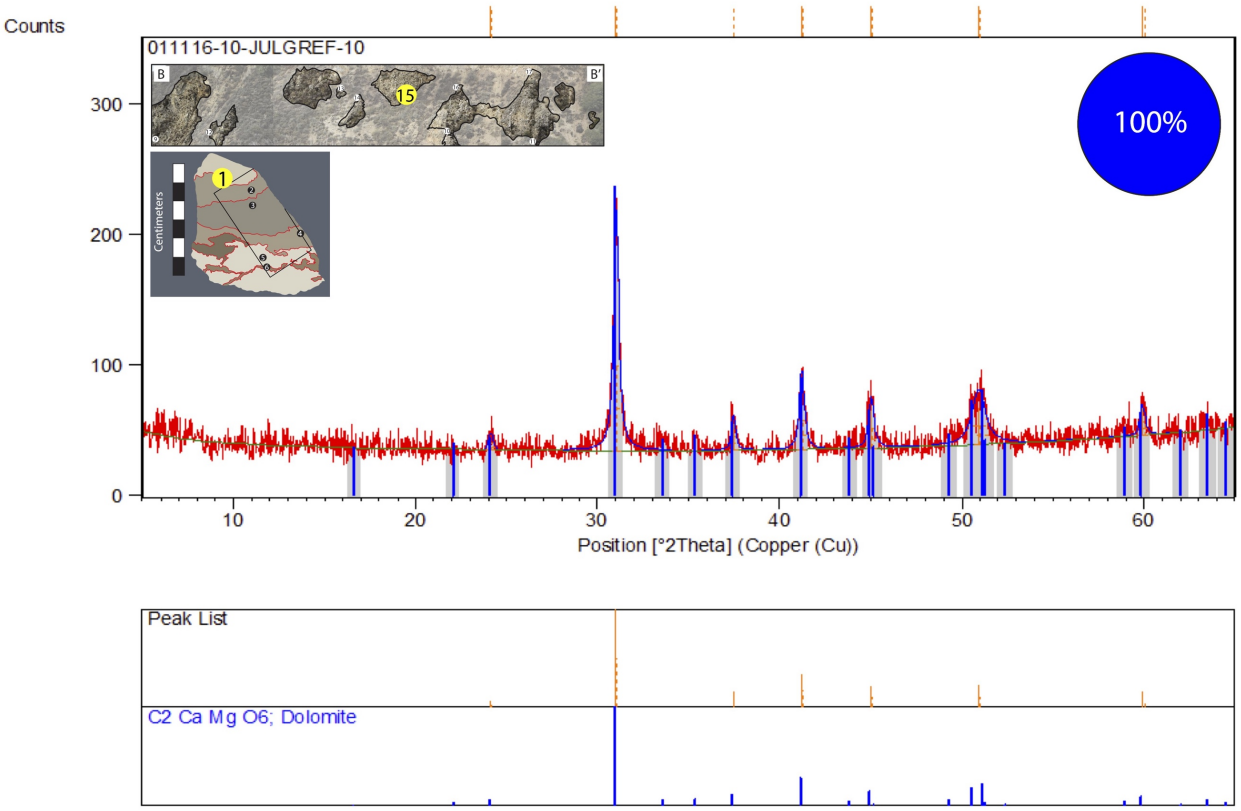
Counts
011116-10-JULGREF-10
B
B'
15
1
Centimeters
100%
300
200
100
0
10
20
30
40
50
60
Position [°2Theta] (Copper (Cu))
Peak List
C2 Ca Mg O6; Dolomite

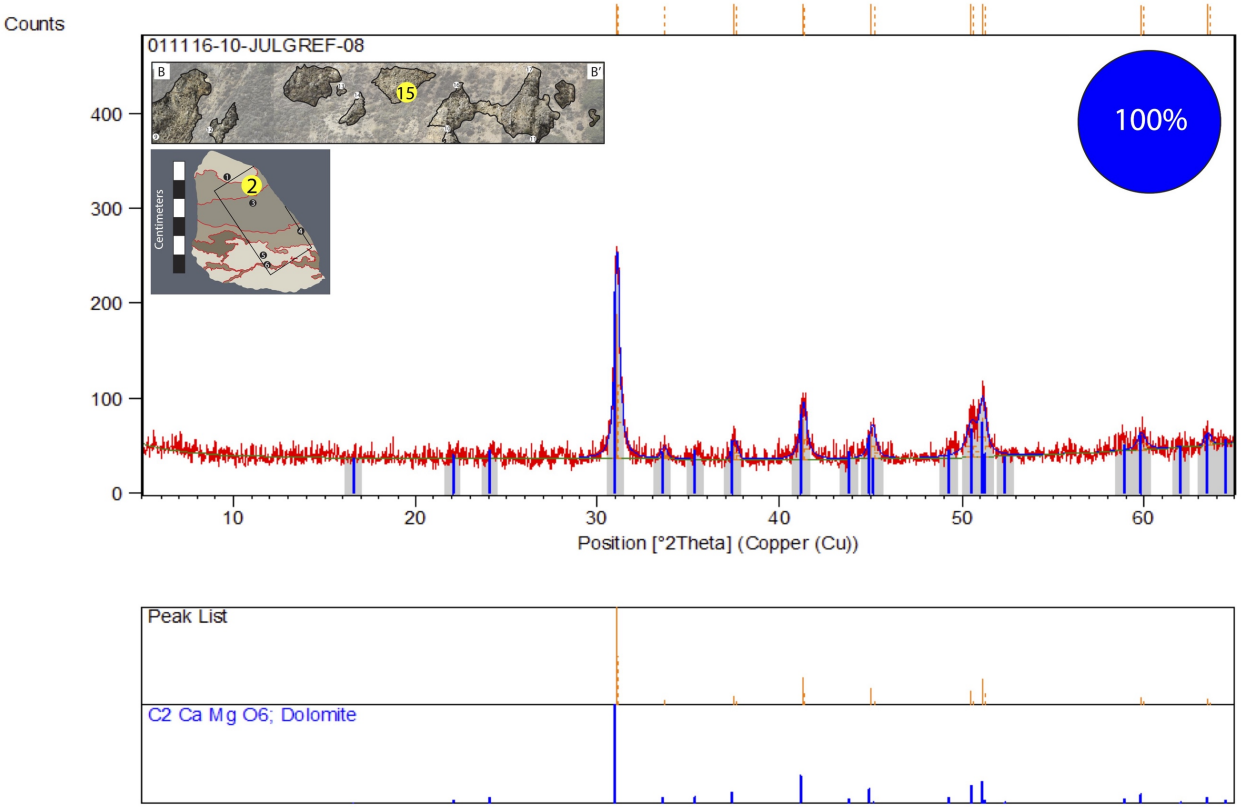
Counts
011116-10-JULGREF-08
B
B'
15
2
Centimeters
100%
400
300
200
100
0
10
20
30
40
50
60
Position [°2Theta] (Copper (Cu))
Peak List
C2 Ca Mg O6; Dolomite

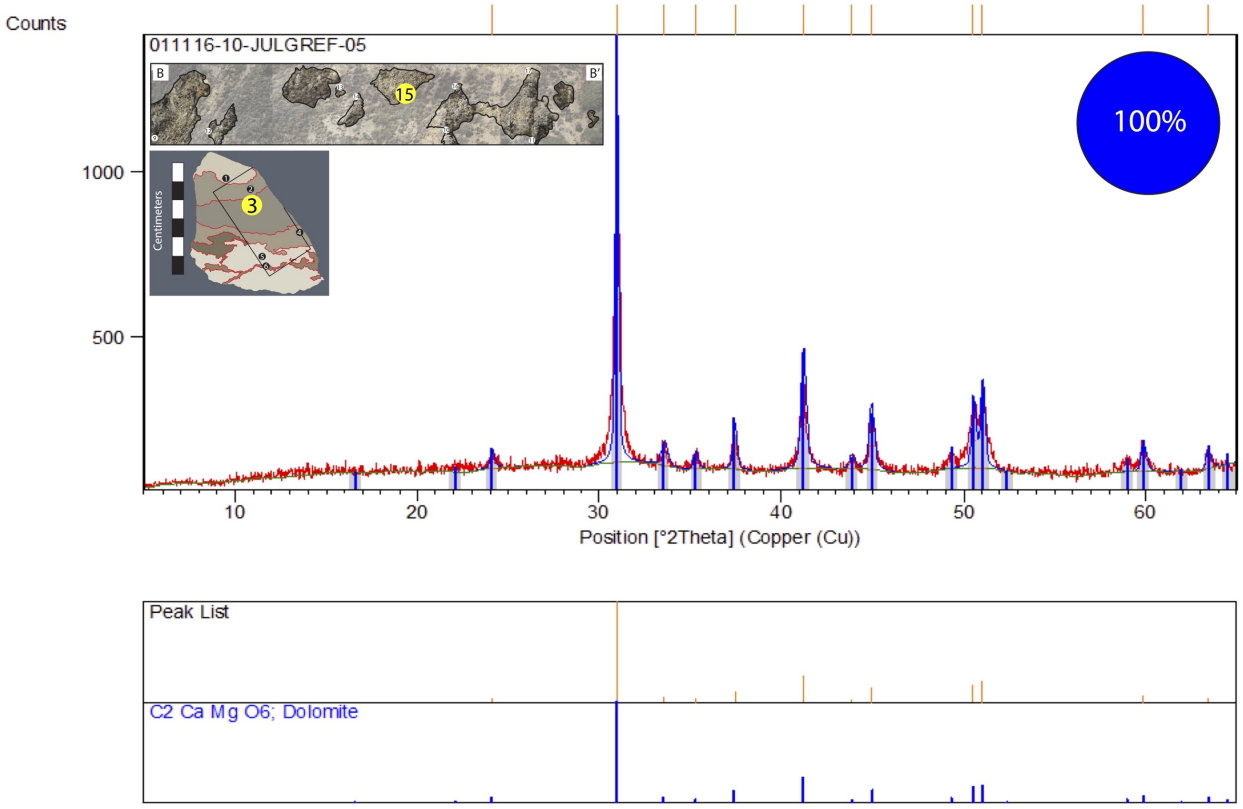
Counts
011116-10-JULGREF-05
B
B'
15
3
Centimeters
100%
1000
500
10
20
30
40
50
60
Position [°2Theta] (Copper (Cu))
Peak List
C2 Ca Mg O6; Dolomite

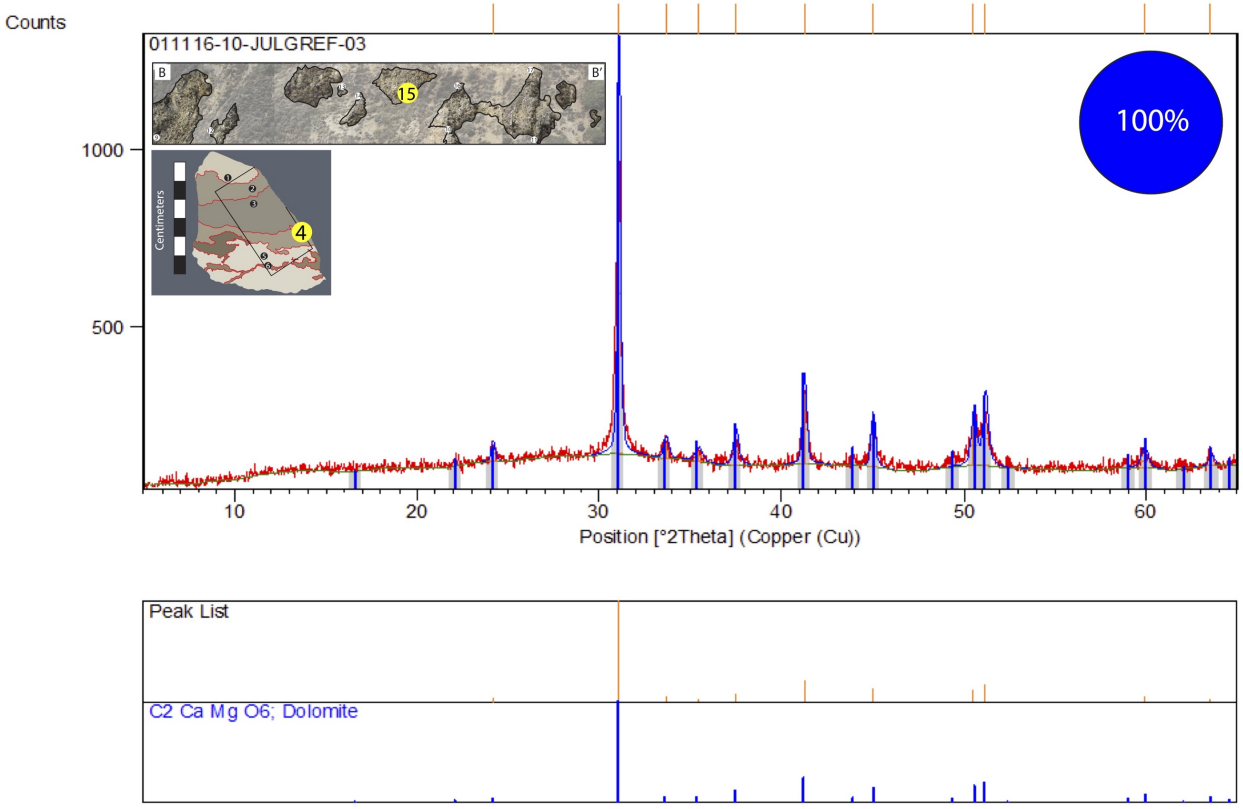
Counts
011116-10-JULGREF-03
B
B'
15
4
Centimeters
100%
1000
500
10
20
30
40
50
60
Position [°2Theta] (Copper (Cu))
Peak List
C2 Ca Mg O6; Dolomite

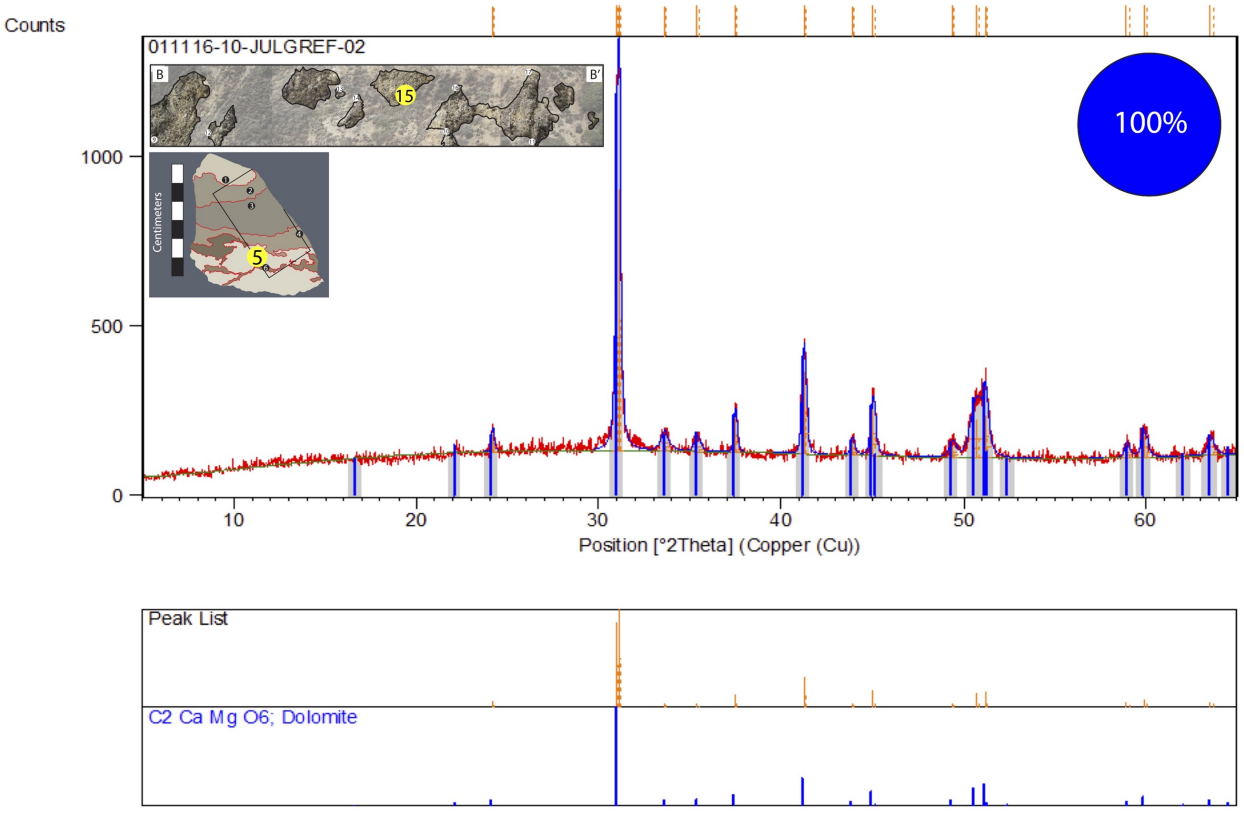
Counts
011116-10-JULGREF-02
B
B'
15
5
Centimeters
100%
1000
500
0
10
20
30
40
50
60
Position [°2Theta] (Copper (Cu))
Peak List
C2 Ca Mg O6; Dolomite

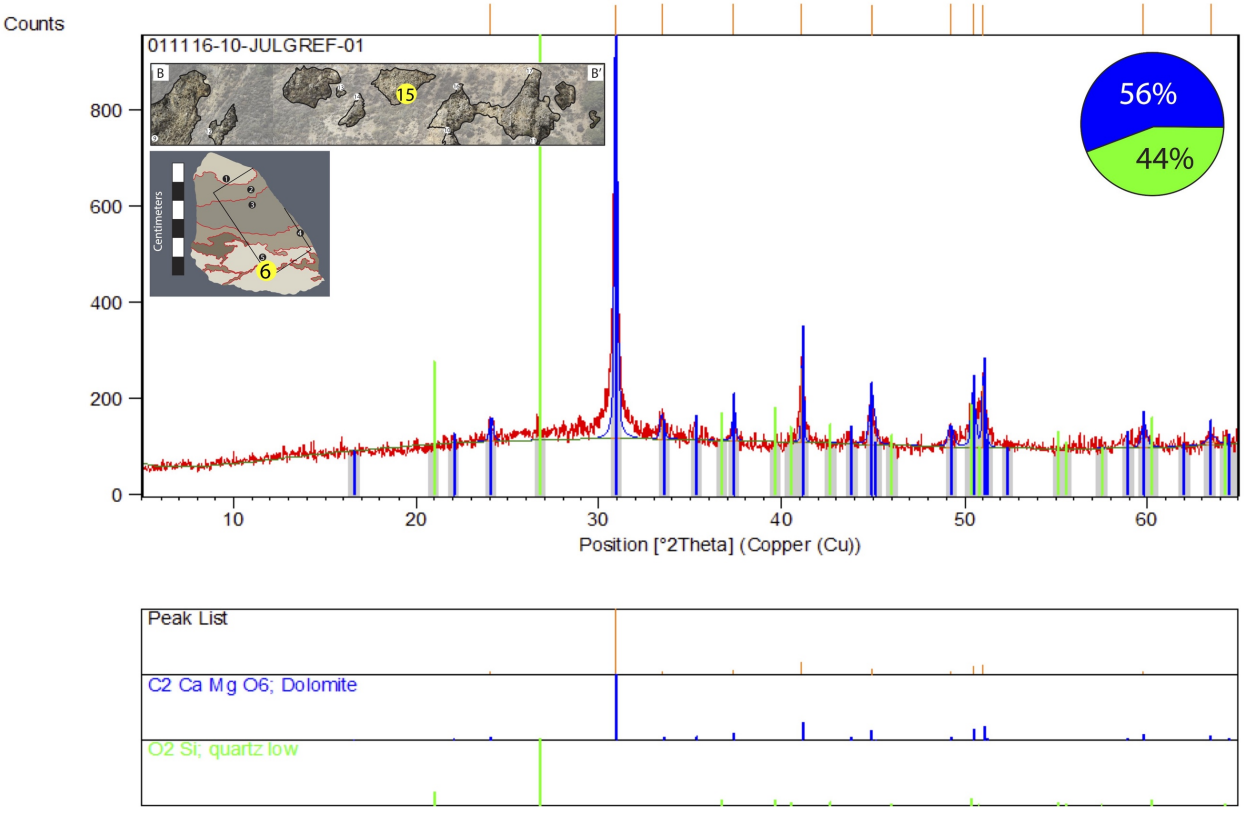
Counts
011116-10-JULGREF-01
B
B'
15
6
Centimeters
56%
44%
800
600
400
200
0
10
20
30
40
50
60
Position [°2Theta] (Copper (Cu))
Peak List
C2 Ca Mg O6; Dolomite
O2 Si; quartz low

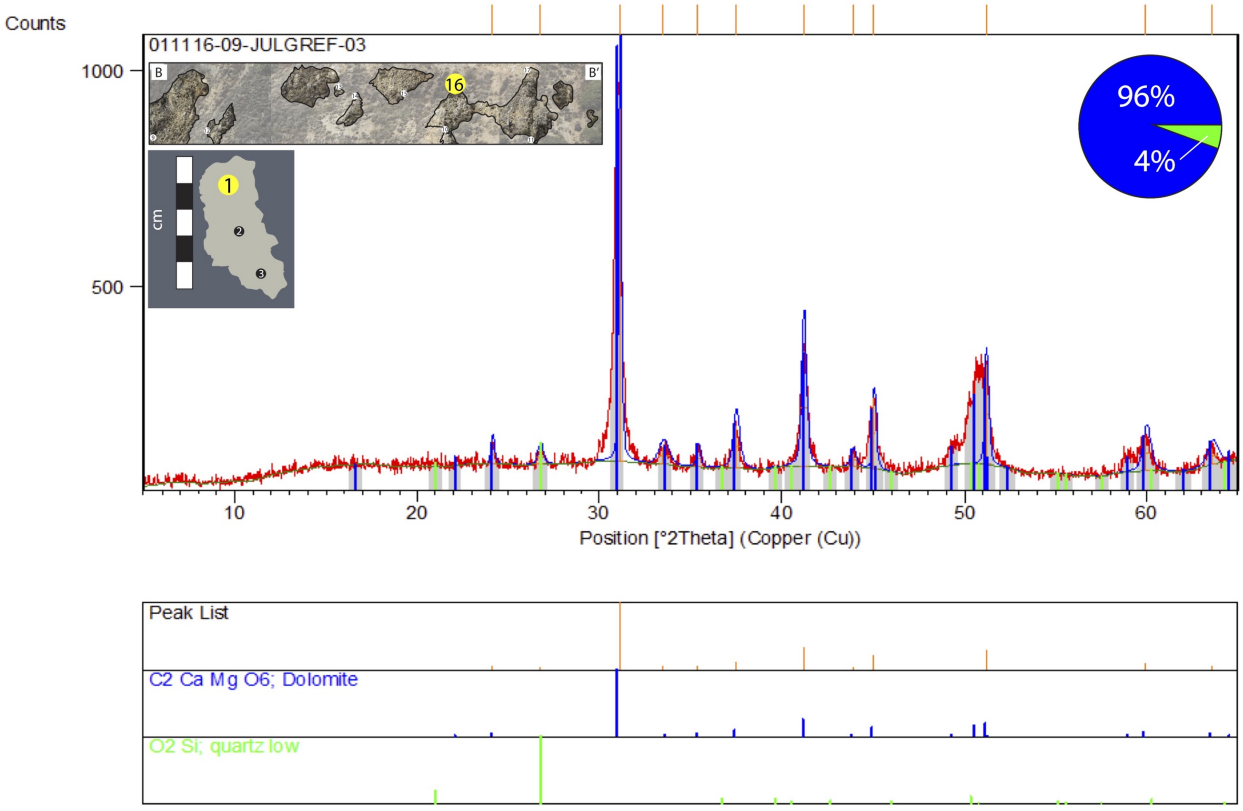
Counts
011116-09-JULGREF-03
1000
500
B
B'
16
1
2
3
cm
96%
4%
10
20
30
40
50
60
Position [°2Theta] (Copper (Cu))
Peak List
C2 Ca Mg O6; Dolomite
O2 Si; quartz low

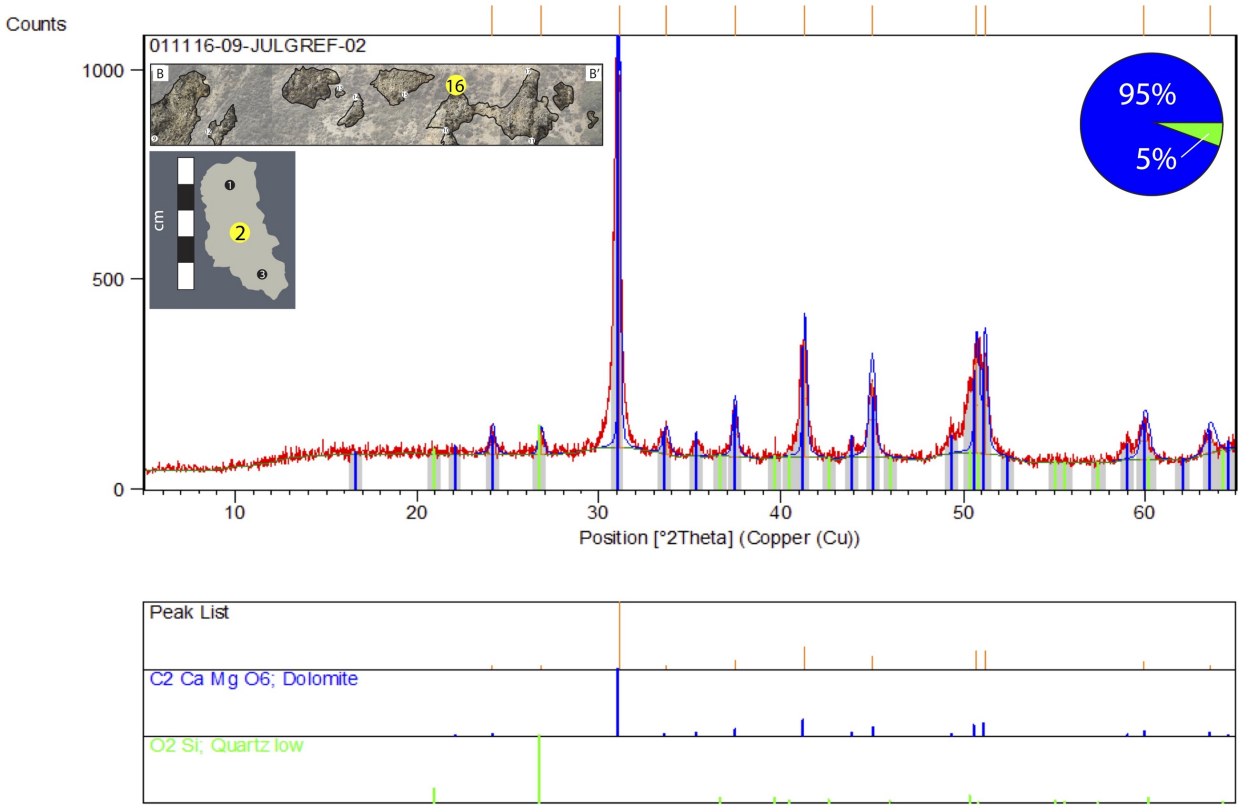
Counts
011116-09-JULGREF-02
1000
500
0
B
B'
16
1
2
3
cm
95%
5%
10
20
30
40
50
60
Position [°2Theta] (Copper (Cu))
Peak List
C2 Ca Mg O6; Dolomite
O2 Si; Quartz low

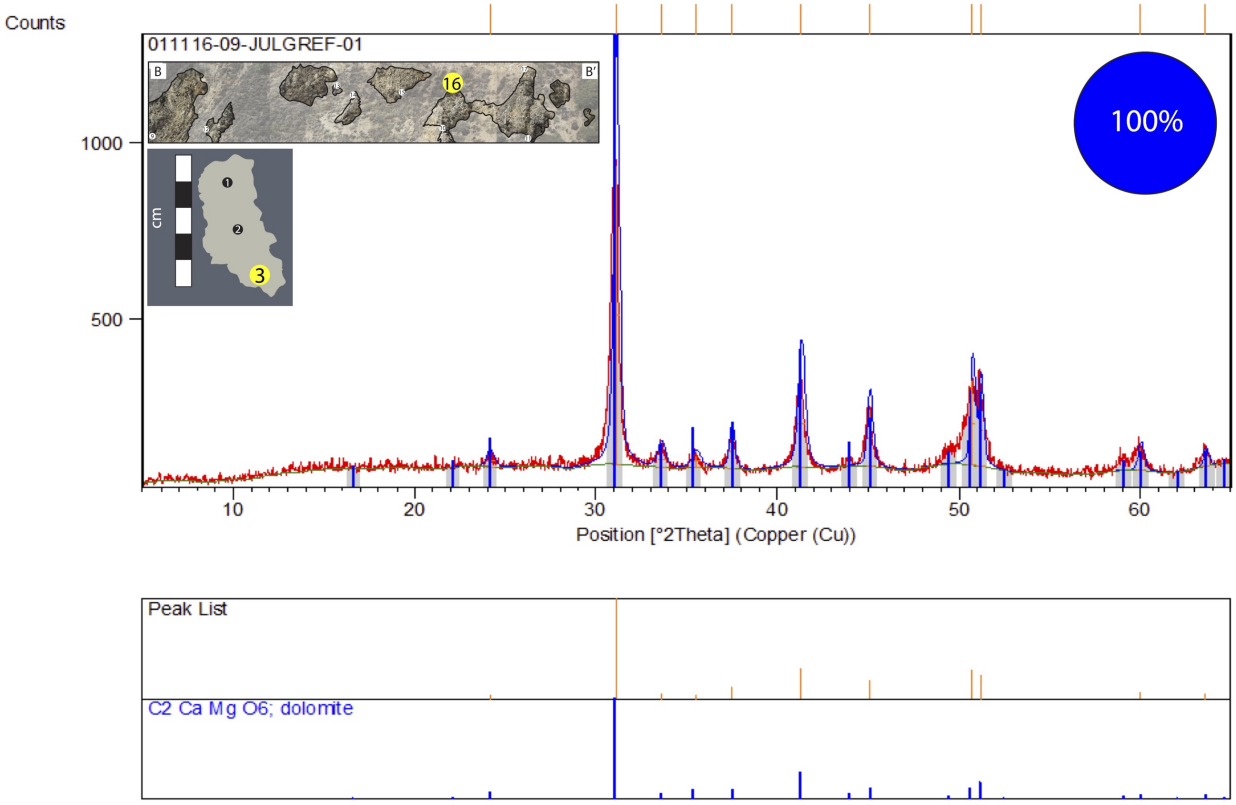
Counts
011116-09-JULGREF-01
B
B'
16
100%
1000
500
cm
3
10
20
30
40
50
60
Position [°2Theta] (Copper (Cu))
Peak List
C2 Ca Mg O6; dolomite

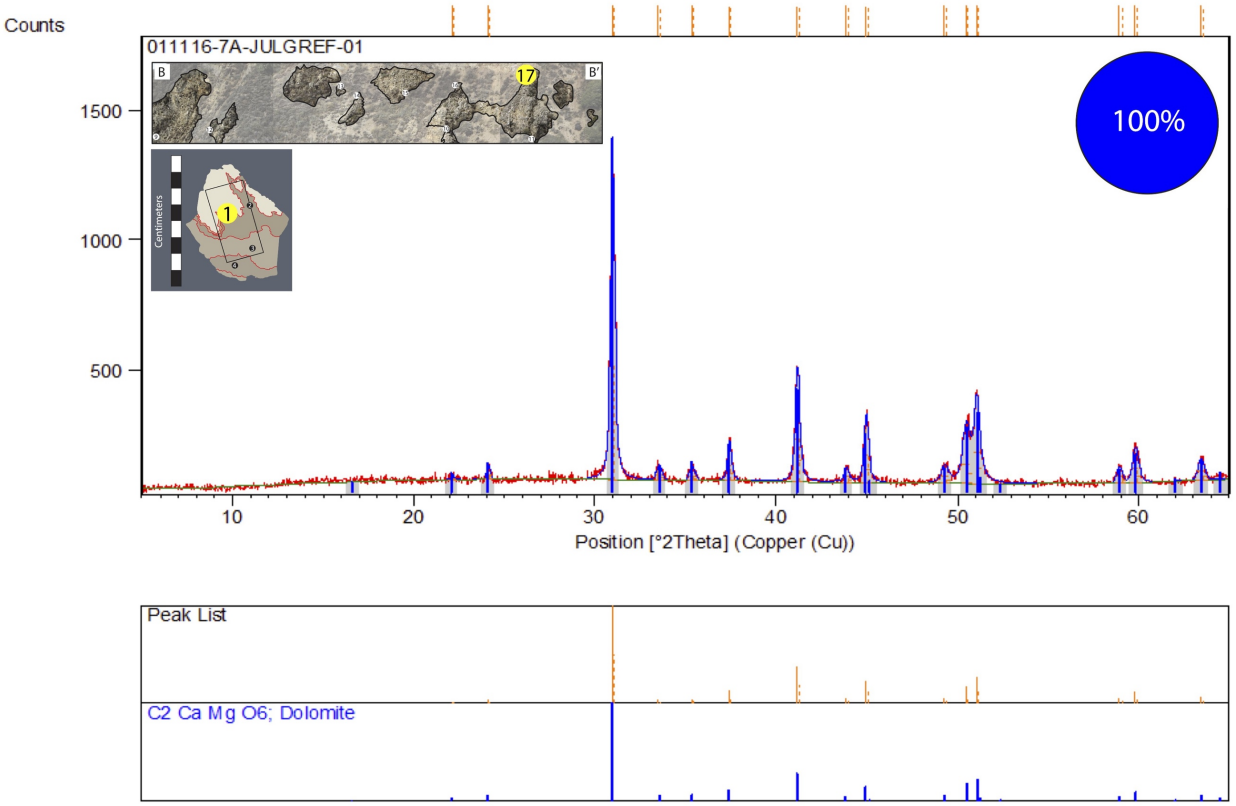
Counts
011116-7A-JULGREF-01
B
B'
17
100%
1500
1000
500
Centimeters
1
10
20
30
40
50
60
Position [°2Theta] (Copper (Cu))
Peak List
C2 Ca Mg O6; Dolomite

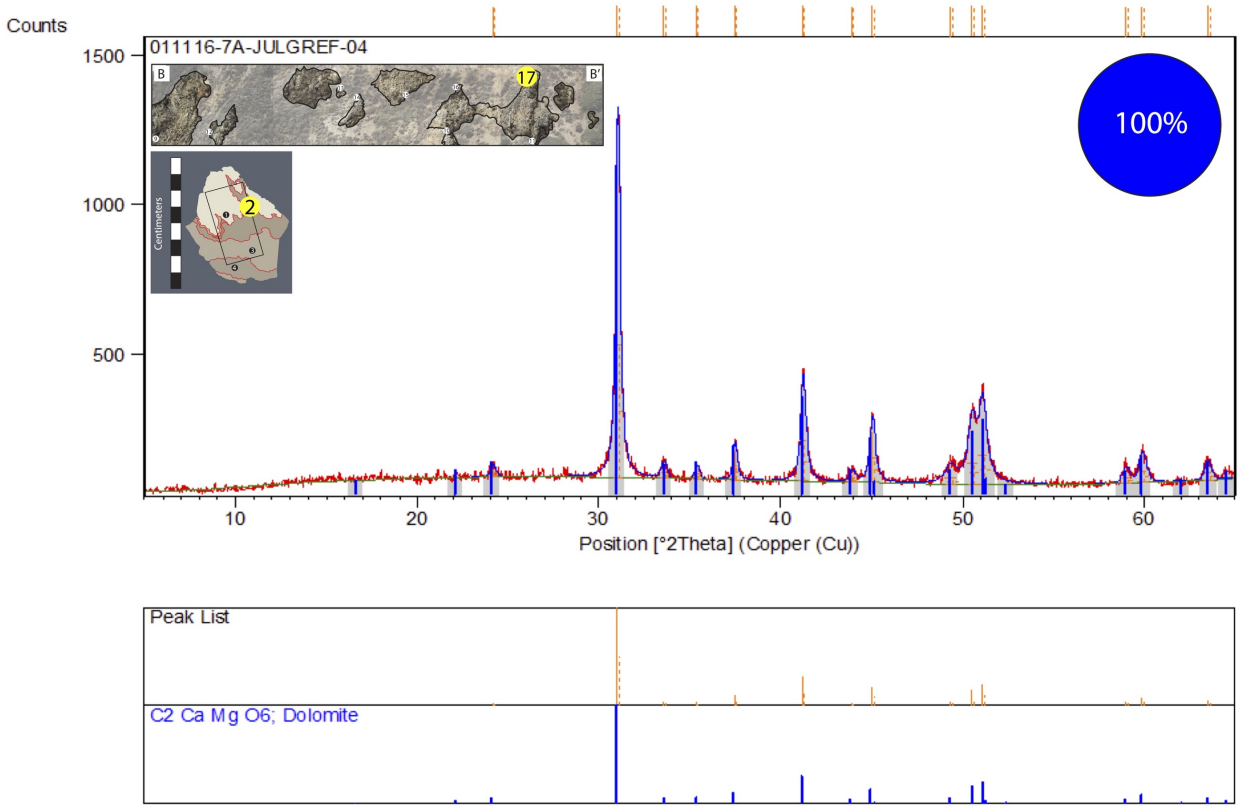
Counts
011116-7A-JULGREF-04
B
B'
17
2
Centimeters
100%
1500
1000
500
10
20
30
40
50
60
Position [°2Theta] (Copper (Cu))
Peak List
C2 Ca Mg O6; Dolomite

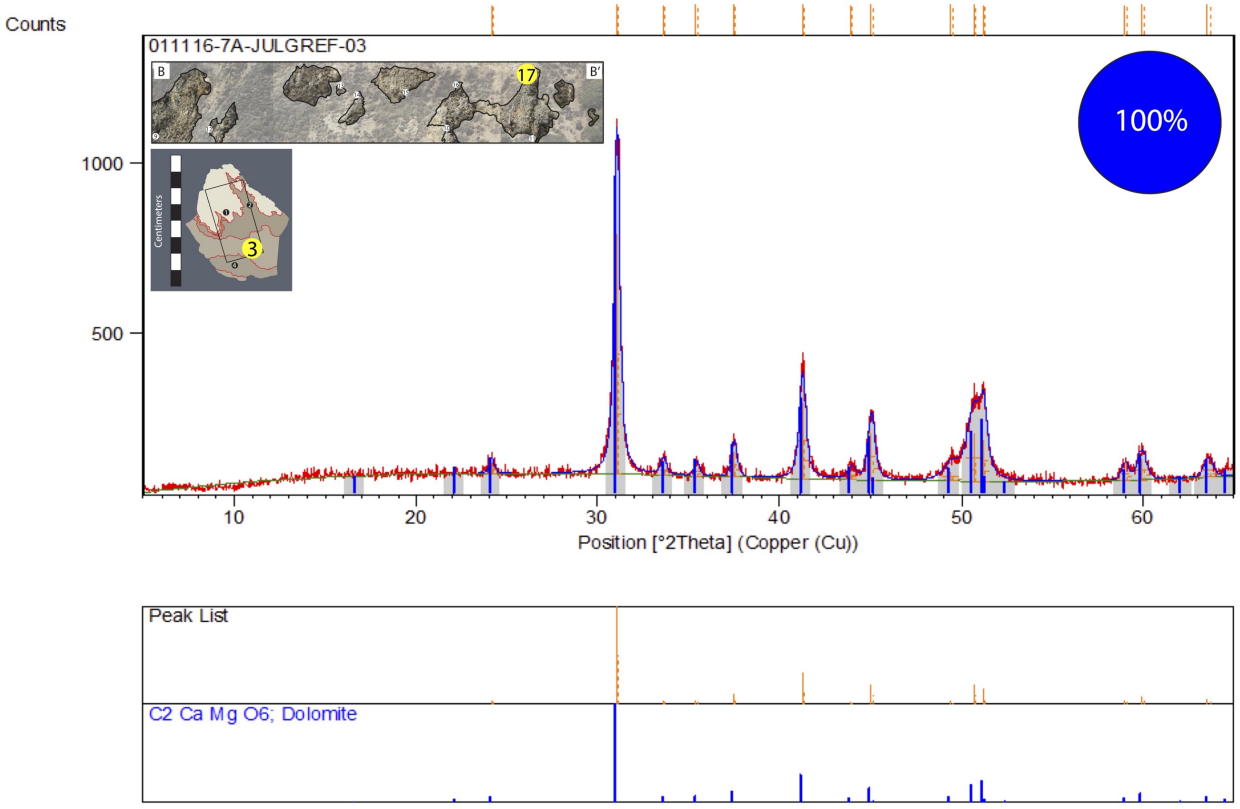
Counts
011116-7A-JULGREF-03
B
B'
17
3
Centimeters
100%
1000
500
10
20
30
40
50
60
Position [°2Theta] (Copper (Cu))
Peak List
C2 Ca Mg O6; Dolomite

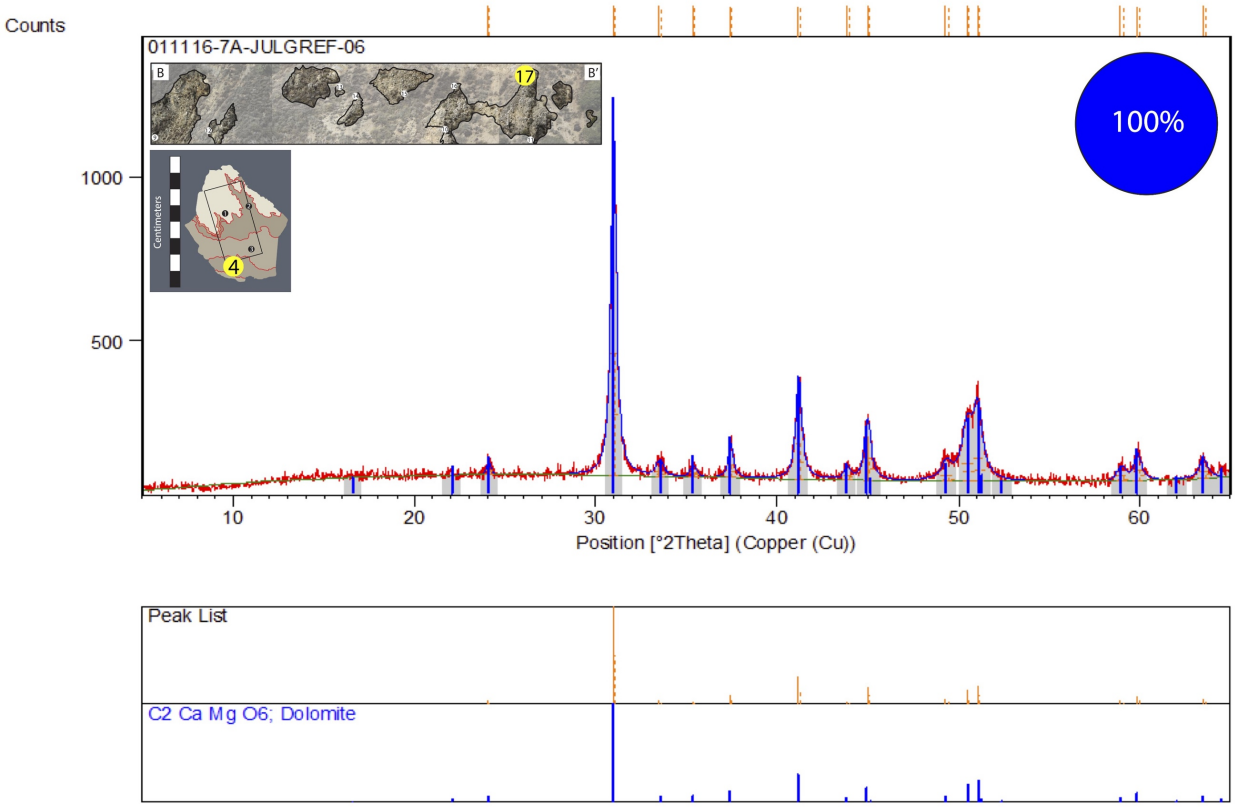
Counts
011116-7A-JULGREF-06
B
B'
17
4
Centimeters
100%
1000
500
10
20
30
40
50
60
Position [°2Theta] (Copper (Cu))
Peak List
C2 Ca Mg O6; Dolomite

APPENDIX C

TRACE ELEMENT CONCENTRATIONS

APPENDIX C: Trace Element Concentrations

	Location on Transect B-B’		
	10	10	10
	Sample Name		
	072815-20B-01	072815-20B-03	072815-20B-06
Element	Concentration (µg/g)		
Be	0.22	0.27	0.13
B	6.81	2.71	5.69
Al	1781.46	539.39	1188.10
Ti	119.80	44.20	92.32
V	100.45	78.46	72.60
Cr	40.57	17.90	28.81
Mn	90.97	133.39	71.88
Fe	2785.30	1787.94	2360.01
Co	0.98	0.40	0.61
Ni	22.63	8.62	18.83
Cu	13.93	5.57	13.37
Zn	27.70	12.35	22.34
As	1.85	0.96	1.08
Se	0.28	0.00	0.21
Sr	274.48	229.88	275.86
Mo	0.91	0.00	0.70
Ag	0.70	0.13	2.45
Cd	1.82	1.14	2.21
Sn	0.23	0.11	0.21
Sb	0.31	0.12	0.14
Ba	181.87	70.28	123.36
Tl	0.12	0.00	0.07
Pb	0.69	0.19	0.72

	Location on Transect B-B’		
	11	14	14
	Sample Name		
	072615-15A-01	011116-11-03	01116-11-07
Element	Concentration (µg/g)		
Be	0.26	0.28	0.24
B	9.29	3.74	3.40
Al	2196.41	928.03	911.31
Ti	153.47	48.11	48.27
V	104.22	109.95	77.71
Cr	42.08	27.06	16.66
Mn	100.79	111.35	99.66
Fe	3158.57	1514.13	1521.29
Co	0.89	0.34	0.35
Ni	37.18	7.03	5.84
Cu	17.21	9.23	6.87
Zn	48.72	18.04	12.15
As	2.28	0.36	0.26
Se	0.28	0.00	0.00
Sr	232.90	208.87	254.95
Mo	1.42	0.00	0.00
Ag	0.61	0.24	0.20
Cd	4.79	1.93	1.34
Sn	0.31	0.13	0.13
Sb	0.34	0.07	0.00
Ba	198.85	105.84	124.88
Tl	0.09	0.00	0.00
Pb	6.00	0.24	0.27

	Location on Transect B-B’		
	15	15	16
	Sample Name		
	011116-10-06	011116-10-07	011116-09-01
Element	Concentration (µg/g)		
Be	0.13	0.17	0.19
B	5.89	8.02	12.04
Al	1292.00	998.75	988.95
Ti	94.18	57.04	49.13
V	70.33	88.59	110.83
Cr	28.41	19.56	17.78
Mn	39.94	92.23	115.20
Fe	2075.02	1615.93	1740.70
Co	0.47	0.53	0.31
Ni	8.35	5.01	4.52
Cu	8.19	4.81	2.43
Zn	18.10	11.39	13.70
As	0.46	0.27	0.25
Se	0.00	0.00	0.00
Sr	334.69	224.59	180.19
Mo	0.86	0.00	0.00
Ag	0.41	0.35	0.19
Cd	2.75	1.43	1.40
Sn	0.16	0.19	0.16
Sb	0.00	0.00	0.00
Ba	175.58	148.10	72.96
Tl	0.00	0.00	0.00
Pb	0.40	0.54	0.66

	Location on Transect B-B’		
	16	17	17
	Sample Name		
	011116-09-03	011116-7A-02	011116-7A-06
Element	Concentration (µg/g)		
Be	0.21	0.13	0.20
B	6.08	5.23	5.35
Al	943.64	1028.50	1010.49
Ti	53.54	69.53	62.68
V	99.87	140.93	116.94
Cr	24.25	29.92	29.98
Mn	107.85	65.30	107.78
Fe	1863.75	1902.28	1996.74
Co	0.32	0.44	0.46
Ni	5.78	9.99	13.12
Cu	2.92	5.32	7.61
Zn	12.50	16.10	24.48
As	0.22	0.81	1.22
Se	0.00	0.00	0.00
Sr	187.65	312.66	253.47
Mo	0.00	0.69	0.82
Ag	0.18	0.30	0.36
Cd	1.49	2.70	4.26
Sn	0.14	0.11	0.16
Sb	0.00	0.15	0.25
Ba	69.43	199.70	139.56
Tl	0.00	0.00	0.00
Pb	0.40	0.49	0.50

REFERENCES

REFERENCES

Behl, R.J., 1992, Chertification in the Monterey Formation of California and deep-sea sediments of the West Pacific [Ph.d thesis]: Santa Cruz, University of California, 302 p.

Behl, R.J., 1998, Relationships between silica diagenesis, deformation, and fluid flow in Monterey Formation cherts, Santa Maria Basin, California, *in* Eichhubl, P., ed., Diagenesis, Deformation, and Fluid Flow in the Miocene Monterey Formation: Pacific Section SEPM Special Publication, book 83, p. 77-83.

Behl, R.J., 2014, Oil and dolomite in the Monterey Formation of California: Abstract adapted from oral presentation given at Pacific Section AAPG, SEG and SEPM Joint Technical Conference, Bakersfield, California, 27-30 April.

Behl, R.J., and Garrison, R.E., 1994, The origin of chert in the Monterey Formation of Californa (USA), *in* Iijima, A., Abed, A., and Garrison, R., eds., Siliceous, Phoshpatic and Glauconitic Sediments of the Tertiary and Mesozoic: Proceedings of the 29th International Geological Congress, Part C, VSP, Utrecht.

Billups, K., and Schrag, D.P., 2002, Paleotemperatures and ice volume of the past 27 Myr revisited with paired Mg/Ca and $^{18}O/^{16}O$ measurements on benthic foraminifera: Paleoceanography, v.17, no.1, 1003, doi: 10.1029/2000PA000567.

Boles, J.R., Eichhubl, P., Garven, G., and Chen, J., 2004, Evolution of a hydrocarbon migration pathway along basin-bounding faults: Evidence from fault cement: AAPG Bulletin, v. 88, no. 7, p. 947-970, doi: 10.1306/02090403040.

Bramlette, M.N., 1946, The Monterey Formation of California and the origin of its siliceous rocks: U.S. Geological Survey Professional Paper 212.

Brown, C.P., 2014, A stable isotope study of fluid-rock interaction in serpentinites of the Franciscan Complex, San Rafael Mountains, California [M.S. thesis]: Long Beach, California State University, 231 p.

Claypool G.E., and Kaplan I.R., 1974, The origin and distribution of methane in marine sediments, *in* Kaplan, I.R., ed., Natural Gases in Marine Sediments: New York, Plenum Press, p. 99-140.

Compton, J. S., and Siever, R., 1984, Stratigraphy and dolostone occurrence in the Miocene Monterey Formation, Santa Maria basin area, California, *in* Garrison, R.E., Kastner, M. and Zenger, D.H., eds., Dolomites of the Monterey Formation and Other Organic-Rich Units: Pacific Section, Society for Sedimentary Geology, v. 41, p. 141-153

Curtis C. D., Petrowski C., and Oertel G. (1972) Stable carbon isotope ratios within carbonate concretions: a clue to time and place of origin: Nature v. 235, p. 98–100.

Davies, G.R., and Smith, L.B., Jr., 2006, Structurally controlled hydrothermal dolomite reservoir facies: An overview: AAPG Bulletin, v. 90, p. 1641-1690, doi: 10.1306/05220605164.

Dibblee, T.W., 1950, Geology of Southwestern Santa Barbara County, California: State of California Department of Natural Resources, Bulletin 150.

Dibblee, T.W., 1966, Geology of the central Santa Ynez Mountains, Santa Barbara County, California: Bulletin, California Division of Mines and Geology, v. 186, p. 1-99.

Dibblee, T.W., 1989a, Geologic map of the Casmalia and Orcutt Quadrangles, Santa Barbara County, California: Dibble Geological Foundation Map DF-24, scale 1:24,000.

Dibblee, T.W., 1989b, Geologic map of the Point Sal and Guadalupe Quadrangles, Santa Barbara County, California: Dibble Geological Foundation Map DF-25, scale 1:24,000.

Dibblee, T.W., and Ehrenspeck, H.E., eds., 1986, Geologic map of the Little Pine Mountain quadrangle, Santa Barbara County, California: Dibblee Geological Foundation, Dibblee Foundation Map DF-05, scale 1:24,000.

Dibblee, T.W., and Ehrenspeck, H.E., eds., 1987, Geologic map of the Lake Cachuma quadrangle, Santa Barbara County, California: Dibblee Geological Foundation, Dibblee Foundation Map DF-10, scale 1:24,000.

Dibblee, T.W., and Ehrenspeck, H.E., eds., 1988a, Geologic map of the Solvang and Gaviota quadrangles, Santa Barbara County, California: Dibblee Geological Foundation, Dibblee Foundation Map DF-16, scale 1:24,000.

Dibblee, T.W., and Ehrenspeck, H.E., eds., 1988b, Geologic map of the Santa Rosa Hills and Sacate quadrangles, Santa Barbara County, California: Dibblee Geological Foundation, Dibblee Foundation Map DF-17, scale 1:24,000.

Dibblee, T.W., and Ehrenspeck, H.E., eds., 1988c, Geologic map of the Lompoc Hills and Point Conception quadrangles, Santa Barbara County, California: Dibblee Geological Foundation, Dibblee Foundation Map DF-18, scale 1:24,000.

Dibblee, T.W., and Ehrenspeck, H.E., eds., 1988d, Geologic map of the Point Arguello and Tranquillon Mountain quadrangles, Santa Barbara County, California: Dibblee Geological Foundation, Dibblee Foundation Map DF-19, scale 1:24,000.

Dibblee, T.W., Ehrenspeck, H.E., and Bartlett, W.L., 1994, Geologic map of the Tepusquet Canyon quadrangle, Santa Barbara County, California: Dibblee Geological Foundation, Dibblee Foundation Map DF-52, scale 1:24,000.

Eichhubl, P., and Behl, R.J., 1998, Diagenesis, deformation, and fluid flow in the Miocene Monterey Formation, *in* Eichhubl, P., ed., Diagenesis, Deformation, and Fluid Flow in the Miocene Monterey Formation: Pacific Section, Society of Sedimentary Geologists Special Publication, Book 83, p. 5-13.

Eichhubl, P., and Boles, J.R., 1998, Vein formation in relation to burial diagenesis in the Miocene Monterey Formation, Arroyo Burro Beach, Santa Barbara, California, *in* Eichhubl, P., ed., Diagenesis, Deformation, and Fluid Flow in the Miocene Monterey Formation: Pacific Section, Society of Sedimentary Geologists Special Publication, Book 83, p. 15-36.

Eichhubl, P., and Boles, J.R., 2000a, Focused fluid flow along faults in the Monterey Formation, coastal California: GSA Bulletin, v. 112, no. 11, p. 1667-1679.

Eichhubl, P., and Boles, J.R., 2000b, Rates of fluid flow in fault systems; evidence for episodic rapid fluid flow in the Miocene Monterey Formation, coastal California: American Journal of Science, v. 300.7, p. 571-600, doi: 10.2475/ajs.300.7.57.

Fife, D.L., 1979, The "Basal Member of the Monterey Formation," Lower Aliso Creek Area, Orange County, California: *in* Geologic Guide to the San Onofre Nuclear Generating Station and Adjacent Regions of So. California: American Association of Petroleum Geologists publication, p. A17-A24.

Finger, K.L., 1988, Depositional Paleoecology of Miocene Ostracods in the Monterey Formation, Laguna Hills, Southern California, USA: Developments in Palaeontology and Stratigraphy, v. 11, p. 1101-1111.

Früh-Green, G., 2005, The Lost City Expedition: http://oceanexplorer.noaa.gov/explorations/05 lostcity/background/serp/serpentinization.html (accessed December 2017).

Horita, J., 2014, Oxygen and carbon isotope fractionation in the system dolomite-water-CO2 to elevated temperatures: Geochemica et Cosmochimica Acta, v. 129, p. 111-124.

Hornafius, J.S., Luyendyk, B.P., Terres, R.R., and Kamerling, M.J., 1986, Timing and extent of Neogene tectonic rotation in the western Transverse Ranges, California [abs.]: Geological Society of America Bulletin, v. 97.12, p. 1476-1487.

Ijeoma, I.O., 2014, A test of diagenetic ordering in siliceous lithofacies, Monterey Formation, southwest Casmalia Hills, Santa Maria Basin, California [M.S. thesis]: Long Beach, California State University, 148 p.

International Centre for Diffraction Data, 2008, Quantitative analysis: Reference intensity ratio (RIR): http://www.icdd.com/resources/tutorials/pdf/Quantitative%20Analysis%20 RIR.pdf (accessed May 2017).

Isaacs, C.M., 1981, Outline of diagenesis in the Monterey Formation examined laterally along the Santa Barbara coast, California, *in* Isaacs, C.M., ed., Guide to the Monterey Formation in the California Coastal Areas, Ventura to San Luis Obispo: Pacific Section AAPG, v. 52, p. 25-38.

Kushnir, J. and Kastner, M., 1984, Two forms of dolomite in the Monterey Formation, California: Concretions and layers – a comparative mineralogical, geochemical, and isotopic study, *in* Garrison, R.E., Kastner, M., and Zenger, D.H., eds., Dolomites of The Monterey Formation and Other Organic-Rich Units: Pasivic Sections SEPM, v. 41, p. 171-183.

Loyd, S.J., Berelson, W.M., Lyons, T.W., Hammond, D.E., and Corsetti, F.A., 2012a, Constraining pathways of microbial mediation for carbonate concretions of the Miocene Monterey Formation using carbonate-associated sulfate: Geochemica et Cosmochimica Acta, v. 78, p. 77-98.

Loyd, S.J., Corsetti, F.A., Eiler, J.M., and Tripati, A.K., 2012b, Determining the diagenetic conditions of concretion formation: Assessing temperatures and pore waters using clumped isotopes: Journal of Sedimentary Research, v. 82, p. 1006-1016.

MacKinnon, T.C., 1989, Petroleum geology of the Monterey Formation in the Santa Maria, *in* MacKinnon, T.C., ed., Oil in the California Monterey Formation, Field Trip Guidebook: American Geophysical Union, v. T311, p. 11-27.

Magaritz, M. and Taylor, H.P., 1976 Oxygen, hydrogen, and carbon isotope studies of the Franciscan Formation, Coast Ranges, California: Geochimica et Cosmochimica Acta, v. 40, p. 215-234.

Malone, M.J., Baker, P.A., and Burns, S.J., 1994, Recrystallization of dolomite: Evidence from the Monterey Formation (Miocene), California: Sedimentology, v. 41, p. 1223-1239.

Malone, M.J., Baker, P.A., and Burns, S.J, 1996, Hydrothermal dolomitization and recrystallization of dolomite breccias from the Miocene Monterey Formation, Tepusquet area, California: Journal of Sedimentary Research, v. 66, no. 5, p. 976-990.

Martin, J.B., and Rymerson, R.A., 1998, Fluid mixing and heterogeneous isotopic compositions of the diagenetic minerals from the Monterey Formation at Jalama Beach, California, *in* Eichhubl, P., ed., Diagenesis, Deformation, and Fluid Flow in the Miocene Monterey Formation: Pacific Section, Society of Sedimentary Geologists Special Publication, Book 83, p. 67-76.

Martin, J.B., and Rymerson, R.A., 2002, A coupled fluid-inclusion and stable isotope record of paleofluids in the Monterey Formation, California: GSA Bulletin, v. 114, no. 3, p. 269-280.

McLean, H., 1995, Distribution and juxtaposition of Mesozoic lithotectonic elements in the basement of Santa Maria Basin, California: U.S. Geological Survey Bulletin 1995-B: Evolution of Sedimentary Basins – Santa Maria Province, p. B1-B12.

Morey, G.W., 1962, The action of water on calcite, magnesite, and dolomite: The American Mineralogist, v. 47, p. 1456-1460.

Murata, K.J., Friedman, I., and Madsen, B.M., 1969, Isotopic Composition of Diagenetic Carbonates in Marine Miocene Formations of California and Oregon: U.S. Geological Survey Professional Paper 614-B, 24 p.

Murata, K.J., Friedman, I., and Cremer, M., 1972, Geochemistry of Diagenetic Dolomites in Miocene Marine Formations of California and Oregon: U.S. Geological Survey Professional Paper 274-C, 12 p.

Namson, J., and Davis, T.L., 1990, Late Cenozoic fold and thrust belt of the southern Coast Ranges and Santa Maria Basin, California: AAPG Bulletin, v. 74, no. 4, p. 467-492.

Nicholson, C., Sorlien, C., Atwater, T., Crowell, J.C., and Luyendyk, B.P., 1994, Microplate capture, rotation of the western Transverse Ranges, and initiation of the San Andreas transform as a low-angle fault system: Geology, v. 22, p. 491- 495.

Onderdonk, N.W., 2005, Structures that accommodated differential vertical axis rotation of the western Transverse Ranges, California: Tectonics, v. 24, TC4018, doi: 10.1029/2004T C001769.

Pisciotto, K.A., 1981, Review of secondary carbonates in the Monterey Formation, California, *in* The Monterey Formation and Related Siliceous Rocks of California: Pacific Section, Society for Sedimentary Geology, p. 273-283.

Pisciotto, K.A., and Garrison, R.E., 1981, Lithofacies and depositional environments of the Monterey Formation, California, *in* The Monterey Formation and Related Siliceous Rocks of California: Pacific Section, Society for Sedimentary Geology, p. 97-122.

Pisciotto, K.A., and Mahoney, J.J, 1981, Isotopic survey of diagenetic carbonates, Deep Sea Drilling Project leg 63: Initial Reports of the Deep Sea Drilling Project, v. 63, p. 595-609.

Redwine, L., 1981, Hypothesis combining dilation, natural hydraulic fracturing, and dolomitization to explain petroleum reservoirs in Monterey Shale, Santa Maria area, California, *in* The Monterey Formation and Related Siliceous Rocks of California: Pacific Section, Society for Sedimentary Geology, p. 221-248.

Roehl, P.O., 1981, Dilation brecciation – A proposed mechanism of fracturing, petroleum expulsion and dolomitization in the Monterey Formation, California, *in* The Monterey Formation and Related Siliceous Rocks of California: Pacific Section, Society for Sedimentary Geology, p. 285-315.

Strickland, H., 2013, Fracture networks and mechanical stratigraphy in the Monterey-equivalent Pismo Formation and its relationship to primary sedimentology and stratigraphy at Montaña De Oro State Park, California [M.S. thesis]: Long Beach, California State University, 154 p.

Tennyson, M. and Isaacs, C.M., 2001, Geologic setting and petroleum geology of Santa Maria and Santa Barbara basins, coastal California, *in* The Monterey Formation: From Rocks to Molecules: New York, Columbia University Press, p. 206-229.

University of Cambridge Department of Earth Sciences, 2015, Carbonate staining: http://www.esc.cam.ac.uk/resources/facilities/laboratories/carbonate-staining (accessed May 2017).

Vasconcelos, C., McKenzie, J.A., Warthmann, R., and Bernasconi, S.M., 2005, Calibration of the $\delta^{18}O$ paleothermometer of dolomite precipitated in microbial cultures and natural environments: Geological Society of America Bulletin, v. 33, no. 4, p. 317-320, DOI: 10.1130/G20992.1.

White, D. E., 1957, Thermal waters of volcanic origin: Geological Society of America Bulletin, v. 68, p. 1637–1658.

Winter, B.L., and Knauth, L.P., 1992, Stable isotope geochemistry of carbonate fracture fills in the Monterey Formation, California: Journal of Sedimentary Petrology, v. 62, no. 2, p. 208-219.

Wirtz, Y., 2017, Strain variation between the Monterey and Sisquoc formations, southern Santa Maria Basin, California, USA: Implications for structural assessment of fold and thrust belts [M.S. thesis]: Long Beach, California State University, 78 p.

Woodring, W.P., and Bramlette, M.N., 1950, Geology and Paleontology of the Santa Maria District, California: U.S. Geological Survey Professional Paper 222, 136 p.